M 2026

U.PORTO
FEUP FACULDADE DE ENGENHARIA
UNIVERSIDADE DO PORTO

Study of the surface functionalisation of leather using natural products to improve hydrophobicity and stain resistance

INÊS PINTO CORREIA DE SOUSA

MASTER'S DEGREE DISSERTATION IN MATERIALS ENGINEERING SUBMITTED TO THE FACULTY OF ENGINEERING OF UNIVERSITY OF PORTO

SUPERVISOR
PROFESSOR CARLOS FONSECA

CO-SUPERVISOR
PROFESSOR JOANA LOUREIRO

U.PORTO
FEUP FACULDADE DE ENGENHARIA
UNIVERSIDADE DO PORTO

CANDIDATO	Inês Sousa	*Código*	202008935
TÍTULO			
DATA			
LOCAL			
JÚRI	*Presidente*		DEMEC/FEUP
	Arguente		DEMEC/FEUP
	Orientador		DEMEC/FEUP
	Co-orientador		DEMEC/FEUP

ABSTRACT

The global leather industry, particularly the Portuguese footwear sector, faces increasing pressure to phase out fluorinated (PFAS) finishing agents in favour of sustainable, high-performance alternatives. This work developed and characterised bio-based hydrophobic and stain-resistant coatings for leather, based on zinc oxide (ZnO) nanoparticles combined with two natural low-surface-energy agents, myristic acid and carnauba wax, applied through three distinct functionalisation methodologies , thereby supporting United Nations Sustainable Development Goals (SDGs), namely SDG 9 (Industry, Innovation and Infrastructure), SDG 12 (Responsible Consumption and Production), and SDG 6 (Clean Water and Sanitation), by replacing persistent, water-contaminating PFAS-based treatments with a sustainable, bio-based alternative.

ZnO nanoparticles were synthesised via a wet chemical route and characterised. Three functionalisation approaches were investigated: sequential immersion with pre-synthesised nanoparticles and myristic acid (Methodology 1), *in-situ* precipitation of ZnO via a tannic acid-mediated route (Methodology 2) and a bilayer system combining ZnO nanoparticles with carnauba wax (Methodology 3). Coatings were characterised by water contact angle (WCA), scanning electron microscopy, energy-dispersive X-ray spectroscopy and Fourier-transform infrared spectroscopy.

Methodology 1 achieved the best overall performance, reaching a maximum WCA of 144.3° ± 5.6, up to 99.7% stability retention after 5 minutes and maintaining substantial hydrophobicity after 50 abrasion cycles. A central finding of this work is that the total quantity of zinc deposited is not a reliable predictor on its own of hydrophobic performance. Rather, the homogeneity of its distribution and the deposition mechanism employed appear more decisive. The developed coatings provided complete resistance to green tea staining and a partial reduction in coffee staining. This work demonstrates the feasibility of fluorine-free, sustainable hydrophobic and stain-resistant leather coatings based on ZnO nanoparticles and natural, bio-based low-surface-energy agents.

Keywords: Leather functionalisation; Zinc oxide nanoparticles; Myristic acid; Carnauba wax; Hydrophobic coating; Stain resistance; Sustainable surface finishing; PFAS-free

RESUMO

A indústria mundial do couro, particularmente o setor do calçado português, enfrenta uma pressão crescente para eliminar os agentes de acabamento fluorados (PFAS), em favor de alternativas sustentáveis e de alto desempenho. Este trabalho desenvolveu e caracterizou revestimentos hidrofóbicos e resistentes a nódoas, de base sustentável, para couro, baseados em nanopartículas de óxido de zinco (ZnO) combinadas com dois agentes naturais de baixa energia superficial, o ácido mirístico e a cera de carnaúba, aplicados através de três metodologias de funcionalização distintas, contribuindo assim para os Objetivos de Desenvolvimento Sustentável (ODS) das Nações Unidas, nomeadamente o ODS 9 (Indústria, Inovação e Infraestruturas), o ODS 12 (Produção e Consumo Sustentáveis) e o ODS 6 (Água Potável e Saneamento), ao substituir tratamentos de couro à base de PFAS, persistentes e contaminantes da água, por uma alternativa sustentável e de base biológica.

Foram sintetizadas e caracterizadas nanopartículas de ZnO por via química húmida. Foram investigadas três abordagens de funcionalização: imersão sequencial com nanopartículas pré-sintetizadas e ácido mirístico (Metodologia 1), precipitação in situ de ZnO através de uma via mediada por ácido tânico (Metodologia 2) e um sistema bicamada combinando nanopartículas de ZnO com cera de carnaúba (Metodologia 3). Os revestimentos foram caracterizados por ângulo de contacto com a água (WCA), microscopia eletrónica de varrimento, espetroscopia de raios-X por dispersão de energia e espetroscopia de infravermelho por transformada de Fourier.

A Metodologia 1 alcançou o melhor desempenho global, atingindo um WCA máximo de 144,3°± 5,6 e uma retenção de estabilidade de até 99,7% após 5 minutos, mantendo hidrofobicidade substancial após 50 ciclos de abrasão. Uma conclusão central deste trabalho é que a quantidade total de zinco depositado não é, por si só, um fator de previsão fiável do desempenho hidrofóbico. Pelo contrário, a homogeneidade da sua distribuição e o mecanismo de deposição aparentam ser mais decisivos. Os revestimentos desenvolvidos proporcionaram resistência completa a nódoas de chá verde e uma redução parcial nas nódoas de café. Este trabalho demonstra a viabilidade de revestimentos de couro hidrofóbicos e resistentes a nódoas, sem flúor e sustentáveis, baseados em nanopartículas de ZnO e agentes naturais de baixa energia superficial de base biológica.

Palavras-chave: Funcionalização de couro; Nanopartículas de óxido de zinco; Ácido mirístico; Cera de carnaúba; Revestimento hidrofóbico; Resistência a nódoas; Acabamento superficial sustentável; Sem PFAS

ACKNOWLEDGEMENTS

I would like to begin by thanking my supervisor, Professor Carlos Fonseca. His constant availability to discuss ideas and work through problems together created the kind of environment where I felt genuinely supported throughout the development of this work, one I don't believe it would have gone as well without. That openness also made room for growth beyond the dissertation itself, both personally and professionally.

I am equally grateful to my co-supervisor, Professor Joana Loureiro, for her valuable input and support.

I would also like to thank the technical staff who made the experimental work possible, in particular D. Cândida and Eng.ª Arminda, from DEQB.

My deepest thanks go to my parents, without whose unconditional love, support and sacrifice none of this would have been possible. Everything I have achieved, I owe to you.

To the rest of my family, thank you for your continued support throughout this journey.

Finally, to my friends, especially those who shared this university path with me — Francisco, Isabel, Leonor, Daniela, and Leonor — thank you for the friendship, support, and for the countless moments that made this experience so much better. I don't think I could have done this without our coffee breaks and without sharing both the frustrations and the victories along the way.

The author thanks the financial support of the project BioShoes4All—"Inovação e capacitação da fileira do calçado para a bioeconomia sustentável", (PRR 000011)—funded by the European Union/NextGenerationEU under the Recovery and Resilience Programme through the 'Environmental Fund', and of project UIDB/50006/2020 | UIDP/50006/2020, through national funds.

INDEX

ABSTRACT ..... **i**
RESUMO ..... **ii**
ACKNOWLEDGEMENTS ..... **iii**
INDEX ..... **iv**
LIST OF FIGURES ..... **vii**
LIST OF TABLES ..... **x**
1. Introduction **1**
1.1. Leather and its role in the Portuguese Footwear Industry 1
1.2. Overview of the Tanning Process 1
1.3. Conventional finishings 2
1.4. Sustainable alternatives 3
1.5. Research aims 4
2. Literature Review **4**
2.1. Leather surface structure and chemistry 4
2.1.1. Hierarchical architecture of collagen fibres 4
2.1.2. Surface reactive functional groups 5
2.1.3. Surface charge and isoelectric point 6
2.1.4. Chemical modifications from tanning and fatliquoring 7
2.1.5. Surface topography and roughness 7
2.2. Fundamentals of hydrophobicity and stain resistance 7
2.2.1. Surface energy, contact angle and Young's equation 7
2.2.2. Wetting on rough surfaces: Wenzel and Cassie-Baxter models 8
2.3. Multi-functional properties of ZnO nanoparticles 10
2.3.1. Physicochemical basis and surface reactivity 10
2.3.2. UV Shielding and antimicrobial properties 10
2.4. Low-surface-energy agents: fatty acids and natural waxes 11
2.4.1. Chemical structure and amphiphilic nature 11
2.5. Recent advances in fabrics bio-based functionalization 12
3. Materials and Methods **13**
3.1. Leather substrate (as-received) 13
3.2. Leather cleaning methodologies 13
3.3. Synthesis and characterisation of ZnO nanoparticles 15

3.3.1. Synthesis of ZnO nanoparticles 15
3.3.2. Dynamic Light Scattering (DLS) 16
3.4. Surface functionalisation 16
3.4.1. Methodology 1 - Sequential immersion with pre-synthesised nanoparticles 16
3.4.2. Methodology 2 – *In-situ* synthesis with *in-situ* precipitation 17
3.4.3. Methodology 3 - Bilayer system with ZnO nanoparticles and carnauba wax 19
3.4.4. Sample nomenclature and experimental design 20
3.5. Characterization of functionalised leather 21
3.5.1. Scanning Electron Microscopy and Energy-Dispersive X-ray Spectroscopy (SEM/EDS) 22
3.5.2. Fourier-Transform Infrared Spectroscopy (FTIR) 22
3.5.3. Water Contact Angle (WCA) 22
3.5.4. Abrasion resistance 23
3.5.5. Stain resistance 23
3.6. Statistical analysis 23
4. Results and Discussion 24
4.1. Nanoparticle synthesis and characterisation 24
4.1.1. Particle size distribution (DLS) 24
4.1.2. Selection of zinc acetate concentration for functionalisation 26
4.2. Methodology 1 26
4.2.1. WCA response to process variables: statistical analysis and mechanistic discussion 28
4.2.2. Surface morphology and chemistry (SEM/EDS, FTIR) 31
4.2.3. Selection of best-performing conditions 37
4.3. Methodology 2 38
4.3.1. Effect of zinc salt, base, solvent and final bath conditions on WCA 38
4.3.2. Surface morphology and chemistry (SEM/EDS, FTIR) 40
4.3.3. Selection of best-performing conditions 44
4.4. Methodology 3 44
4.4.1. Preliminary trials (M3-(1B+3W) / M3-(2B+3B)) vs. standardised protocol 45
4.4.2. Effect of number of bilayers on WCA 47
4.4.3. Surface morphology and chemistry (SEM, FTIR) 48
4.5. Comparison across methodologies 51
4.5.1. WCA comparison 51
4.6. Durability and functional performance of selected coatings 52

4.6.1. Abrasion resistance 52
4.6.2. Stain resistance 55
5. Conclusion 57
6. Future works 58
7. References 60

LIST OF FIGURES

Figure 1 - General scheme of leather processing [12] 2
Figure 2 - Hierarchical and molecular structure of type I collagen. The diagram illustrates the macromolecular triple helix organization (top), the specific amino acid sequence of the alpha-chain (middle), and the chemical representation of the fundamental Gl [19] 5
Figure 3 - Cross-sectional schematic of leather morphology [21] 5
Figure 4 - Molecular interactions within the collagen triplet (Gly-Pro-Hyp)[23] 6
Figure 5 - Schematic representation of Young's equation [28] 8
Figure 6 - Wetting regimes defined by the contact angle: superhydrophilic, hydrophilic, hydrophobic, and superhydrophobic states [24] 8
Figure 7 - Schematic representation of the Cassie-Baxter and Wenzel models [30]..... 9
Figure 8 - Structural representation of ZnO wurtzite lattice [36] 10
Figure 9 - Chemical structure and molecular models of a fatty acid, illustrating the hydrophilic carboxyl head and the hydrophobic hydrocarbon tail [39] 11
Figure 10 - Myristic acid, adapted from[44]..... 12
Figure 11 - Schematic representation of Cleaning Approach 1 (simple cleaning protocol) 14
Figure 12 - Schematic representation of Cleaning Approach 2 (extended cleaning protocol with acetic acid treatment) 14
Figure 13 - Schematic representation of the initial steps of ZnO nanoparticle synthesis: precursor dissolution (zinc acetate in absolute ethanol and ethylene glycol) and dropwise addition of 0.25 M KOH under stirring, in a water bath at 55 °C..... 15
Figure 14 - Schematic representation of the sequential functionalization process for the leather samples. (a) One cycle of n-ZnO dispersion immersion; (b) One cycle of MA solution immersion. The complete coating is formed by performing three consecutive cycles of step (a) followed by three consecutive cycles of step (b). 17
Figure 15 - Schematic representation of the in-situ synthesis functionalisation process for the leather samples (M2). (a) preparation of the tannic acid (TA) and zinc salt (acetate or nitrate) solutions, with the pH adjusted to 5–6 using 0.1 M NaOH; (b) immersion sequence, consisting of TA immersion, water rinsing, zinc salt immersion, and a further water rinse, repeated twice in total; (c) final bath, in which a base (MEA or

ammonia) was added dropwise, at a controlled temperature (50 °C or room temperature), until reaching a pH of approximately 8.5, followed by a 30-minute reaction period; (d) oven drying at 70 °C; (e) immersion in a 1% MA solution in isopropanol (10 min immersion, 20 min drying). Steps (e) was repeated three times in total, as described for Methodology 1 (Section 3.4.1). 18
Figure 16 - Schematic representation of the bilayer functionalisation process for the leather samples (M3). (a) Immersion in the tannic acid (TA) solution for 15 minutes, followed by oven drying at 70 °C for 20–30 minutes; (b) One bilayer cycle, consisting of immersion in the ZnO nanoparticle dispersion for 10 minutes, a water rinse, immersion in the carnauba wax dispersion for 10 minutes, and a further water rinse; (c) oven drying overnight at 65 °C. Step (b) was repeated according to the number of bilayers tested (1, 3 or 5).)..... 20
Figure 17 - Water contact angle (WCA) at t=0 min and t=5 min for all samples prepared under Methodology 1, compared to the untreated (control) leather. Error bars represent standard deviation across replicate measurements 27
Figure 18 - Backscattered electron SEM micrographs of the untreated (control) leather surface at 100× (panoramic) and 1000× (detail) magnification, showing the characteristic fibrous topography of the collagen network. Inset: corresponding water contact angle 32
Figure 19 - Backscattered electron SEM micrographs at 100× (panoramic) and 1000× (detail) magnification of the four ZnO-0.22 conditions: M1-A1-0.22-100Et, M1-A1-0.22-50Et, M1-A2-0.22-100Et, and M1-A2-0.22-50Et. Insets show the corresponding water contact angle for each condition..... 32
Figure 20 - Backscattered electron SEM micrographs at 100× (panoramic) and 1000× (detail) magnification of the four ZnO-1.1-c conditions: M1-A1-1.1c-100Et, M1-A1-1.1c-50Et, M1-A2-1.1c-100Et, and M1-A2-1.1c-50Et. Insets show the corresponding water contact angle for each condition..... 34
Figure 21 - FTIR-ATR spectra of the untreated (Control) leather, all Methodology 1 conditions, and pure myristic acid (MA)..... 36
Figure 22 - Water contact angle (WCA) at t=0 min and t=5 min for the untreated control and all Methodology 2 conditions (M2-1 to M2-6). Error bars represent standard deviation across replicate measurements 39

Figure 23 - Backscattered electron SEM micrographs at 100× (panoramic) and 1000× (detail) magnification of the untreated control and Methodology 2 conditions M2-2 to M2-6. Insets show the corresponding water contact angle for each condition 41
Figure 24 - FTIR-ATR spectra of the untreated (Control) leather, M2-2 to M2-6 conditions from Methodology 2, and pure myristic acid (MA) 43
Figure 25 - Water contact angle (WCA) at t=0 min and t=5 min for the untreated control, the preliminary trial conditions (M3-(1B+3W) and M3-(2B+3B)), and the standardised bilayer protocol conditions (M3-1B, M3-3B, M3-5B). Error bars represent the standard deviation a 45
Figure 26 - SEM micrographs of sample M3-(1B+3W): (left) backscattered electron image at 100× (panoramic) and 1000× (detail) magnification, with inset showing the corresponding water contact angle (125.0° ± 3.08); (right) secondary electron image at 50 48
Figure 27 - SEM micrographs of samples M3-1B (a, b) and M3-3B (c, d): (a, c) backscattered electron images at 100× magnification, with insets showing the corresponding water contact angle; (b) secondary electron image at 5000× magnification of sample M3-1B, showing surface detail; (d) backscattered electron image at 5000× magnification of sample M3-3B, corresponding to a higher-magnification view of the region shown in (c). 49
Figure 28- ATR-FTIR spectra of the untreated (control) leather Methodology 3 conditions M3-(1B+3W), M3-1B, and M3-3B 50
Figure 29- Water contact angle (WCA) at t=0 min and t=5 min for M1-A1-1.1c-50Et and M1-A2-1.1c-50Et before abrasion (0 cycles) and after 20 and 50 abrasion cycles 53
Figure 30- Backscattered electron SEM micrographs of sample M1-A1-1.1c-50Et after 0, 20 and 50 abrasion cycles, at 100× (top row) and 1000× (bottom row) magnification 54
Figure 31- Backscattered electron SEM micrographs of sample M1-A2-1.1c-50Et after 0, 20 and 50 abrasion cycles, at 100× (top row) and 1000× (bottom row) magnification 54
Figure 32- Leather specimens used for stain resistance testing: M1-A1-1.1c-50Et, M1-A2-1.1c-50Et, and the untreated control 56
Figure 33- Stain resistance testing on M1-A1-1.1c-50Et, M1-A2-1.1c-50Et, and the untreated control, using coffee (a–c) and green tea (d–f) as staining agents. Rows show, from top to bottom: immediately after droplet deposition, after 10 minutes, and after droplet removal 56

Figure 34- Final appearance of the coffee-stained specimens after droplet removal and complete drying 57

LIST OF TABLES

Table 1 - Zinc acetate precursor concentrations used in the synthesis of ZnO nanoparticles 16
Table 2 - Variables and corresponding levels tested within Methodology 1(M1) 17
Table 3 - Conditions tested within Methodology 2 (M2) 19
Table 4 - Sample codes and corresponding conditions for Methodology 1 21
Table 5 - Sample codes and corresponding conditions for Methodology 2 21
Table 6 - Sample codes and corresponding conditions for Methodology 3 21
Table 7 - Overview of the characterisation techniques used to evaluate the functionalised leather samples. 22
Table 8 – Z-average particle size and PDI of commercial and synthesised ZnO nanoparticles, as measured by DLS. 24
Table 9 - KOH-to-precursor ratio for each synthesis condition, relative to the stoichiometric requirement. 26
Table 10 - Three-way factorial ANOVA for WCA at t = 5 min 28
Table 11 - Marginal means for each factor level (averaged over the other two factors) . 28
Table 12 - Tukey HSD grouping of the eight Methodology 1 conditions (WCA at t = 5 min, α = 0.05). Conditions sharing a letter are not significantly different from each other 29
Table 13 - Effect of cleaning protocol (IPA/AA − IPA) on WCA at t = 5 min, by ZnO concentration and dispersion medium 30
Table 14 - Effect of ZnO concentration (1.1 − 0.22) on WCA at t = 5 min, by dispersion medium (averaged over cleaning protocol) 30
Table 15 - Semi-quantitative EDS analysis of zinc content on the leather surface for the control and all Methodology 1 conditions. 35
Table 16 - Ranking of Methodology 1 conditions by mean WCA at t = 5 min, from best to worst-performing 37

Table 17 - Ranking of Methodology 2 conditions by mean WCA at t = 5 min, with Games-Howell statistical grouping (α = 0.05). Conditions sharing a letter are not significantly different from each other. 39
Table 18 - Semi-quantitative EDS analysis of zinc content on the leather surface for Methodology 2 conditions (M2-1 to M2-6) 43
Table 19 - Games-Howell grouping of WCA at t = 5 min for the untreated control and all Methodology 3 conditions (α = 0.05). Conditions sharing a letter are not significantly different from each other 46
Table 20 - Summary of water contact angle (WCA) at t=0 and t=5 min, retention, and surface zinc content (where available) for the best-performing conditions identified within each methodology 51
Table 21 - Tukey HSD pairwise comparisons between abrasion cycle counts, for each condition (α = 0.05) 53

LIST OF ABBREVIATIONS

AA – Acetic Acid

ANOVA – Analysis of Variance

ATR – Attenuated Total Reflectance

BSED – Backscattered Electron Detection

DLS – Dynamic Light Scattering

ECHA – European Chemicals Agency

EDS – Energy-Dispersive X-ray Spectroscopy

EG – Ethylene Glycol

EPA – Environmental Protection Agency

EU – European Union

FTIR – Fourier-Transform Infrared Spectroscopy

HSD – Honestly Significant Difference

IPA – Isopropyl Alcohol

MA – Myristic Acid

MEA – Monoethanolamine

n-ZnO – Zinc Oxide Nanoparticles

PDI – Polydispersity Index

PFAS – Per- and Polyfluoroalkyl Substances

PFOA – Perfluorooctanoic Acid

PFOS – Perfluorooctane Sulfonate

REACH – Registration, Evaluation, Authorisation and Restriction of Chemicals

ROS – Reactive Oxygen Species

SD – Standard Deviation

SDG – Sustainable Development Goal

SEM – Scanning Electron Microscopy

SSbD – Safe-and-Sustainable-by-Design

SVHC – Substances of Very High Concern

TA – Tannic Acid

UV – Ultraviolet

WCA – Water Contact Angle

ZnO – Zinc Oxide

1. Introduction

1.1. Leather and its role in the Portuguese footwear industry

Leather is one of the oldest and most versatile materials used globally [1] due to its exceptional combination of mechanical resistance, flexibility, breathability and aesthetic look. The fact that leather is a by-product from the meat and dairy sectors and not a primary product from an independent industry, makes it interesting sustainability-wise. The hides and skins that would otherwise be discarded as residues, are collected and transformed by a tanning process into a reliable material, which gives leather a great advantage when it comes to the circular economy in comparison to synthetic alternatives [1–3].

At its core, leather derives its unique properties from a hierarchically organized network of collagen fibres that make up the dermal layer of animal skin. This fibrous architecture grants the material its intrinsic tensile strength and porosity [4]. The specific properties of leather vary considerably according to the animal species of origin: cattle, sheep and goat skins differ substantially in total thickness, fibre bundle size and weave pattern, offering tanners a range of raw materials suited to different end uses, with the tanning process itself capable of further modifying this natural weave to achieve the physical properties required for a given application [5]. Ovine leather has been reported to present approximately half the tear strength of bovine leather, a difference closely correlated with the degree of collagen fibril alignment within the plane of the tissue, limiting its suitability for high-value applications such as footwear [6]. However, this same porous and chemically reactive structure makes leather inherently susceptible to moisture absorption and the formation of surface stains, limitations that are particularly critical in high-performance applications, like footwear [1,7].

Portugal holds a prominent position in the European footwear industry, ranking second among the continent's producers, after Italy. In 2024, the Portuguese industry produced 80 million pairs and exported 67 million pairs to 170 countries, with the cluster’s total turnover reaching €2.22 billion [8]. The average exportation price comes up to €27,32 per pair thus reflecting a well-established position in the premium segment of the global market [9]. Leather footwear is the cornerstone of this strategy, currently accounting for 83% of the sector’s foreign trade [8]. Beyond footwear, the Portuguese leather goods and apparel segment has also shown notable growth: exports of leather goods manufactured in Portugal reached €273 million in 2022, a 39% year-on-year increase, with the number of companies operating in this sector growing by 42% over the preceding decade to 142 businesses and employment nearly tripling to 3,324 [10]. This focus on the value-added segment makes the surface finish of the leather a critical factor: a finish that loses its water-repellent properties or develops stains with use compromises not only the product’s functionality but also the brand’s reputation.

1.2. Overview of the tanning process

Leather processing involves a series of sequential physical and chemical operations that

transform raw animal hides into a stable and durable material. As illustrated in Figure 1, the process is divided into four main stages: pre-tanning, tanning, post-tanning and finishing. In the pre-tanning phase, the hides undergo soaking, fleshing, depilation and liming to remove non-collagenous components and prepare the fibrous structure for subsequent stages [11].

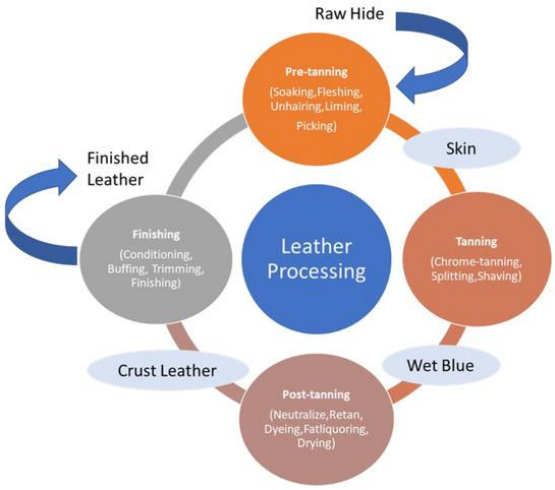


Figure 1 - General scheme of leather processing [12]

Tanning itself is the central stage of the process, with chrome tanning being the most widely used method in industry. In this case, trivalent chromium salts form stable coordination complexes with the collagen fibres, imparting thermal and hydrothermal resistance to the material and producing the intermediate product known as wet blue.

Post-tanning operations, which include neutralisation, retanning, dyeing and fat-tanning, adjust the material's mechanical and aesthetic properties, producing what is known as crust leather, ready for the final stage [11].

It is at this final stage, the finishing, that the functional surface properties of the leather are defined, namely its appearance, feel, abrasion resistance, water repellence and stain resistance. Conventional finishing treatments have historically relied on synthetic agents, such as fluorocarbon-based compounds, to achieve these properties [13]. However, growing environmental concerns and increasingly restrictive regulations have fuelled demand for more sustainable alternatives, a topic explored in greater depth in the following sections.

1.3. Conventional finishings

As the industry staple, the leather processing has relied heavily on per- and polyfluoroalkyl substances (PFAS) to achieve high-performance surface finishes. These synthetic chemicals are characterised by their extreme hydrophobicity and lipophobicity, chemical inertness and resistance to elevated temperatures.

These properties result directly from the extremely stable and low-energy carbon-fluorine (C–F) bond, which is known as one of the strongest bonds in organic chemistry [14,15]. Due to these characteristics, PFAS-based treatments have historically become the standard for imparting water, oil and stain repellence to leather and textile articles, with long-chain perfluoroalkylated compounds, such as perfluorooctanoic acid (PFOA) and

perfluorooctane sulfonate (PFOS)[13,16].

However, the very chemical structure that gives PFAS their unique functional properties also makes them highly resistant to environmental degradation. Scientific research has shown that PFAS are extremely persistent, bioaccumulative and mobile in the environment, traits which have led to them being labelled '*forever chemicals*' [14,16].

Throughout the entire life cycle of a treated product, PFAS are continuously released into ecosystems. Furthermore, their toxicity is now widely recognised as the exposure to PFAS has been linked to serious health risks, including carcinogenic, hepatotoxic, immunotoxic and endocrine-disrupting effects, as well as reproductive harm and damage to fetal development [14,15].

In response to these alarming environmental and health impacts, increasingly restrictive legislation has been introduced worldwide. Regulatory bodies such as the US Environmental Protection Agency (EPA) and the European Union, through its REACH Regulation (Registration, Evaluation, Authorisation and Restriction of Chemicals), have identified numerous PFAS as substances of remarkably high concern (SVHC) [15]. Several long-chain PFAS, including PFOA and PFOS, are already effectively banned in the EU. More recently, a proposal for a universal restriction given to ECHA by the national authorities of Germany, Denmark, the Netherlands, Norway and Sweden propose a near-total ban on the intentional use of PFAS in sectors such as textiles, leather and clothing [15,16]. This proposal, currently undergoing scientific evaluation, stands for one of the most significant regulatory developments in European chemicals law in recent years, with formal legislation expected in 2027 [15].

This shift in the regulatory landscape has made the transition away from fluorocarbon-based finishes an urgent industry priority. The leather sector, already under scrutiny for the environmental footprint of the tanning process, faces added pressure to reformulate its finishing chemistry. This reality has driven current research to focus on developing safer, PFAS-free alternatives capable of delivering equivalent or superior functional performance [7,14].

1.4. Sustainable alternatives

The need to find alternatives to PFAS in leather finishes has driven intensive research over recent decades, guided by the *Safe-and-Sustainable-by-Design* (SSbD) principle. SSbD consists of the idea that new materials should be designed with safety and sustainability built in, rather than merely assessed after the fact [16]. In this context, various classes of alternative compounds have been explored, ranging from polyurethanes and silicones to natural waxes and biopolymers, with varying results in terms of performance, durability and environmental profile [14,16].

Bio-based solutions are among the most promising approaches, notably the use of naturally occurring fatty acids as low surface energy agents. These compounds are abundant, renewable and biodegradable and their ability to reduce the surface free energy of solid substrates through the orientation of non-polar alkyl chains makes them remarkable candidates aligned with the principles of green chemistry [14,17]. However, their use alone proves insufficient to achieve superhydrophobicity, as obtaining high

contact angles requires not only low surface energy but also structural roughness at the nanoscale [14].

This requirement has been addressed through the incorporation of inorganic nanoparticles, inspired by the lotus effect, a phenomenon where natural surfaces combine hydrophobic components with hierarchical microstructures to achieve extreme water repellency [14,17]. Zinc oxide (ZnO) nanoparticles have emerged as a particularly attractive choice in this context, not only for their ability to generate surface roughness, but also for their intrinsic multifunctional properties, including UV-shielding and antimicrobial activity [14,18]. The interesting combination of ZnO nanoparticles with fatty acids represents a double sustainable approach — biologically safe and functionally effective — which forms the focus of this dissertation.

1.5. Research aims

The overall aim of this study is to develop and characterise a sustainable surface coating for leather, based on a combination of ZnO nanoparticles with naturally occurring low-surface-energy agents, namely myristic acid and carnauba wax, with a view to imparting hydrophobicity and stain resistance. ZnO nanoparticles were selected, among other reasons, for their recognised potential to confer additional functional properties to leather, such as UV shielding and antimicrobial activity; while these properties were not experimentally assessed within the scope of the present work, they are considered a relevant direction for future development.

To this end, the following specific goals were defined:

- To synthesise and characterise the ZnO nanoparticles;
- To optimise the application parameters of the surface treatment;
- To evaluate hydrophobicity by measuring the contact angle;
- To characterise the obtained coatings chemically and morphologically;
- To evaluate the stain resistance and mechanical durability (abrasion resistance) of the functionalised leather.

2. Literature Review

2.1. Leather surface structure and chemistry

For the development of effective treatments, it is essential to have an insight into the structure and chemistry of leather. The protein-based, porous and chemically heterogeneous nature of this substrate determines how finishing agents interact, adhere and distribute themselves across the surface, directly influencing the performance and durability of the final coating.

2.1.1. Hierarchical architecture of collagen fibres

Leather derives its mechanical properties from the hierarchical organisation of type I collagen, which is the dominant structural protein in the animal dermis. The fundamental

unit is the collagen triple helix, consisting of three polypeptide chains stabilised by hydrogen bonds between glycine, proline and hydroxyproline residues [19] . These molecules progressively aggregate into microfibrils, fibrils, fibres and fibre bundles — a multi-scale organisation that confers the material an exceptional combination of tensile strength and flexibility, see Figure 2 [19].

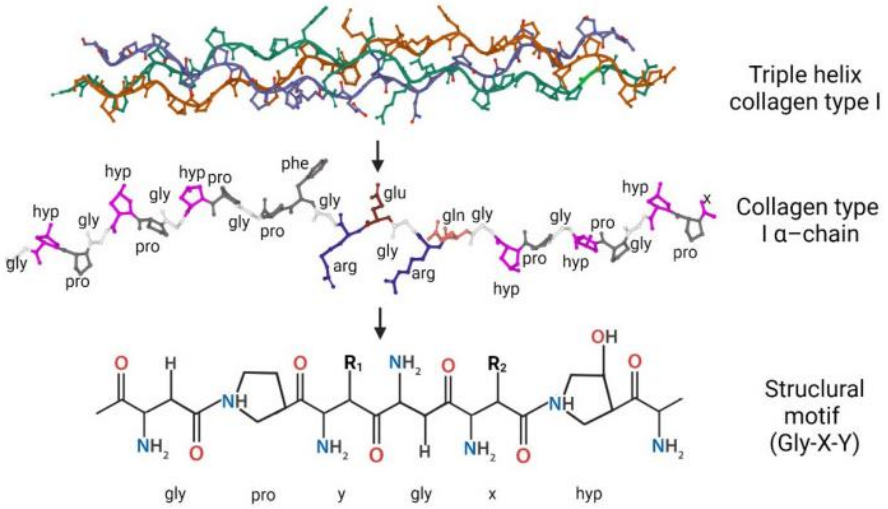


Figure 2 - Hierarchical and molecular structure of type I collagen. The diagram illustrates the macromolecular triple helix organization (top), the specific amino acid sequence of the alpha-chain (middle), and the chemical representation of the fundamental Gl [19]

As illustrated in Figure 3, the skin has two morphologically distinct layers. The grain layer is characterised by fine, densely packed fibres oriented parallel to the surface. The underlying reticular dermis (corium) is composed of thicker fibre bundles interwoven in multiple directions and is responsible for the overall mechanical strength [11]. It is in the grain layer that finishing agents primarily interact with the substrate, and the grain layer's microstructure determines the adhesion and distribution of the nanomaterials. The natural porosity of this fibrous network facilitates the penetration of colloidal dispersions, allowing for deeper anchoring of the modifying agents [7,20].

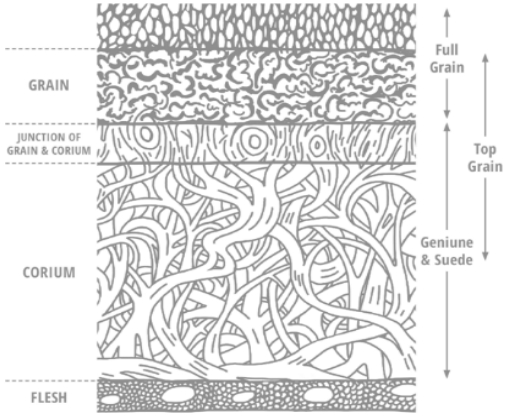


Figure 3 - Cross-sectional schematic of leather morphology [21]

2.1.2. Surface reactive functional groups

The surface of leather is richly endowed with reactive functional groups, originating from the amino acid composition of collagen. The groups most relevant to surface

functionalisation are the primary amine groups (-NH_2), derived from lysine and hydroxylysine residues, the carboxylate groups (-COOH), present in aspartic and glutamic acid residues and hydroxyl groups (-OH), associated with serine, threonine and hydroxyproline residues (Figure 4) [22,23]. These groups are exposed on the surface of collagen fibres and constitute the main sites for anchoring functionalising agents, including metal oxide nanoparticles [7,17].

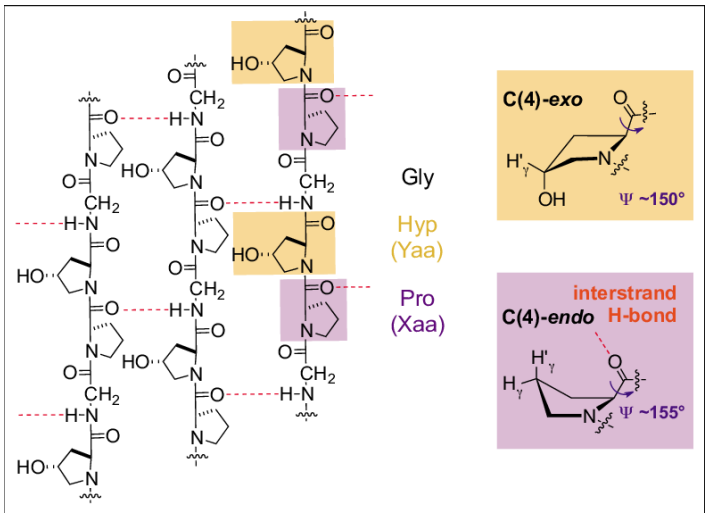


Figure 4 - Molecular interactions within the collagen triplet (Gly-Pro-Hyp)[23]

The natural hydrophilicity of leather results largely from the ability of these polar groups to form hydrogen bonds with water molecules. The -NH_2 and -COOH groups are particularly relevant in this context, given their highly polar nature and their abundance on the fibre surface [7,22]. It is precisely this intrinsic affinity for water that hydrophobic treatments aim to neutralise, by replacing or blocking these groups with entities of low surface energy.

2.1.3. Surface charge and isoelectric point

The surface of leather has a variable electrical charge depending on the pH of the environment, which is determined by the balance between protonation and deprotonation of the amine and carboxylate groups. At pH values below the isoelectric point (pI), the amine groups are predominantly protonated (-NH_3^+) - the surface has a positive net charge. Above the pI, deprotonation of the carboxylate groups (-COO^-) predominates - surface overall negative [20,22] . For chrome-tanned leather, the pI typically lies between 6 and 7, whilst for vegetable-tanned leathers this value is generally lower, in the range of 3 to 4 [22].

Understanding the pI is important not only for the application of functionalising agents, but also for understanding the behaviour of the substrate during post-tanning operations in an aqueous system. Surface charge influences the penetration and fixation of retanning agents, dyes and fatliquors, predominantly anionic or cationic compounds, thus determining the electrostatic affinity between the substrate and each product class [22]. The surface charge state at the time of applying the hydrophobic finish is, for this reason, a factor that determines the quality of the initial interaction between the substrate and the functionalising agent [20,22].

2.1.4. Chemical modifications from tanning and fatliquoring

The tanning process profoundly alters the surface chemistry of leather compared with raw hide, with direct implications for subsequent functionalisation. In chrome tanning, the most widely used industrial method, Cr (III) ions interact with collagen through coordination reactions, especially with carboxyl groups, forming stable complexes that reduce the number of available reactive sites for later interactions with finishing agents [22] . Vegetable tanning proceeds through a different chemical pathway, in which tannins interact with collagen and modify its surface chemistry in a way that produces a distinct material with different reactivity, wettability, and pH-dependent behaviour [22].

Fatliquoring operations, carried out during post-tanning, introduce lipid compounds into the fibrous structure, lubricating the collagen network, improving softness and flexibility and lowering the initial surface free energy of the leather. This can be beneficial for the adhesion of hydrophobic coatings, but heterogeneous fatliquor distribution may also lead to non-uniform deposition of subsequent functional layers [22,24]. In parallel, surfactants employed during processing can modify local wettability and influence the spreading, anchoring and final performance of functionalising agents [24,25].

2.1.5. Surface topography and roughness

The outer layer of leather displays a characteristic natural roughness, due to the microstructure of the grain layer and the pattern of hair follicles, which varies depending on the animal species, the anatomical region, and the applied processing methods [26]. This intrinsic roughness, visible at micrometre scales, has direct implications for the wettability of the substrate — a rough surface does not behave like an ideal surface, and the contact angle observed results not only from surface chemistry but also from its physical texture [27]. The relationship between roughness and wettability will be discussed in detail in section 2.2, in the context of the Wenzel and Cassie-Baxter models.

Mechanical finishing operations, such as buffing and polishing, alter the natural roughness profile of the leather and may increase or reduce surface roughness depending on the intended objective [26]. In the context of surface functionalisation, the topographical state of the substrate before coating application is a key factor, as it influences the uniformity of coating agent deposition and the effective contact area between the coated layer and the substrate [26,27].

2.2. Fundamentals of hydrophobicity and stain resistance

A surface’s resistance to water and the adhesion of contaminants is determined by two interdependent factors: the material’s free surface energy and its micro- and nanoscale topography. Understanding the physicochemical principles governing surface wettability is essential for the rational design of hydrophobic coatings.

2.2.1. Surface energy, contact angle and Young's equation

The wettability of a solid surface by a liquid is determined by the balance between the liquid's cohesive forces — which tend to minimise the area of contact with the solid — and the adhesive forces between the liquid and the solid — which promote spreading.

This balance is quantified by the surface free energy (γ), which represents the excess energy associated with the existence of an interface. High-energy surfaces, such as metals and metal oxides, interact strongly with water, whilst low-energy surfaces, such as waxes and fluorinated polymers, minimise these interactions [14]. The most used experimental parameter to characterise wettability is the contact angle (θ), defined as the angle formed between the liquid-vapour interface and the solid surface at the point of contact on the three-phase line. For an ideal surface, perfectly smooth and chemically homogeneous, this angle is described by Equation 1, Young's equation [18], as illustrated in Figure 5:

$$\gamma_{sv} = \gamma_{sl} + \gamma_{lv} \cos \theta_Y \quad (1)$$

, where γ_{sv} is the surface free energy, γ_{sl} is the interfacial tension between the liquid and the solid, γ_{lv} is the surface tension of the liquid, and θ_Y is the contact angle on a surface.

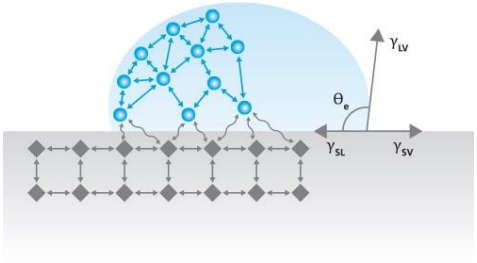


Figure 5 - Schematic representation of Young's equation [28]

Based on the value of θ, surfaces are classified as hydrophilic (θ < 90°), hydrophobic (90° < θ < 150°) or superhydrophobic (θ > 150°) [1,7], as illustrated in Figure 6. Untreated leather typically exhibits contact angles of less than 90°, reflecting the intrinsic hydrophilic nature of collagen, and the aim of finishing treatments is to shift this value into the hydrophobic or superhydrophobic range [7].

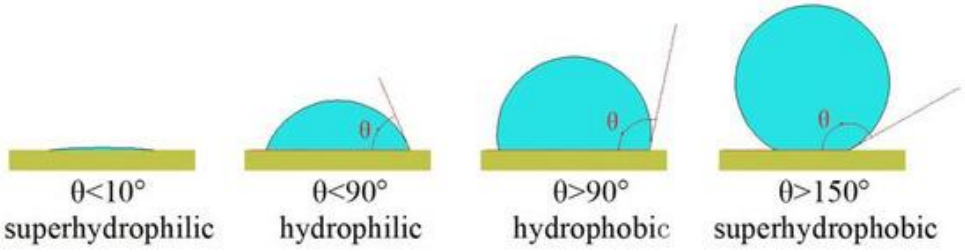


Figure 6 - Wetting regimes defined by the contact angle: superhydrophilic, hydrophilic, hydrophobic, and superhydrophobic states [24]

2.2.2. Wetting on rough surfaces: Wenzel and Cassie-Baxter models

Young's equation applies exclusively to ideal, smooth and homogeneous surfaces, conditions that are rarely found in real materials. Rough surfaces, such as leather or substrates functionalised with nanoparticles, exhibit wetting behaviour that deviates significantly from that predicted by Young's model, making it necessary to use models that explicitly incorporate the effect of surface topography. The two fundamental models in this context are the Wenzel model and the Cassie-Baxter model, which describe two distinct wetting regimes on rough surfaces [29], as seen in Figure 7.

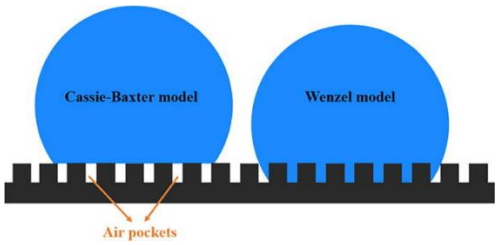


Figure 7 - Schematic representation of the Cassie-Baxter and Wenzel models [30]

In the Wenzel model, the liquid fully fills the cavities and irregularities of the rough surface, maintaining close contact with the solid across the entire interfacial area. In this regime, roughness amplifies the intrinsic behaviour of the surface: if the surface is hydrophilic, it becomes more hydrophilic; if it is hydrophobic, it becomes more hydrophobic. This effect is quantified by the Wenzel roughness factor (r), defined as the ratio of the actual surface area to the projected area, and which features in the modified Equation 2 [31]:

$$cos\theta_W = r \cdot cos\theta_Y \quad (2)$$

where θ_W is the apparent contact angle in the Wenzel regime and θ_W is the Young's angle of the equivalent smooth surface. Although this regime can produce high contact angles on intrinsically hydrophobic surfaces, the droplets tend to adhere strongly to the surface, making it difficult for them to detach, which limits self-cleaning [29].

The Cassie-Baxter model describes a fundamentally different regime, in which the liquid does not penetrate the cavities of the rough surface, which remain filled with air. The drop thus rests on a composite interface, partly solid, partly gaseous, which drastically reduces the effective contact area between the liquid and the solid. The apparent contact angle in this regime is given by Equation 3 [31] :

$$cos\theta_{CB} = f_s(cos\theta_Y + 1) - 1 \quad (3)$$

where f_s represents the fraction of solid area in contact with the liquid. As f_s decreases, fraction of trapped air increases, the contact angle approaches 180°, corresponding to ideal superhydrophobicity. It is in this regime that the so-called lotus effect is observed: water droplets take on an almost spherical shape, roll easily over the surface at very low angles of inclination (roll-off angle < 10°) and carry away deposited dirt particles, giving the surface self-cleaning properties [14].

The transition between the Wenzel and Cassie-Baxter regimes is determined by the surface roughness geometry and scale, as well as the pressure applied to the droplet. Surfaces with multi-scale hierarchical roughness, such as combining micrometre- and nanometre-scale structures, favour the stabilisation of the Cassie-Baxter regime and hinder the collapse into the Wenzel regime and this is the principle that justifies the incorporation of nanoparticles as a strategy for achieving durable superhydrophobicity on substrates such as leather [7]. In leather, this hierarchical roughness results from combining the microscale texture naturally present in the grain layer with the nanoscale roughness introduced by nanoparticle deposition. Together, these two scales create a network of micro- and nano-cavities that trap air pockets, supporting the droplet and minimising solid-liquid contact — a necessary condition for contact angles above 150° [32,33].

2.3. Multi-functional properties of ZnO nanoparticles

2.3.1. Physicochemical basis and surface reactivity

At the nanoscale, ZnO nanoparticles exhibits a wurtzite crystal structure (Figure 8) with an extraordinarily high surface area-to-volume ratio compared to its bulk forms, which maximises the number of contact sites available for interaction with the collagen fibres of the substrate [17,34]. The surface of ZnO nanoparticles is naturally terminated in hydroxyl groups (Zn–OH), resulting from the adsorption of water molecules and the incomplete coordination of surface zinc ions [17,18,35].

These groups confer an amphoteric character on the ZnO surface which allows it to behave as a Lewis acid or base depending on the pH of the medium. Accordingly, ZnO nanoparticles exhibit a characteristic isoelectric point, generally reported around pH 9 [32,33], below which the surface carries a net positive charge, and above which it becomes negatively charged. They are also fundamental for subsequent functionalisation with fatty acids, via esterification or coordination reactions between the fatty acid carboxylate groups and the surface Zn^{2+} ions [17,18,35]. This surface reactivity is therefore the central mechanism linking ZnO deposition to the hydrophobic modification discussed in section 2.4.

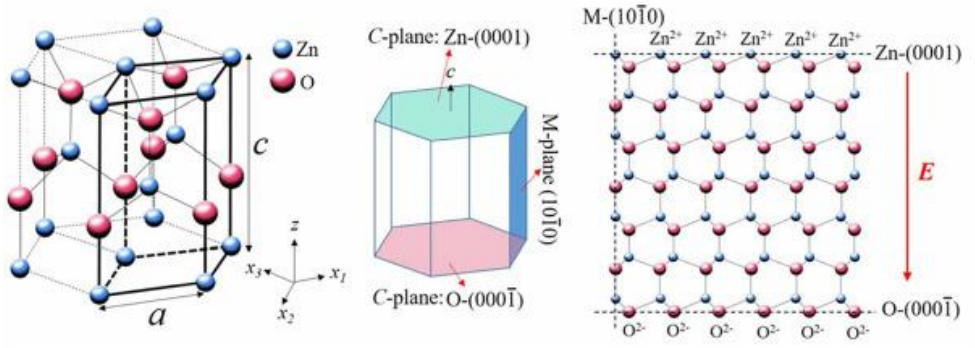


Figure 8 - Structural representation of ZnO wurtzite lattice [36]

2.3.2. UV Shielding and antimicrobial properties

The ability of ZnO to absorb ultraviolet radiation stems from its band structure; photons with energy above the band gap are absorbed, promoting electrons from the valence band to the conduction band [17]. When applied to leather, this mechanism protects collagen fibres against UV-induced photodegradation, which is responsible for the fading and progressive weakening of the material under conditions of sun exposure [1,18] .This property represents significant added value for footwear and leather goods applications subject to prolonged outdoor exposure.

The antimicrobial properties of ZnO derive from multiple complementary mechanisms: the controlled release of Zn^{2+} ions in an aqueous medium, the generation of reactive oxygen species (ROS) via photocatalysis under UV irradiation, and the direct contact of the nanoparticles with the cell membranes of microorganisms, compromising their structural integrity [37].The demonstrated inhibitory effect against bacteria such as *Staphylococcus aureus* and *Escherichia coli* is particularly relevant in the context of leather, a protein-based substrate which, under humid conditions, provides a favourable

environment for microbial growth [1].

2.4. Low-surface-energy agents: fatty acids and natural waxes

Naturally occurring fatty acids and natural waxes are one of the most extensively studied classes of bio-based compounds as a sustainable alternative to fluorinated agents in surface finishing [14]. Their ability to reduce the surface free energy of solid substrates, combined with their abundance, biodegradability and low toxicity, makes them candidates that are naturally aligned with the principles of green chemistry and the *Safe-and-Sustainable-by-Design* (SSbD) paradigm [14,16,17,38].

2.4.1. Chemical structure and amphiphilic nature

Fatty acids are amphiphilic molecules consisting of two functionally distinct regions: a polar head, corresponding to the carboxyl group (–COOH), which has a high affinity for polar surfaces and aqueous media, and a non-polar aliphatic tail, consisting of a hydrocarbon chain of variable length, which is responsible for the molecule's hydrophobic nature [14] (Figure 9). This structural duality determines the adsorption behaviour of fatty acids at solid-liquid interfaces: the polar head anchors to the surface, whilst the aliphatic tail orients itself outwards, exposing low-energy methyl groups (–CH_3) that impart hydrophobicity to the substrate [14,17] .

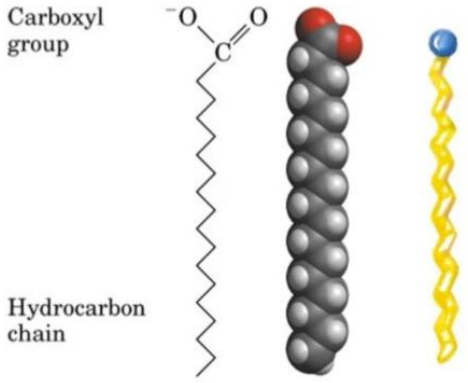


Figure 9 - Chemical structure and molecular models of a fatty acid, illustrating the hydrophilic carboxyl head and the hydrophobic hydrocarbon tail [39]

The degree of unsaturation of the aliphatic chain significantly influences molecular packing and the properties of the coating formed. Myristic acid (C14:0), a saturated fatty acid, forms fully extended chains that allow for dense and ordered packing, maximising van der Waals interactions between adjacent chains and producing coatings with greater rigidity and moisture barrier properties [14,17] (Figure 10). This packing density is a key determinant of hydrophobic performance: longer, saturated chains establish more extensive van der Waals interactions with neighbouring molecules, favouring a more compact, ordered layer and, consequently, a more effective low-surface-energy barrier [14,40].



Figure 10 - Myristic acid, adapted from[44]

Natural waxes, such as carnauba wax, share a closely related chemistry: rather than existing as free fatty acids, they are predominantly composed of esters formed between long-chain fatty acids and long-chain fatty alcohols [38,41,42], alongside smaller amounts of free fatty acids, alcohols and hydrocarbons. Despite lacking a free carboxylic acid head group, these esters retain the same fundamental amphiphilic logic: a more polar ester linkage, capable of interacting with hydroxylated or reactive surfaces, and long, non-polar aliphatic chains that dominate the molecule's overall behaviour and confer its characteristic hydrophobicity [14,38,41] . This structural similarity underlies the shared potential of fatty acids and natural waxes as low-surface-energy coating agents.

2.5. Recent advances in fabrics bio-based functionalization

Driven by the transition towards a circular economy and the Safe-and-Sustainable-by-Design (SSbD) paradigm, the leather industry is undergoing a significant shift to replace hazardous chemicals — particularly PFAS-based finishing agents — with bio-based alternatives [16]. Recent research has demonstrated that naturally occurring compounds can be effectively integrated into both the tanning and finishing stages, yielding high-performance leathers with a significantly reduced environmental footprint [14,20].

For surface finishing, the replacement of fluorinated compounds has driven the exploration of natural materials with intrinsically low surface energy, such as natural waxes and fatty acids [14,24]. Natural polymers like zein, a highly hydrophobic protein extracted from corn, have been employed to construct nanoscale rough topographies via self-assembly. When combined with beeswax, these systems create highly durable, superhydrophobic, and self-cleaning coatings without the use of toxic solvents [14,24]. Polysaccharides such as chitosan and modified starches are also extensively studied as green binders that not only enhance surface roughness but also impart intrinsic antimicrobial properties to the substrate [14].

Interestingly, the application of biological catalysts such as enzymes is transforming surface modification operations in leather processing. Lipases have been investigated as green agents to selectively modify surface topography, creating the hierarchical roughness necessary for subsequent hydrophobic treatments while avoiding harsh chemical degradation [14]. Similarly, their use in degreasing processes enables the effective breakdown of natural animal fats without synthetic surfactants, significantly reducing the chemical oxygen demand of industrial effluents [43].

Furthermore, while strictly bio-based coatings offer excellent environmental profiles, they often suffer from limited durability, exhibiting poor mechanical robustness, low thermal stability, and susceptibility to fast leaching when applied in isolation [14]. The development of an organic-inorganic hybrid system — combining the dense, low-surface-

energy organic layer of of fatty acids or natural waxes with the rigid, inorganic architecture of ZnO nanoparticles — effectively overcomes these limitations. The inorganic counterpart not only establishes the necessary hierarchical roughness but also provides robust anchoring sites that significantly enhance the mechanical resistance and overall durability of the coating [1,14]. For instance, Sani et al. demonstrated that cotton fabrics functionalised with ZnO nanoparticles and a mixture of stearic and myristic acids achieved a water contact angle of 164º and a sliding an angle of only 5º [17]. This hybrid coating remained stable, retaining a contact angle of approximately of 160º after five cycles of immersion in boiling water [17]. Similarly, Arfaoui et al. grew ZnO nanorods on jute fibres via hydrothermal synthesis, followed by stearic acid modification [18]. Stearic acid alone increased the contact angle to only 115º, whereas adding the ZnO nanorod underlayer raised it to 148º, confirming the essential role of the inorganic component in stabilising the Cassie-Baxter regime [18]. Beyond fatty acids, similar hybrid systems have been built using natural waxes. Bashari et al. deposited bilayers of carnauba wax nanoparticles and chitosan onto cotton and nylon fabrics, achieving contact angles up to 135º alongside durable antibacterial activity [44].

Despite these promising synergistic effects, the specific combination of ZnO nanoparticles with bio-based fatty acids and natural waxes applied to leather finishing remains underexplored. In particular, the systematic optimisation of deposition parameters and the quantitative evaluation of durability under real-use conditions have yet to be fully addressed in the literature. The present work aims to contribute to filling this gap, providing a comprehensive characterisation of this hybrid ZnO combined with myristic acid and carnauba wax coating and its performance as a highly durable, sustainable and fluorine-free finishing system for leather.

3. Materials and Methods

3.1. Leather substrate (as-received)

The leather substrate used throughout this work was supplied by Dias Ruivo, a Portuguese tannery (Avintes, Vila Nova de Gaia) specialised in the tanning and finishing of bovine and ovine hides for the fashion, footwear and leather goods industries [45]. The material consisted of bovine (cow) leather, chrome-tanned and dyed in a dry pink shade, in the wet blue state. To minimise batch variability and provide a suitable and consistent control base for laboratory experimentation, the leather was processed following a simplified and lighter finishing treatment compared to standard commercial production. This reduced processing was intended to limit the number of chemical additives and finishing layers already present on the surface, thereby providing a more homogeneous and reproducible substrate for the subsequent functionalisation treatments described in section 3.4.

3.2. Leather cleaning methodologies

Prior to functionalisation, several preliminary cleaning trials were conducted to define a protocol capable of effectively removing surface contaminants (e.g., residual finishing

agents, dust and superficial greases) while preserving the structural integrity and surface characteristics of the leather. Based on these preliminary tests, two distinct cleaning approaches were selected and applied to the leather samples used throughout the remainder of this work.

Approach 1 – Simple cleaning protocol

As shown in Figure 11, the leather samples were immersed in isopropanol for 10 minutes, then gently rubbed with a microfibre cloth in circular motions to remove loose surface residues. The samples were then briefly rinsed in water and dried in an oven at 70 °C for 20-30 minutes.

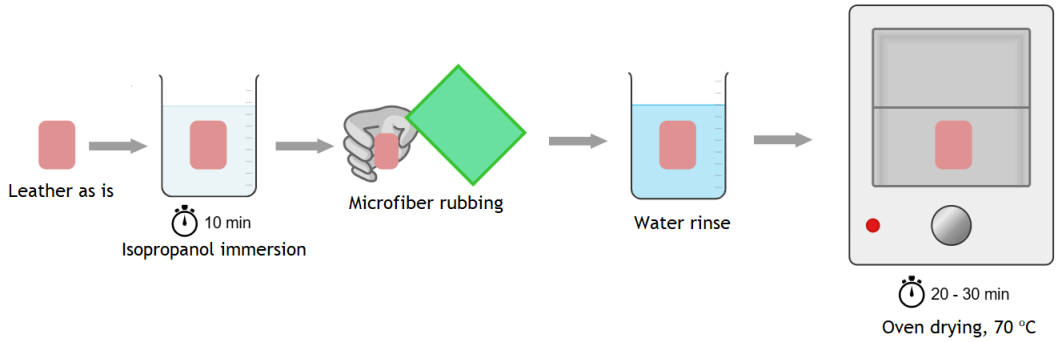


Figure 11 - Schematic representation of Cleaning Approach 1 (simple cleaning protocol)

Approach 2 – Extended cleaning protocol with acetic acid treatment

This protocol followed the same initial steps as Approach 1 (isopropanol immersion, microfibre cloth rubbing). Following the cloth-rubbing step, the samples were immersed in water for 2 minutes, then immersed in an acetic acid solution (0.3 % concentration) for 10 minutes. The samples were subsequently washed in two sequential water rinses and dried in an oven under the same conditions as Approach 1 (70 °C, 20-30 minutes). This is illustrated in Figure 12. Acetic acid is said to help open the collagen fibre structure, thus preparing the surface for a more efficient functionalisation.

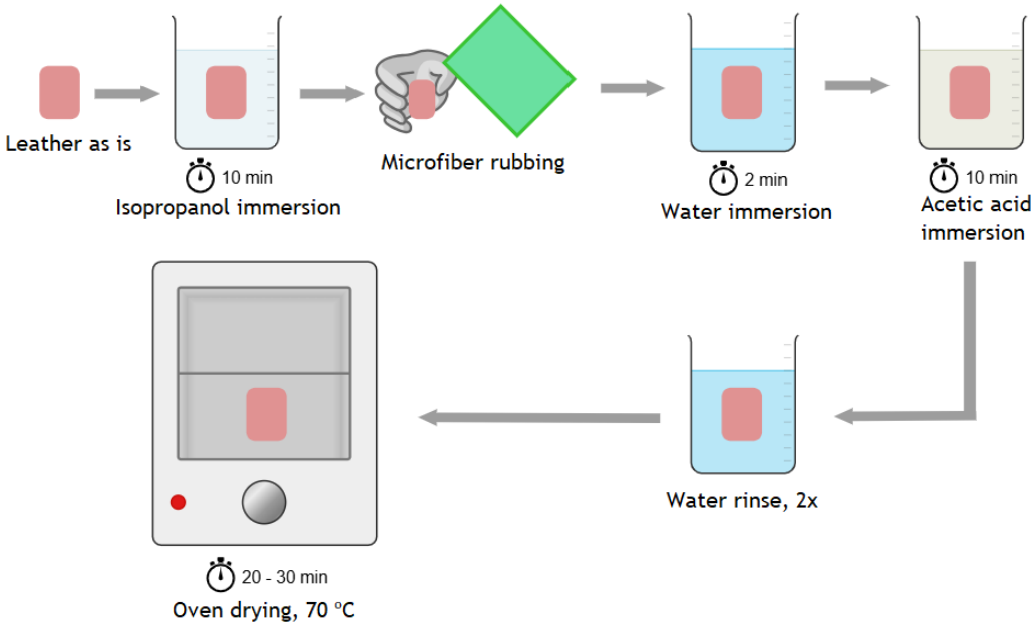


Figure 12 - Schematic representation of Cleaning Approach 2 (extended cleaning protocol with acetic acid treatment)

3.3. Synthesis and characterisation of ZnO nanoparticles

This section describes the synthesis route developed to produce zinc oxide nanoparticles (n-ZnO) used in the surface functionalisation treatments (section 3.4.), as well as their physiochemical characterisation by Dynamic Light Scattering (DLS) (section 3.3.2.).

3.3.1. Synthesis of ZnO nanoparticles

The zinc oxide nanoparticles were synthesised via a wet chemical route in an ethanolic medium. The precursor, zinc acetate dihydrate, was dissolved in a solution of 45 mL of absolute ethanol and 5 mL of ethylene glycol (EG), with a final volume of 50 mL. Precursor solutions were initially prepared at four different zinc acetate concentrations, 2.2%, 1.1%, 0.55%, and 0.22% (w/v), to evaluate the influence of precursor concentration on nanoparticle size and dispersion.

A potassium hydroxide (KOH) solution (0.25 M) was then added slowly dropwise under constant stirring, with the reaction carried out in a water bath at 55 ºC (Figure 13). Under these conditions, the reaction is generally understood to proceed through the initial formation of zinc hydroxide.

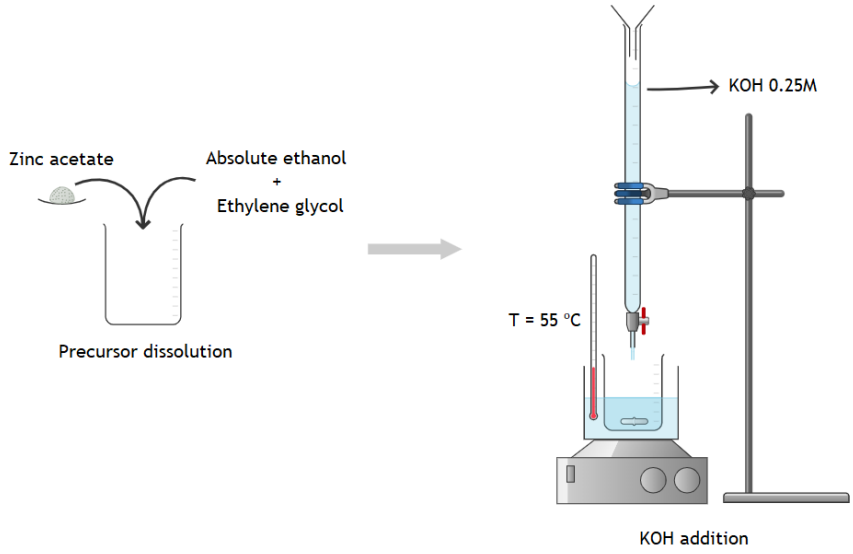


Figure 13 - Schematic representation of the initial steps of ZnO nanoparticle synthesis: precursor dissolution (zinc acetate in absolute ethanol and ethylene glycol) and dropwise addition of 0.25 M KOH under stirring, in a water bath at 55 °C.

Following the reaction, the resulting suspension was centrifuged (Hermle Z 200 A, Hermle Labortechnik, Germany) and the nanoparticles were washed by discarding the supernatant and redispersing the particles in fresh ethanol, with a final volume of 30 mL. This washing step was repeated twice to ensure adequate removal of reaction by-products. The purified nanoparticles were stored under refrigeration until further use. All reagents used were of reagent grade.

For the initial screening of precursor concentrations, all four conditions (Table 1) — ZnO-2.2, ZnO-1.1-i, ZnO-0.55 and ZnO-0.22 — were synthesised using KOH volumes that were substoichiometric relative to the intended reaction, in order to keep a low concentration of n-ZnO. For 1.1% the KOH volume was recalculated according to the correct stoichiometry, giving rise to a second condition at this same concentration: ZnO-1.1-c, as

distinct from the original, substoichiometric ZnO-1.1-i. As such, the leather functionalisation trials described in Section 3.4. were carried out using nanoparticles synthesised at two conditions: 0.22% zinc acetate (with substoichiometric KOH) and 1.1% zinc acetate (with the corrected, stoichiometric KOH volume).

Table 1 - Zinc acetate precursor concentrations used in the synthesis of ZnO nanoparticles

Code	Zinc acetate mass (g)	Concentration (% w/v)
ZnO-2.2	1.1	2.20%
ZnO-1.1-i	0.55	1.10%
ZnO-0.55	0.27	0.55%
ZnO-0.22	0.108	0.22%
ZnO-1.1-c	0.55	1.10%

3.3.2. Dynamic Light Scattering (DLS)

The particle size distribution of the n-ZnO suspensions was analysed by Dynamic Light Scattering (DLS) using a Zetasizer Advance (Malvern Panalytical Instrument, UK). This analysis was performed both on the synthesised n-ZnO suspensions, at the precursor concentrations described in Table 1, and on the commercial n-ZnO (Sigma-Aldrich, ref.544906) originally intended for use in this study, to assess its actual particle size and dispersion behaviour in suspension. Prior to measurement, suspensions were diluted 1:100 in isopropanol. Measurements were performed in manual mode, with 11 runs per sample.

3.4. Surface functionalisation

Three distinct methodologies were developed and tested for the surface functionalisation of leather with n-ZnO and the hydrophobic agents selected for this study.

3.4.1. Methodology 1 - Sequential immersion with pre-synthesised nanoparticles

In this approach, leather samples previously cleaned, according to both cleaning protocols described in section 3.2., were functionalised through a sequential immersion process.

Samples were first subjected to three consecutive immersion cycles in the n-ZnO dispersion, each cycle consisting of 10 minutes of immersion under gentle agitation followed by 20 minutes of oven drying at 75 ºC. Upon completion of these three cycles, the same immersion-drying sequence (10 minutes of immersion, 20 minutes of drying, repeated three times) was applied using a 1% myristic acid (MA) solution in isopropanol. This way, the final coating consists of 3 layers of n-ZnO and 3 layers of MA (Figure 14).

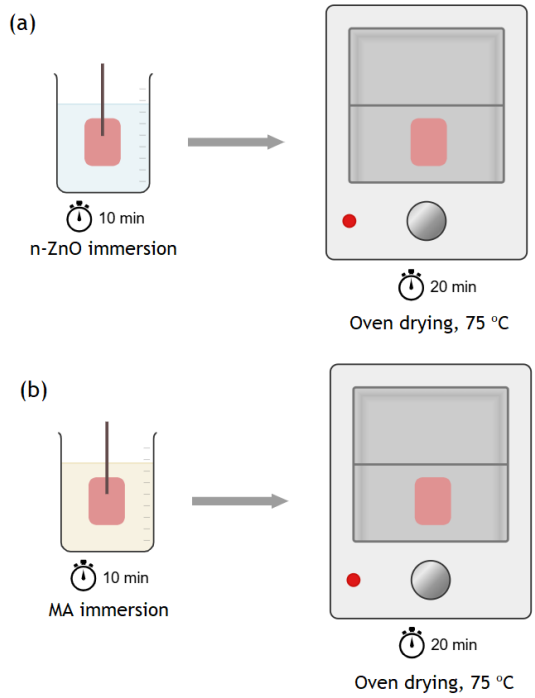


Figure 14 - Schematic representation of the sequential functionalization process for the leather samples. (a) One cycle of n-ZnO dispersion immersion; (b) One cycle of MA solution immersion. The complete coating is formed by performing three consecutive cycles of step (a) followed by three consecutive cycles of step (b).

Within this methodology, three variables were tested: (i) the leather cleaning protocol used (section 3.2.); (ii) the zinc acetate concentration used in n-ZnO synthesis (ZnO-0.22 and ZnO-1.1-c, section 3.3.1.); (iii) the nanoparticle dispersion medium, comparing the as-prepared ethanolic dispersion against a re-centrifuged and redispersed version in a 50% ethanol/50% water mixture (Table 2).

Table 2 - Variables and corresponding levels tested within Methodology 1(M1)

Variable	Levels tested
Cleaning protocol	Approach 1 (A1) / Approach 2 (A2)
Zinc acetate concentration	0.22% / 1.10%
Dispersion medium	100% ethanol (100Et) / 50% ethanol-50% water (50Et)

Prior to use, dispersions prepared with the higher-concentration nanoparticles (ZnO-1.1-c) were additionally sonicated for 2 minutes (30 s on/off cycles, amplitude 60-70%) in an ice bath, using a Qsonica Q55 sonicator equipped with a CL-188 converter, in order to counteract the faster sedimentation rate observed for this condition compared to the lower-concentration dispersions (ZnO-0.22). For the condition of 50% ethanol/water as the dispersion medium, the pH was specifically monitored and, when necessary, adjusted through the addition of acetic acid, to be at pH 7-7,5. The aim was to keep the pH below the isoelectric point of ZnO in order to favour electrostatic attraction between the nanoparticles and the leather surface. This step was not applicable to the as-prepared ethanolic dispersion, given the non-aqueous nature of the medium.

3.4.2. Methodology 2 – *In-situ* synthesis with *in-situ* precipitation

In this methodology, nanoparticle synthesis took place directly on the leather surface.

The tannic acid (TA) solution was prepared by dissolving 0.5 g of TA in 100 mL of 70% ethanol, and the zinc salt solution was similarly prepared in 100 mL of 70% ethanol; in both cases, the pH was adjusted to 5–6 using 0.1 M NaOH (Figure 15a). Leather samples were then subjected to two full immersion cycles, each consisting of 10 minutes of immersion in the TA solution, followed by 1 minute of rinsing in distilled water, then 10 minutes of immersion in the zinc salt solution, followed again by 1 minute of rinsing in distilled water (Figure 15b). This sequence (TA → water → zinc salt → water) was repeated twice in total. In sample M2-6, ethanol was entirely replaced by isopropanol in both solutions.

Samples were subsequently immersed in a final bath prepared using the same solvent system, to which a small additional amount of zinc salt was added in some conditions (Table 3). This bath was maintained at a controlled temperature (50 °C, or room temperature in one condition) while a base (monoethanolamine, MEA, at 0.2 %(w/v) or ammonia at 1%, depending on the condition) was added dropwise, gradually raising the pH and inducing localised precipitation of zinc oxide onto the leather surface. Base addition was stopped upon reaching a pH of approximately 8.5, after which the reaction was allowed to proceed for a further 30 minutes (Figure 15c). Samples were then oven-dried at 70 °C for 20–30 minutes, until fully dried (Figure 15d). Finally, samples were immersed in a 1% myristic acid (MA) solution in isopropanol, following the same three-cycle immersion–drying sequence described for Methodology 1, section 3.4.1. (Figure 15e).

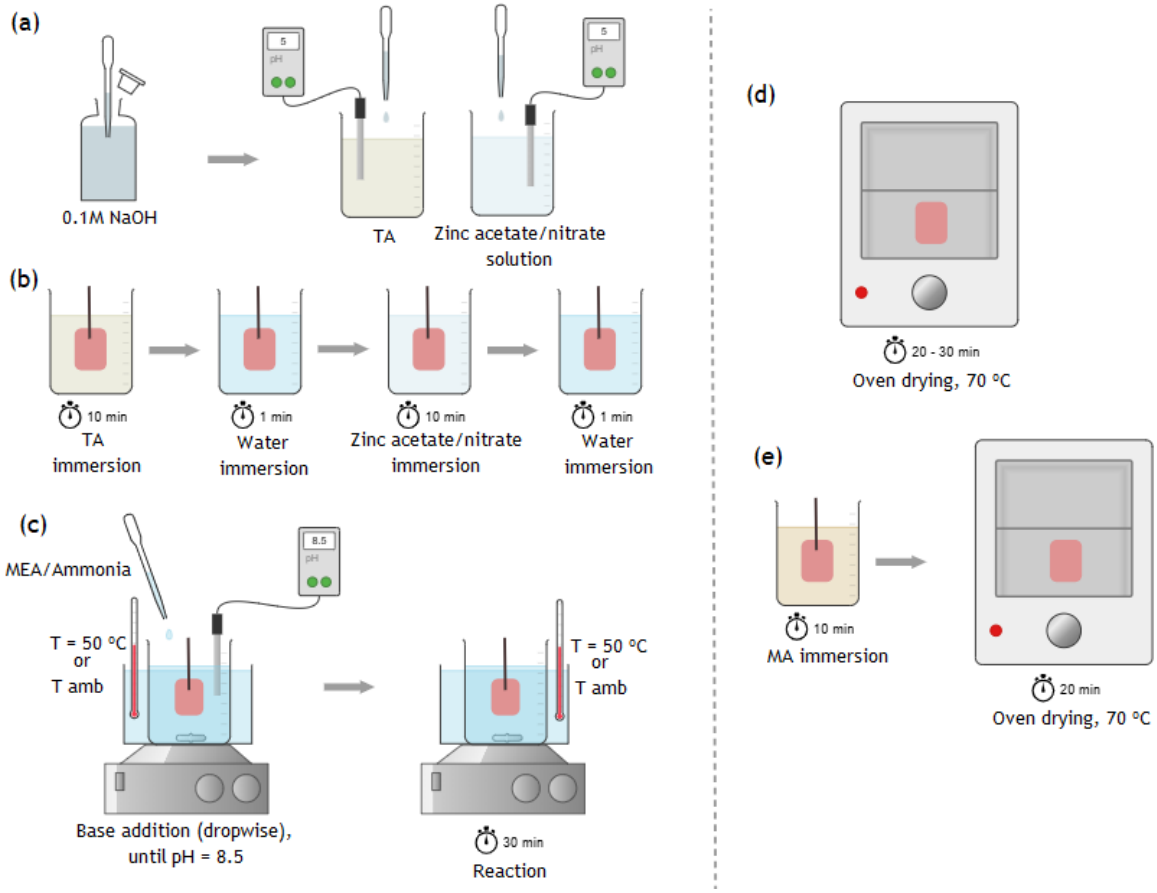


Figure 15 - Schematic representation of the *in-situ* synthesis functionalisation process for the leather samples (M2). (a) preparation of the tannic acid (TA) and zinc salt (acetate or nitrate) solutions, with the pH adjusted to 5–6 using 0.1 M NaOH; (b) immersion sequence, consisting of TA immersion, water rinsing, zinc salt immersion, and a further

water rinse, repeated twice in total; (c) final bath, in which a base (MEA or ammonia) was added dropwise, at a controlled temperature (50 °C or room temperature), until reaching a pH of approximately 8.5, followed by a 30-minute reaction period; (d) oven drying at 70 °C; (e) immersion in a 1% MA solution in isopropanol (10 min immersion, 20 min drying). Steps (e) was repeated three times in total, as described for Methodology 1 (Section 3.4.1).

Given the exploratory nature of this methodology, the tested conditions were not organised as a full factorial design, but rather as a series of targeted pairwise comparisons, summarised in Table 3. In Trial 1 the synthesis was done using zinc acetate as the zinc salt and monoethanolamine (MEA) as the base to trigger zinc precipitation. Following this experiment, zinc nitrate was adopted as the zinc salt and ammonia as the base for the remaining conditions (Trials 2 to 6), due to practical difficulties encountered in fully dissolving zinc acetate and achieving the target pH with MEA. Trials 3 and 4 allowed the effect of heating during the final bath to be assessed, under otherwise identical conditions (2% (w/v) zinc nitrate, ethanol). Trials 5 and 6 enabled a comparison between ethanol and isopropanol as the reaction solvent, at a lower zinc nitrate concentration (1% (w/v)). Trials 2 and 3 enabled evaluations of the effect of adding a supplementary zinc salt during the final precipitation bath.

Table 3 - Conditions tested within Methodology 2 (M2)

Trial	Zinc salt	Salt conc. (%w/v)	Solvent	Final bath conc. (%w/v)	Heating	Base
1	Zinc acetate	1.0	Ethanol	0.022	Yes	MEA
2	Zinc nitrate	2.0		0.090		Ammonia
3		2.0		None		
4		2.0			No	
5		1.0			Yes	
6		1.0	Isopropanol			

3.4.3. Methodology 3 - Bilayer system with ZnO nanoparticles and carnauba wax

In this methodology, n-ZnO synthesised at the higher precursor concentration (1.10%) was re-centrifuged and redispersed in a 50:50 ethanol/water mixture. Prior to use, the dispersion was sonicated for 2 minutes (30 s on/off cycles, amplitude 60–70%) in an ice bath and the pH was checked and, where necessary, adjusted with HCl or NaOH to within the range of 7–7.5.

The carnauba wax dispersion was prepared by first heating water to 90 ºC in a water bath, after which the wax was added at a concentration of 3% (w/v) to achieve wax melting. The dispersion was then processed using an IKA T25 digital Ultra-Turrax homogeniser (IKA, Germany) at 16 000 rpm for 2 minutes, followed by rapid cooling in a water bath, resulting in a fine particulate wax dispersion. The final dispersion presented a pH of approximately 7.

Leather samples were first immersed in a 0.5% tannic acid (TA) solution (pH 4.5–5) for 15 minutes, then oven-dried at 70 °C until dry. The TA immersion step was performed once, prior to the bilayer deposition. Each bilayer was formed by immersing the samples in the n-ZnO dispersion for 10 minutes, rinsing in distilled water, then immersing them in the carnauba wax dispersion for 10 minutes, followed by a final rinse in distilled water. Samples were then oven-dried at 65 ºC overnight. This bilayer sequence (n-ZnO → water

→ wax → water → drying) could be repeated multiple times to build up the coating (Figure 16).

Preliminary trials were conducted with one and two bilayers, in which additional wax layers or bilayers were applied on top of an already-dried base coating. As these reinforcement steps did not follow a consistent or directly comparable pattern between samples, a more systematic approach was subsequently adopted, applying a fixed number of bilayers consecutively, without intermediate reinforcement steps. Based on this revised approach, samples with 1, 3 and 5 bilayers were prepared.

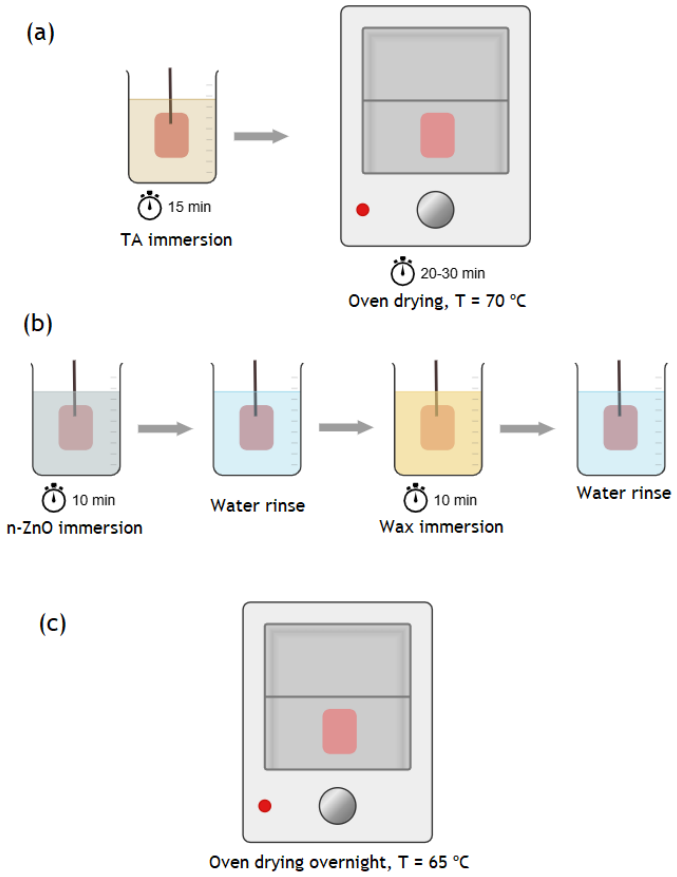


Figure 16 - Schematic representation of the bilayer functionalisation process for the leather samples (M3). (a) Immersion in the tannic acid (TA) solution for 15 minutes, followed by oven drying at 70 °C for 20–30 minutes; (b) One bilayer cycle, consisting of immersion in the ZnO nanoparticle dispersion for 10 minutes, a water rinse, immersion in the carnauba wax dispersion for 10 minutes, and a further water rinse; (c) oven drying overnight at 65 °C. Step (b) was repeated according to the number of bilayers tested (1, 3 or 5).)

3.4.4. Sample nomenclature and experimental design

This section summarises the complete set of conditions tested across the three functionalisation methodologies described above, along with the corresponding sample codes used throughout this work. Sample codes follow the format [Methodology]-[variable levels], where only the variables that were varied within each methodology are included in the code, while conditions common to all samples within a given methodology are stated before the respective table.

- M1 — Sequential immersion with pre-synthesised nanoparticles

Within this methodology, three variables were investigated: the leather cleaning protocol (Approach 1 or Approach 2), the ZnO precursor concentration (ZnO-0.22 or ZnO-1.1-c),

and the nanoparticle dispersion medium (100% ethanol or 50% ethanol/water). Table 4 presents the eight resulting combinations and their corresponding sample codes.

Table 4 - Sample codes and corresponding conditions for Methodology 1

Code	Cleaning protocol	ZnO conc. (%w/v)	Dispersion medium
M1-A1-0.22-100Et	Approach 1	0.22	100% ethanol
M1-A1-0.22-50Et			50% ethanol/water
M1-A1-1.1c-100Et		1.1	100% ethanol
M1-A1-1.1c-50Et			50% ethanol/water
M1-A2-0.22-100Et	Approach 2	0.22	100% ethanol
M1-A2-0.22-50Et			50% ethanol/water
M1-A2-1.1c-100Et		1.1	100% ethanol
M1-A2-1.1c-50Et			50% ethanol/water

- M2 — *In-situ* synthesis by localised precipitation

All samples prepared under this methodology used leather cleaned according to Approach 1. Six conditions were tested, corresponding to the trials described in Section 3.4.2, and were assigned the codes M2-1 to M2-6, in the same order in which they were introduced. Table 5 details the specific parameters distinguishing each of these conditions.

Table 5 - Sample codes and corresponding conditions for Methodology 2

Code	Description
M2-1	Zinc acetate (1.0 %), ethanol, 50 °C, MEA as base, 0.022% acetate final bath
M2-2	Zinc nitrate (2.0 %), ethanol, 50 °C, ammonia as base, 0.090% nitrate final bath
M2-3	Zinc nitrate (2.0 %), ethanol, 50 °C, ammonia as base, no addition to final bath
M2-4	Zinc nitrate (2.0 %), ethanol, room temperature, ammonia as base, no addition to final bath
M2-5	Zinc nitrate (1.0 %), ethanol, 50 °C, ammonia as base, no addition to final bath
M2-6	Zinc nitrate (1.0 %), isopropanol, 50 °C, ammonia as base, no addition to final bath

- M3 — Bilayer system with ZnO nanoparticles and carnauba wax

All samples prepared under this methodology used leather cleaned according to Approach 1, nanoparticles synthesised at the ZnO-1.1-c concentration, and a dispersion medium of 50% ethanol/water. Table 6 presents the sample codes corresponding to the preliminary trials and to the standardised protocol described in Section 3.4.3.

Table 6 - Sample codes and corresponding conditions for Methodology 3

Code	Description
M3-(1B+3W)	Preliminary trial: 1 bilayer, oven-dried, followed by 3 additional consecutive wax (W) layers
M3-(2B+3B)	Preliminary trial: 2 bilayers, oven-dried, followed by 3 additional bilayers (B), with intermediate drying
M3-1B	Standardised protocol: 1 bilayer
M3-3B	Standardised protocol: 3 bilayers
M3-5B	Standardised protocol: 5 bilayers

3.5. Characterization of functionalised leather

The functionalised leather samples, obtained through the different cleaning methodologies (Section 3.2.), nanoparticles synthesis conditions (Section 3.3.) and

functionalisation approaches (Section 3.4.), were characterised using a set of complementary techniques to assess their surface morphology, chemical composition, wettability, mechanical durability and stain resistance. Table 7 summarises the techniques used, their main purpose and the samples to which each was applied.

Table 7 - Overview of the characterisation techniques used to evaluate the functionalised leather samples.

Technique	Purpose	Samples analysed
SEM/EDS	Surface morphology and elemental distribution (Zn presence)	All coating conditions
FTIR	Surface chemical composition	
WCA	Surface wettability and hydrophobicity	
Stain resistance	Resistance to common staining agents	Best coating conditions
Abrasion resistance	Mechanical durability of the coating	

3.5.1. Scanning Electron Microscopy and Energy-Dispersive X-ray Spectroscopy (SEM/EDS)

The surface morphology of the leather samples, coated and uncoated, was examined using a high-resolution (Schottky) Environmental Scanning Electron Microscope with X-ray microanalysis and electron backscattered diffraction capabilities (FEI Quanta 40O FEG ESEM / EDAX Genesis X4M, FEI Company, USA). Prior to analysis, all samples were coated with a thin Au/Pd film by sputtering, using an SPI Module Sputter Coater, for 100 seconds with a 15 mA current. Imaging was performed using both secondary electron and backscattered electron modes, at 100x magnification for panoramic overview images and 1000x magnification for detailed surface analysis. In a few specific cases, magnifications of up to 5000x were used to examine features of interest in greater detail.

Energy-dispersive X-ray spectroscopy (EDS) was performed at an accelerating voltage of 15 kV and was primarily used to confirm the presence and distribution of zinc (Zn) on the leather surface, providing an indication of nanoparticle deposition and coverage. In addition to spectral acquisition, semi-quantitative elemental analysis was performed to obtain a general overview of the elemental composition of the coated samples. However, given the organic nature of fatty acids and carnauba wax used in functionalisation treatments (sector 3.4.), their direct detection and quantification by this technique is inherently limited, as EDS is primarily suited to the identification of inorganic and elemental components.

3.5.2. Fourier-Transform Infrared Spectroscopy (FTIR)

Surface chemical changes resulting from the applied coatings were evaluated by Fourier-transform infrared spectroscopy (FTIR) in attenuated total reflectance mode (FTIR-ATR), using a JASCO FT/IR-4100 spectrometer (JASCO Europe, Italy) fitted with an ATR accessory. Spectra were collected over the 4000-400 cm^{-1} range and data acquisition was carried out through Spectra Manager software (v1.2). Post-acquisition spectral processing and analysis were performed in Spectragryph (v1.2.16.1).

3.5.3. Water Contact Angle (WCA)

The wettability of leather surfaces was evaluated through static contact angle

measurements, performed by the sessile drop technique under ambient laboratory conditions. Measurements were carried out on a Theta Life tensiometer (Attention®, Biolin Scientific, Gothenburg, Sweden), controlled through OneAttension® software (version 4.0.2). A 5 µL droplet of ultrapure water was placed on each sample surface, with the contact angle recorded both at the moment of deposition and after a 5-minute interval, in order to capture any change in wetting behaviour over time. For each sample, five independent measurements were taken across different surface locations (one in the centre and one in each corner), and results are expressed as the mean value with the corresponding standard error.

3.5.4. Abrasion resistance

The mechanical durability of the coatings was assessed through cyclic abrasion testing, carried out using a custom-built crockmeter apparatus. Coated leather specimens measuring 3 cm x 4 cm were affixed, using double-sided adhesive tape, to the base of a steel cube. This cube was then positioned on a polishing cloth with the coated face in contact with the cloth and subjected to a repeated back-and-forth movement over a 20 cm stroke length, at a rate of 20 cycles per minute. A constant pressure of 15 kPa was applied to the surface throughout testing.

Since the standard sample size used in the remaining characterisation test was smaller than that required for the abrasion setup, non-abraded specimens with the same larger dimensions (3 cm x 4 cm) were additionally prepared as controls. This ensured reproducibility and a consistent applied pressure across the tested surface area. Samples were subjected to either 20 or 50 cycles abrasion cycles and this test was applied to the two coating conditions that exhibited the highest WCA values.

3.5.5. Stain resistance

The resistance of the coatings to common staining agents was evaluated using two substances with distinct chemical and colouring properties: capsule-brewed coffee and green tea (La Route des Comptoirs, ‘Cueillette Gourmande’ range). The tea was prepared according to the manufacturer’s instructions, with the infusion left to steep in boiled water for 3 minutes, using a volume of 200 mL to replicate the typical concentration of a standard cup of tea.

A single drop of each staining substance was deposited onto the test specimens, which were left undisturbed for 10 minutes before the droplet was removed, allowing the assessment of any residual staining after drying. Photographic records were taken at three stages: immediately after droplet deposition, after the 10-minute resting period and following droplet removal. As with the abrasion testing (section 3.5.4.), this evaluation was carried out on the two coating conditions exhibiting the highest WCA values, as well as on the untreated (as-received) control leather.

3.6. Statistical analysis

Statistical analysis was performed on water contact angle (WCA) data throughout this work, with all comparisons carried out at t = 5 min, given the metastable nature of the Cassie-Baxter wetting regime discussed in Section 2.2.2: initial WCA (t = 0 min) does not

necessarily reflect coating durability, whereas the value at t = 5 min provides a more stable and comparable measure of hydrophobic performance across conditions. All tests used n = 5 replicate measurements per condition, with a significance threshold of $\alpha = 0.05$.

For Methodology 1, the eight functionalised conditions were analysed using a full 2×2×2 three-way factorial ANOVA, with ZnO concentration, dispersion medium, and cleaning protocol as the three process variables. Given the marked heterogeneity in standard deviation across conditions, the robustness of these results was additionally verified using a Welch/Satterthwaite approach, which does not assume equal variance across groups. A Tukey HSD multiple-comparison test was subsequently used to determine which conditions were statistically distinguishable from one another, to identify the best-performing conditions for further testing.

For Methodology 2, the experimental design did not correspond to an orthogonal factorial structure, as each pair of conditions isolated a single process variable at a time. The seven samples (control plus six treated conditions) were therefore compared using a Welch's one-way ANOVA, which does not assume equal variance across groups, followed by Games-Howell post-hoc pairwise comparisons.

For Methodology 3, given the substantial differences in standard deviation between conditions, the six samples (control plus five treated conditions) were similarly compared using a Welch's one-way ANOVA followed by Games-Howell post-hoc pairwise comparisons. For the abrasion resistance testing (Section 4.6.1), a one-way ANOVA was performed separately for each selected condition across the three abrasion cycle counts (0, 20, 50), followed by Tukey HSD pairwise comparisons. The two selected conditions were additionally compared directly to one another at each cycle count using a one-way ANOVA.

4. Results and Discussion

4.1. Nanoparticle synthesis and characterisation

4.1.1. Particle size distribution (DLS)

Table 8 presents the Z-average particle size and polydispersity index (PDI) obtained by DLS for the commercial n-ZnO and for the nanoparticles synthesised at the four zinc acetate concentrations tested (section 3.3.1.).

Table 8 – Z-average particle size and PDI of commercial and synthesised ZnO nanoparticles, as measured by DLS.

Code	Z-average/ nm	PDI
ZnO-Commercial	1385 ± 184	0.80 ± 0.27
ZnO-0.22	458 ± 5	0.34 ± 0.01
ZnO-0.55	468 ± 14	0.22 ± 0.03
ZnO-1.1-i	715 ± 24	0.47 ± 0.09
ZnO-2.2	2737 ± 61	0.56 ± 0.12

Although the commercial n-ZnO is specified by the supplier as having a particle size below 50 nm, the measured Z-average (1385 ± 184 nm) was substantially higher. This was accompanied by the highest PDI recorded across all conditions (0.80 ± 0.27), a value indicative of a highly heterogeneous and polydisperse particle population, well above the

threshold typically considered acceptable for a stable and uniform suspension [46]. Considering these values, it's likely that the commercial nanoparticles were in an aggregated state rather than as individually dispersed particles due to the result of poor colloidal stability. This behaviour is commonly observed in commercial nanoparticle powders, which typically lack a surface stabilising agent [47].

Among the synthesised conditions, particle size did not increase proportionally with zinc acetate concentration. Instead, a marked, non-linear increase was observed between zinc acetate concentration and Z-average particle size. The two lowest precursor concentrations showed similar small Z-average values and corresponding PDI values, which can suggest a relatively consistent and moderately dispersed particle populations. In contrast, a marked increase in particle size was observed between ZnO-1.1-i (715 ± 24 nm) and ZnO-2.2 (2737 ± 61 nm), the latter representing the highest precursor concentration tested. The PDI followed a broadly similar pattern, decreasing from 0.56 at the highest precursor concentration to 0.22 at one of the lowest, indicating that the lower-concentration conditions not only yielded smaller particles on average, but also more uniform batches, with less variability in particle size within each suspension.

This trend can be interpreted considering the classic LaMer model of nucleation and growth [48], which describes how the relative availability of reactive species during a reaction governs the balance between the formation of new nuclei and the growth of existing ones. More specifically, in the precipitation of ZnO from zinc acetate and KOH, the availability of hydroxide ions directly governs the rate of hydrolysis and condensation, through which zinc hydroxide is first formed and subsequently converted to zinc oxide. A higher hydroxide ion availability is therefore expected to accelerate this process, promoting the rapid, widespread nucleation events characteristic of the LaMer model.

Under this model, an abundant base relative to precursor promotes rapid, widespread nucleation, yielding many small nuclei that compete for the limited precursor and grow only modestly. Conversely, a relative base deficit limits nucleation, so the remaining precursor is distributed among fewer sites, allowing each particle to grow more extensively into larger final particles.

In this synthesis, all four precursor concentrations were prepared using a substoichiometric KOH volume. However, the relative base deficit per unit of precursor was proportionally more pronounced at the higher precursor concentrations, as summarised in Table 9. ZnO-2.2 and ZnO-1.1-i were synthesised with approximately 22 mL of KOH per gram of zinc acetate, whereas ZnO-0.55 and ZnO-0.22 used approximately 30 mL per gram, relative to a stoichiometric requirement of approximately 36 mL per gram.

Table 9 - KOH-to-precursor ratio for each synthesis condition, relative to the stoichiometric requirement.

Code	Precursor mass (g)	KOH volume (mL)	KOH : precursor ratio (mL/g)
ZnO-2.2	1.1	24	21.8
ZnO-1.1-i	0.55	12	21.8
ZnO-0.55	0.27	8	29.6
ZnO-0.22	0.108	3.2	29.6
ZnO-1.1-c	0.55	20	36.4 *

* *stoichiometric requirement*

Following the LaMer model, this more pronounced relative base deficit at higher precursor concentrations likely limited the number of nuclei formed, allowing the remaining precursor to promote more extensive particle growth. This is consistent with the substantially larger particle size observed for ZnO-2.2. At lower precursor concentrations, the comparatively smaller relative base deficit likely supported the formation of a greater number of nuclei, distributing the precursor more evenly and resulting in smaller final particle sizes.

4.1.2. Selection of zinc acetate concentration for functionalisation

Based on the DLS results discussed above, ZnO-0.22 was initially selected for the leather functionalisation trials described in Section 3.4, despite presenting a slightly higher PDI than ZnO-0.55. This choice was primarily driven by its smaller Z-average particle size, together with its substantially lower reagent consumption. This latter consideration is particularly relevant when developing a coating system with potential for future industrial adaptation, where reagent efficiency and cost-effectiveness are practical factors alongside performance.

At a later stage of this work, the zinc acetate concentration was increased to 1.10% (ZnO-1.1-c), following observations from SEM/EDS characterisation of the functionalised leather that indicated limited nanoparticle coverage at the lower concentration. It was at this stage that the substoichiometric KOH volume used throughout the initial DLS screening was identified and the synthesis of ZnO-1.1-c was subsequently carried out using the correct, stoichiometric KOH volume originally intended for the reaction. As this correction was introduced after the DLS characterisation stage, the particle size and PDI of the ZnO-1.1-c dispersion were not measured and are therefore not directly comparable to the other conditions reported in Section 4.1.1. Characterising the ZnO-1.1-c dispersion by DLS would allow a more direct comparison with the substoichiometric conditions discussed above, and is suggested as a direction for future work, to complete the particle size characterisation across all conditions used in this study.

4.2. Methodology 1

As described in Section 3.4.1, leather samples were functionalised through a sequential immersion process, involving three cycles of n-ZnO nanoparticle deposition followed by three cycles of immersion in a myristic acid (MA) solution. Figure 17 presents the water

contact angle (WCA) results obtained for all conditions tested under this methodology, compared to the untreated leather (control).

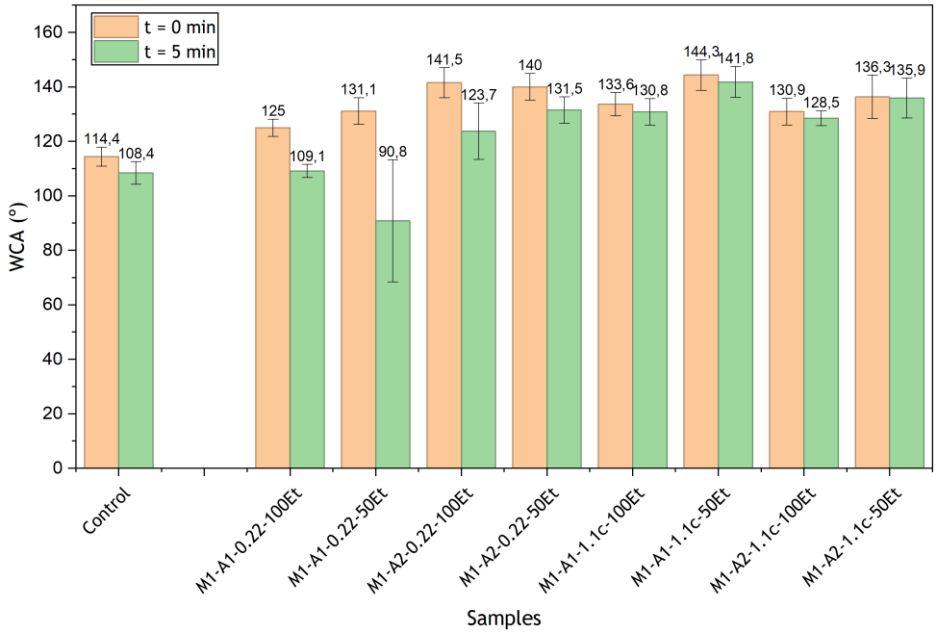


Figure 17 - Water contact angle (WCA) at t=0 min and t=5 min for all samples prepared under Methodology 1, compared to the untreated (control) leather. Error bars represent standard deviation across replicate measurements

The control presented a WCA of approximately 114°, which shows that the substrate already possessed a degree of intrinsic hydrophobicity prior to functionalisation. This can be primarily attributed to both the natural roughness of the leather surface and the presence of waterproof fatliquoring agents and post-tanning operations conventionally applied on the grain side of the leather [20,26]. These hydrophobic agents partially close the leather surface, limiting initial water absorption and resulting in a relatively high baseline contact angle [20,26]. As shown in Figure 17, all functionalised conditions tested within Methodology 1 initially exhibited higher WCA values than the control, confirming the effectiveness of the applied coatings in enhancing surface hydrophobicity beyond the leather's intrinsic behaviour.

The leather surface presents reactive functional groups arising from the collagen structure, including amine, carboxyl, and hydroxyl groups exposed at the fibre surface. The nanoparticle dispersions were maintained at a working pH of approximately 7–7.5, which lies above the isoelectric point of chrome-tanned leather (approximately 6–7) but below that of ZnO (approximately 9). Under these conditions, the leather surface is expected to carry a net negative charge, due to deprotonated carboxylate groups, while the ZnO nanoparticle surface is expected to carry a net positive charge [22,49]. This charge difference is expected to favour electrostatic attraction between the positively charged nanoparticles and the negative collagen fibre surface, promoting nanoparticle deposition and retention during the immersion cycles [49,50] .

Once deposited, the ZnO nanoparticles are expected to introduce nanoscale surface roughness across the leather surface. Their surface, naturally terminated in hydroxyl groups (Zn–OH) due to incomplete coordination of surface Zn^{2+} ions, provides reactive sites for the subsequent binding of myristic acid. As a long-chain saturated fatty acid, MA is expected to react with these surface hydroxyl groups primarily through the carboxylate

head group, via coordination with surface Zn^{2+} ions, leaving the long hydrophobic alkyl chain oriented outward, away from the surface [17,18].

4.2.1. WCA response to process variables: statistical analysis and mechanistic discussion

(I) Statistical analysis

While Figure 17 provides a qualitative overview of the differences between conditions, comparing WCA values and standard deviations by eye alone cannot establish whether these differences are statistically meaningful, particularly given the marked heterogeneity in standard deviation across conditions (ranging from 2.41° to 22.41° at t = 5 min). To address this, the eight functionalised conditions were analysed as a full 2×2×2 factorial design, with ZnO concentration (A), dispersion medium (B) and cleaning protocol (C) as the three process variables, each at two levels, with n = 5 replicate contact-angle measurements per condition. The untreated control was excluded from this analysis, as it does not correspond to any combination of factor levels.

Table 10 summarises which process variables and their interactions significantly affect WCA (significance threshold $p < 0.05$). ZnO concentration and cleaning protocol emerge as the dominant single factors, with three of the four interaction terms also reaching significance.

Table 10 - Three-way factorial ANOVA for WCA at t = 5 min

Effect	Significant?
ZnO concentration (A)	Yes
Dispersion medium (B)	No
Cleaning protocol (C)	Yes
A × B	Yes
A × C	Yes
B × C	No
A × B × C	Yes

ZnO concentration and cleaning protocol were the only two factors with significant main effects, ZnO concentration being by a wide margin the dominant single factor. Dispersion medium showed no significant effect on its own, but became significant in combination with ZnO concentration, through both the A × B and the three-way A × B × C interactions — indicating that its influence on WCA is entirely conditional on the concentration used, rather than acting as a standalone determinant. Corresponding marginal means are shown in Table 11. Table 11 confirms the relative magnitude of each significant main effect: ZnO concentration produces by far the largest shift in mean WCA (+20.5°), followed by cleaning protocol (+11.8°), while the dispersion medium's marginal effect is negligible (+2.0°), consistent with its lack of a significant main effect in Table 10.

Table 11 - Marginal means for each factor level (averaged over the other two factors)

Factor	Level 1	Mean WCA	Level 2	Mean WCA	Difference
ZnO concentration	0.22%	113.8°	1.1%	134.3°	+20.5°
Dispersion medium	100Et	123.0°	50Et	125.0°	+2.0°
Cleaning protocol	A1	118.1°	A2	129.9°	+11.8°

Most notably, ZnO concentration interacts strongly with both cleaning protocol (A × C) and dispersion medium (A × B), meaning that none of these three factors can be interpreted independently of the others. These two interactions are examined in detail in the following two sections, which discuss the influence of the cleaning solution and of the ZnO concentration, respectively.

Given the heterogeneity in standard deviation noted above, the conventional ANOVA's assumption of equal within-group variance is not strictly satisfied by this dataset. Robustness was therefore verified using a Welch/Satterthwaite approach, which does not assume equal variance across groups; all effects identified as significant under the standard ANOVA remained significant under this more conservative test, including the A × B interaction, confirming the results are not an artefact of unequal variance across conditions.

A Tukey HSD multiple-comparison test was performed on the eight functionalised conditions (WCA at t = 5 min, n = 5) to determine whether the top-performing conditions are statistically distinguishable from one another. The results, summarised in Table 12, show that the four highest-performing conditions — M1-A1-1.1c-50Et, M1-A2-1.1c-50Et, M1-A2-0.22-50Et and M1-A1-1.1c-100Et — all fall within the same statistical group (a), differing by no more than 11.0°, well below the Tukey critical difference of 19.9° at α = 0.05.

Table 12 - Tukey HSD grouping of the eight Methodology 1 conditions (WCA at t = 5 min, α = 0.05). Conditions sharing a letter are not significantly different from each other

Condition	Mean WCA ± SD (°)	Tukey group
M1-A1-1.1c-50Et	141.8 ± 5.69	a
M1-A2-1.1c-50Et	135.9 ± 7.30	a
M1-A2-0.22-50Et	131.5 ± 4.80	a
M1-A1-1.1c-100Et	130.8 ± 4.87	a
M1-A2-1.1c-100Et	128.5 ± 2.70	ab
M1-A2-0.22-100Et	123.7 ± 10.38	ab
M1-A1-0.22-100Et	109.1 ± 2.41	bc
M1-A1-0.22-50Et	90.8 ± 22.41	c

The highest mean WCA was obtained for M1-A1-1.1c-50Et, but this condition is not statistically distinguishable from the next five best-performing conditions (group a/ab) and is only significantly higher than M1-A1-0.22-100Et and M1-A1-0.22-50Et. Notably, M1-A2-0.22-50Et achieves a WCA statistically equivalent to the best condition while using five times less zinc acetate precursor. The two clearly worst-performing conditions, both prepared with the lower ZnO concentration and Approach 1 (IPA-only) cleaning, confirm the strong dependence of coating performance on the interaction between these two factors already indicated by the significant A × C term.

(II) Influence of the cleaning solution

The significant A × C interaction identified in the statistical confirms that the effect of the cleaning protocol on WCA is not independent of ZnO concentration. This is illustrated in Table 13, which shows that Approach 2 (IPA/AA) increases WCA substantially relative to Approach 1 (IPA) at low ZnO concentration, whereas at high ZnO concentration the two

protocols perform similarly, with Approach 2 offering no improvement or even a slight decrease.

Table 13 - Effect of cleaning protocol (IPA/AA − IPA) on WCA at t = 5 min, by ZnO concentration and dispersion medium

ZnO concentration	Dispersion medium	IPA	IPA/AA	IPA/AA - IPA
0.22%	100Et	109.1°	123.7°	+14.6°
	50Et	90.8°	131.5°	+40.7°
1.1%	100Et	130.8°	128.5°	-2.3°
	50Et	141.8°	135.9°	-5.9°

The additional acetic acid immersion in Approach 2 is expected to lower the leather surface pH, promoting protonation of exposed collagen carboxylate groups ($-COO^- \rightarrow -COOH$) [50,51] and neutralising residual alkalinity from previous wet-processing steps [21,52,53].

However, the subsequent rinsing step likely attenuates this pH effect, while some carboxylate groups may remain available for Zn^{2+} complexation and interactions with ZnO at the collagen surface. Because surface deprotonation determines the charge available for electrostatic attraction with positively charged ZnO nanoparticles, acid treatment may either favour or hinder deposition depending on the resulting surface charge [20,54,55]. As modelled by Ballantyne & Davis (2019), protonation of collagen carboxylate and amine groups varies non-linearly with pH, so relatively small pH changes can modify leather surface charge and ZnO binding capacity. This may explain the statistically significant dependence of the cleaning protocol on ZnO concentration: at low concentration, Approach 2 may improve nanoparticle deposition by modifying the availability of anchoring sites, whereas at high concentration this effect becomes negligible, possibly because surface coverage is already approaching saturation.

(III) Influence of the ZnO concentration

Building on the dominant main effect of ZnO concentration identified in Table 10, this section examines its interaction with dispersion medium (A × B) and the underlying stability differences between the two concentrations. Table 14 shows that the increase in WCA associated with raising ZnO concentration from 0.22% to 1.10% is roughly twice as large when the dispersion medium is 50% ethanol/water as when it is 100% ethanol.

Table 14 - Effect of ZnO concentration (1.10% − 0.22%) on WCA at t = 5 min, by dispersion medium (averaged over cleaning protocol)

Dispersion medium	WCA at 0.22%	WCA at 1.10%	Effect of increasing concentration
100Et	116.4°	129.7°	+13.3°
50Et	111.2°	138.9°	+27.7°

Beyond this interaction, the initial WCA values (t = 0 min) were similar for both concentrations, averaging 134.4° for ZnO-0.22 and 136.3° for ZnO-1.1-c (Figure 17). After 5 min, however, the mean WCA decreased to 113.8° for ZnO-0.22 (84.7% retention), compared with 134.3° for ZnO-1.1-c (98.5% retention). Variability was also greater for ZnO-0.22, with standard deviations ranging from 2.41° to 22.41°, particularly for M1-A1-0.22-50Et (90.8° ± 22.41°), whereas ZnO-1.1-c showed a narrower range of 2.7° to 7.3°

The cleaning protocol further affected WCA retention. ZnO-1.1-c conditions retained 97–99% of their initial WCA after 5 min under both protocols, indicating comparatively stable hydrophobicity. In contrast, ZnO-0.22 was more sensitive to cleaning: M1-A1-0.22-50Et retained only 69% of its initial WCA, whereas the corresponding Approach 2 condition retained 94%. Nevertheless, M1-A2-0.22-100Et, despite having the second-highest initial WCA (141.5°), showed the largest drop among Approach 2 conditions (17.8°, 87.4% retention). Thus, the lower-concentration coating remained less stable even after modification of the cleaning protocol.

This difference may be explained by two complementary effects. First, the Cassie-Baxter wetting state is metastable: although high initial WCA can result from surface roughness and low surface energy, its persistence depends on sufficiently dense and continuous surface features capable of maintaining trapped air beneath the droplet [56]. Lower or discontinuous nanoparticle coverage may expose more collagen fibres, facilitating water penetration and gradual transition towards a Wenzel-type state [57].

Second, the higher zinc acetate precursor mass and stoichiometric KOH volume used for ZnO-1.1-c are expected to produce a higher nanoparticle concentration in the functionalisation bath, promoting denser and more continuous ZnO deposition. This increases the number of available Zn^{2+} anchoring sites [18,58] and, after myristic acid treatment at the same concentration, should favour formation of a more uniform and densely packed aliphatic layer [58]. Fewer exposed hydrophilic collagen regions would therefore remain, improving resistance to water penetration and helping explain the higher WCA retention of ZnO-1.1-c.

The observed A × B interaction may also be related to electrostatic tuning of the 50Et dispersions. As described in Section 3.4.1, their pH was adjusted to approximately 7–7.5 to maintain positively charged ZnO nanoparticles and a negatively charged leather surface, thereby favouring electrostatic attraction. Because pH is defined by the ionisation of water into H^+ and OH^- ions, no meaningful pH adjustment is possible in the non-aqueous 100Et dispersions, which contain no water to ionise. This may explain why increasing ZnO concentration produced a stronger effect in the 50Et dispersions (Table 14).

4.2.2. Surface morphology and chemistry (SEM/EDS, FTIR)

(I) SEM/EDS

Among the two imaging modes available, backscattered electron detection (BSED) images were selected for presentation and analysis throughout this section, rather than secondary electron images. This choice was based on the pronounced charging effects observed in secondary electron mode, which considerably hindered the clear identification of collagen fibres and inter-fibre pores at the leather surface. BSED imaging, by contrast, additionally allows a preliminary qualitative assessment of the presence of higher atomic number species, as brightness contrast in this mode is directly related to atomic number. Since both the leather matrix (collagen) and myristic acid are organic in nature, and therefore present similarly low atomic numbers, any localised regions of higher brightness can be tentatively attributed to the presence of zinc oxide (n-ZnO).

The untreated (control) leather surface (Figure 18) displays the characteristic fibrous topography of the collagen network, with clearly visible interwoven fibre bundles and inter-fibre pores. No localised regions of increased brightness are observed, consistent with the absence of zinc on this untreated sample.

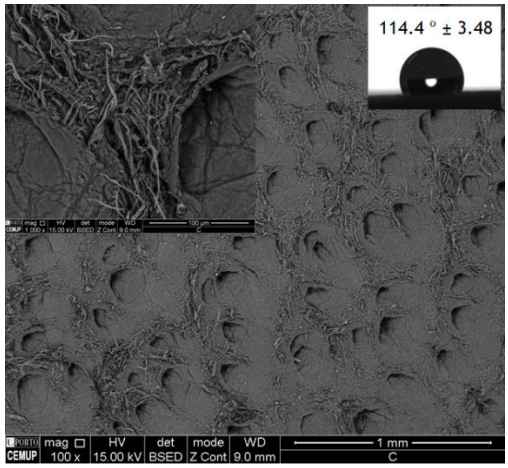


Figure 18 - Backscattered electron SEM micrographs of the untreated (control) leather surface at 100× (panoramic) and 1000× (detail) magnification, showing the characteristic fibrous topography of the collagen network. Inset: corresponding water contact angle

The functionalised samples were subsequently examined by SEM to assess how the ZnO concentration used is reflected in the resulting surface morphology, beginning with the ZnO-0.22 conditions (Figure 19).

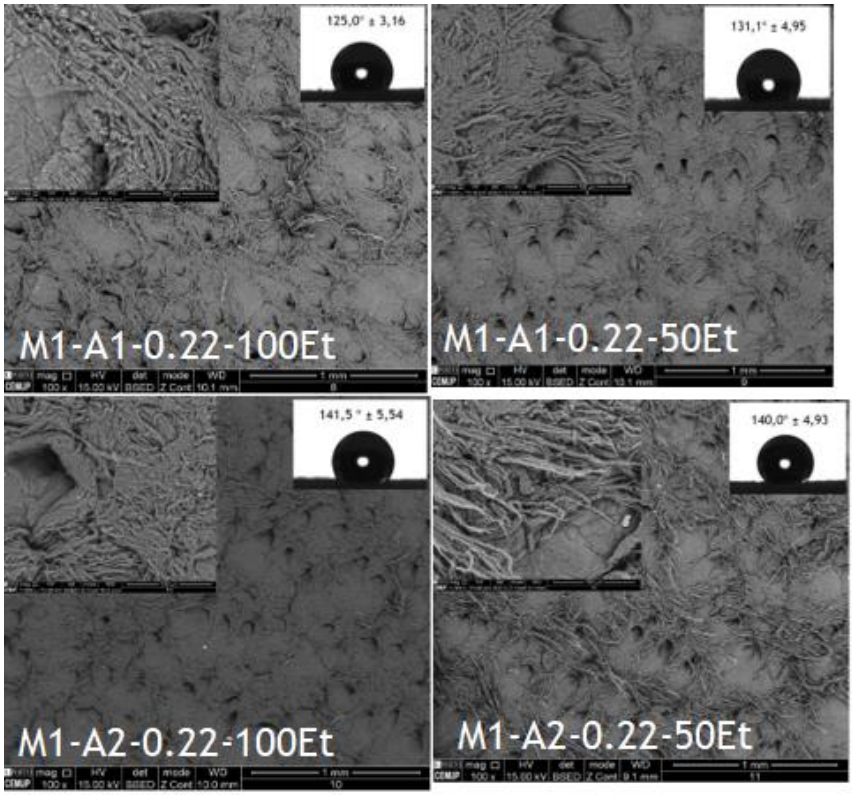


Figure 19 - Backscattered electron SEM micrographs at 100× (panoramic) and 1000× (detail) magnification of the four ZnO-0.22 conditions: M1-A1-0.22-100Et, M1-A1-0.22-50Et, M1-A2-0.22-100Et, and M1-A2-0.22-50Et. Insets show the corresponding water contact angle for each condition

Within the ZnO-0.22 group, all four conditions display a fibrous topography broadly resembling that of the untreated control, with the collagen fibre network remaining visible to varying degrees. This is consistent with the statistically confirmed lower and less stable WCA values recorded for this concentration (Section 4.2.1(III)).

Some differences in surface texture are nonetheless visible between conditions: M1-A2-0.22-100Et presents a smoother, more amorphous surface with fewer resolved fibres, while the remaining three conditions retain a more open, fibrous appearance. Notably, M1-A2-0.22-50Et and M1-A1-0.22-50Et share both ZnO concentration and dispersion medium, differing only in cleaning protocol — yet they represent opposite extremes of WCA stability within this group: M1-A2-0.22-50Et retained one of the better WCA values and was statistically within the top-performing group (Table 12, Section 4.2.1(I)), despite its open fibrous structure, whereas M1-A1-0.22-50Et — visually smoother — showed the poorest stability of all Methodology 1 conditions. This directly illustrates the statistically confirmed A × C interaction (Table 10): the effect of cleaning protocol on coating stability cannot be predicted independently of ZnO concentration, and vice versa. It also indicates that surface morphology alone cannot account for hydrophobic stability, the local distribution or chemical availability of surface Zn^{2+} sites for MA binding likely also plays a role.

In contrast, the ZnO-1.1-c conditions (Figure 20) show a substantially different surface morphology. While the underlying pore structure of the leather remains visible across all four conditions, the loose, individualised fibres characteristic of the control and the ZnO-0.22 conditions are no longer observed. Instead, at 1000× magnification, the surface appears covered by a continuous layer, with the pores framed by this coating rather than by exposed fibre bundles — consistent with the dominant effect of ZnO concentration confirmed by the statistical analysis (Section 4.2.1(I)) and supporting a more robust Cassie-Baxter wetting state at this concentration.

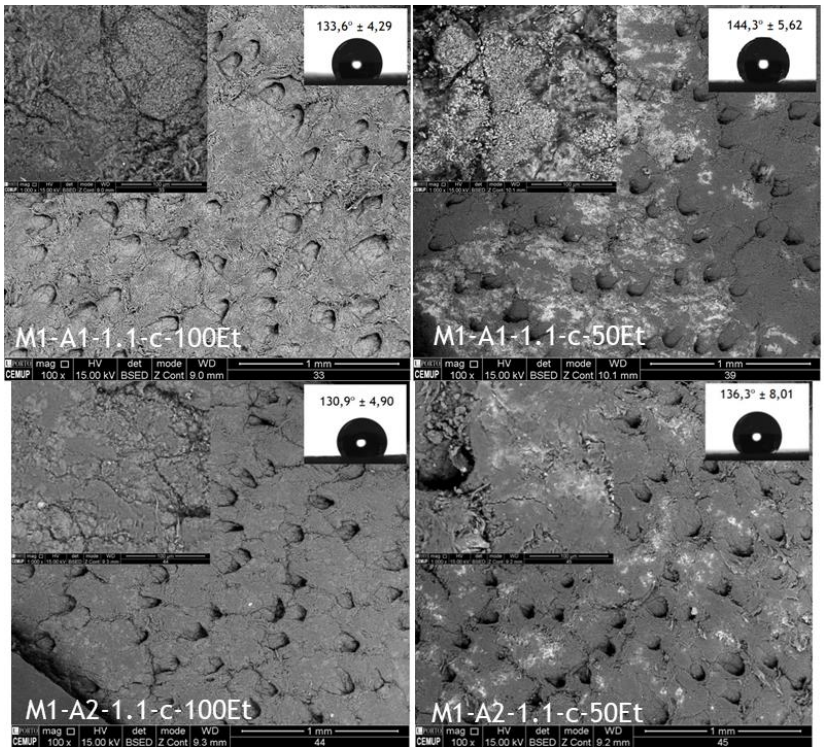


Figure 20 - Backscattered electron SEM micrographs at 100× (panoramic) and 1000× (detail) magnification of the four ZnO-1.1-c conditions: M1-A1-1.1c-100Et, M1-A1-1.1c-50Et, M1-A2-1.1c-100Et, and M1-A2-1.1c-50Et. Insets show the corresponding water contact angle for each condition.

At this higher magnification, localised cracks within the coating layer can also be observed in some conditions, potentially indicating limited flexibility or partial detachment of the deposited material under drying and handling.

Some variation in surface texture is visible between conditions. The 50Et conditions display distinct, comparatively brighter regions across the coating, whereas the 100Et conditions present a more uniform appearance. As brightness contrast in BSED imaging reflects atomic number, this is tentatively attributed to locally denser ZnO deposition — consistent with the significant A × B interaction (Table 10), whereby the benefit of the 50Et medium is only expressed at high ZnO concentration (Table 14). Notably, M1-A1-1.1c-50Et and M1-A2-1.1c-50Et — the two conditions displaying the most pronounced brighter regions — also correspond to the numerically highest and most stable WCA values recorded within Methodology 1, providing an initial visual indication that samples with greater surface zinc content tend to exhibit superior hydrophobic performance. This hypothesis is further examined through semi-quantitative EDS analysis.

Table 15 - Semi-quantitative EDS analysis of zinc content on the leather surface for the control and all Methodology 1 conditions.

Sample	Zn (wt.%)
M1-A1-0.22-100Et	3.79
M1-A1-0.22-50Et	1.04
M1-A2-0.22-100Et	1.96
M1-A2-0.22-50Et	1.60
M1-A1-1.1c-100Et	26.06
M1-A1-1.1c-50Et	29.44
M1-A2-1.1c-100Et	17.18
M1-A2-1.1c-50Et	19.33

Table 15 confirms, quantitatively, the trend predicted by the dominant main effect of ZnO concentration: the ZnO-1.1-c conditions present substantially higher surface zinc content than the ZnO-0.22 conditions, an approximately 10-fold difference. Given the typical EDS interaction volume (approximately 1–3 μm) at the accelerating voltage used, these values reflect the near-surface elemental composition, encompassing both deposited nanoparticles and underlying collagen, rather than the outermost coating layer alone. Nonetheless, this provides direct compositional support for the hypothesis that the higher zinc acetate precursor concentration used in the synthesis of ZnO-1.1-c translates into substantially greater nanoparticle deposition on the leather surface.

Within the ZnO-1.1-c group, Approach 1 conditions consistently present higher Zn content than their Approach 2 counterparts, regardless of dispersion medium, resolving in favour of a hindering effect the ambiguity raised in Section 4.2.1(II) — consistent with the significant A × C interaction (Table 10). This interaction is particularly evident under Approach 1 (IPA), where increasing ZnO concentration produces a much larger rise in WCA (Table 13) than under Approach 2 (IPA/AA), suggesting that the additional acetic acid step somewhat dampens the benefit of higher nanoparticle concentration. Beyond the reduced electrostatic anchoring already discussed in Section 4.2.1(II), two further mechanisms may contribute to this lower Zn content under Approach 2: a residual low-pH microenvironment at the leather surface that keeps the overall surface charge weakly negative or near-neutral even after rinsing, further hindering electrostatic attraction of the positively charged n-ZnO, and a possible minor dissolution of surface ZnO, given its amphoteric nature, in the presence of acetic acid [37]. As these mechanisms were not directly investigated in this work, they remain tentative hypotheses rather than confirmed explanations.

Elemental Zn content, however, does not fully predict WCA performance: within the ZnO-0.22 group, M1-A1-0.22-100Et presented the highest Zn content yet the lowest initial WCA — an apparent discrepancy that is, in fact, consistent with the A × C interaction, since this condition combines low ZnO concentration with the cleaning protocol shown to underperform at this concentration (Table 13). This is further supported by M1-A2-0.22-100Et, which achieved a higher WCA despite a lower Zn content and the smoother, more amorphous surface previously noted by SEM. A similar pattern emerges within the ZnO-1.1-c group: despite its lower Zn content, Approach 2 did not underperform in terms of

WCA stability — M1-A2-1.1c-50Et, in fact, achieved the highest retention recorded across all Methodology 1. Taken together, these observations reinforce that the spatial distribution and uniformity of nanoparticle coverage, rather than total zinc quantity alone, play the more decisive role in hydrophobic performance[32,58] .

(II) FTIR

ATR-FTIR spectra of the untreated control, all Methodology 1 conditions, and pure myristic acid (MA) are presented in Figure 21.

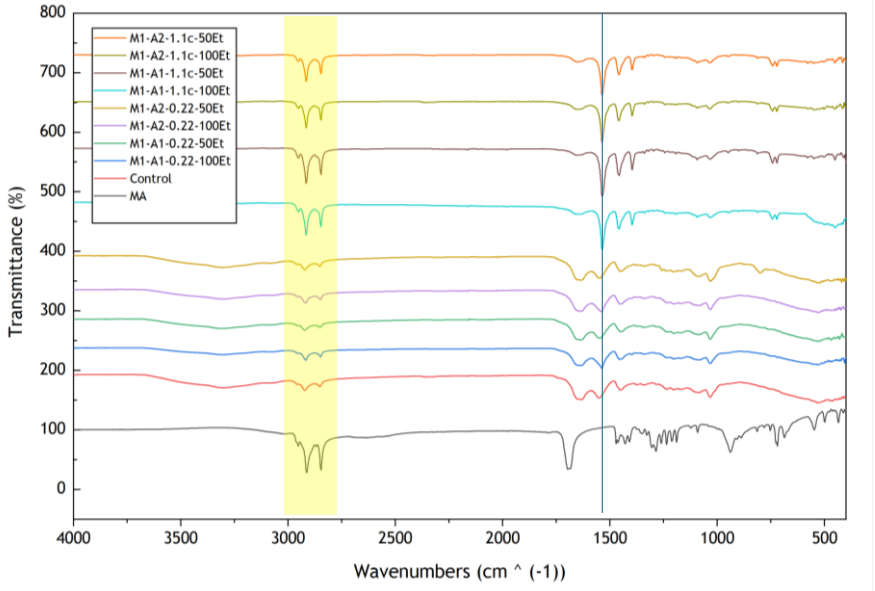


Figure 21 - FTIR-ATR spectra of the untreated (Control) leather, all Methodology 1 conditions, and pure myristic acid (MA)

The ZnO-0.22 spectra remain largely similar to the control, with no substantial new features attributable to MA. The ZnO-1.1-c spectra, by contrast, show clear changes relative to the control, more closely resembling pure MA — consistent with the dominant main effect of ZnO concentration established statistically (Table 10).

In the 2800–2960 cm^{-1} region, corresponding to C-H stretching of the long aliphatic MA chain, the ZnO-1.1-c spectra closely resemble pure MA, whereas the ZnO-0.22 spectra remain comparable to the control — in agreement with the higher Zn content measured by EDS for this group (Table 15) and the greater number of surface Zn^{2+} sites proposed for MA coordination [17,18,57].

The spectrum of pure MA displays a distinct band at ~1700 cm^{-1}, characteristic of the carbonyl stretch (C=O) of the free carboxylic acid group. This band is absent from all leather samples, including ZnO-1.1-c, suggesting that MA is not present in its free acid form but is instead chemically bound, most likely via coordination of the carboxylate group with surface Zn^{2+} ions [17,57].

This is further supported by the band at 1540 cm^{-1}, characteristic of Zn–COO^- coordination, which is clearly visible for the ZnO-1.1-c conditions but not for ZnO-0.22 — an indication that more MA is present at the higher concentration. This band lies close to the Amide II region of collagen (N-H bending and C-N stretching), present across all samples given the substrate's collagenous nature [7,20] but its distinct emergence in the

ZnO-1.1-c spectra reflects an additional Zn-coordinated carboxylate contribution absent at the lower concentration, consistent with the ~10-fold difference in surface Zn content measured by EDS (Table 15) [17,18,58].

Taken together, the absence of the free C=O band and the presence of a resolved Zn–COO^- coordination band support the same conclusion for the ZnO-1.1-c samples: MA is chemically bound to the surface via carboxylate coordination with Zn^{2+}, rather than physically deposited in its free acid form [17,57,58]. This is consistent with the hypothesis that denser ZnO deposition promotes more effective MA binding and, in turn, superior and more stable hydrophobic performance, as established by the statistical analysis (Section 4.2.1(I)).

4.2.3. Selection of best-performing conditions

Table 16 shows the WCA ranking of the Methodology 1 conditions, from best to worst-performing.

Table 16 - Ranking of Methodology 1 conditions by mean WCA at t = 5 min, from best to worst-performing

Rank	Condition	Mean WCA ± SD (°)
1	M1-A1-1.1c-50Et	141.8 ± 5.7
2	M1-A2-1.1c-50Et	135.9 ± 7.3
3	M1-A2-0.22-50Et	131.5 ± 4.8
4	M1-A1-1.1c-100Et	130.8 ± 4.9
5	M1-A2-1.1c-100Et	128.5 ± 2.7
6	M1-A2-0.22-100Et	123.7 ± 10.4
7	M1-A1-0.22-100Et	109.1 ± 2.4
8	M1-A1-0.22-50Et	90.8 ± 22.4

Statistically, WCA alone does not identify a single best-performing condition, nor does it justify prioritising the ZnO-1.1-c conditions over M1-A2-0.22-50Et on WCA grounds alone. This condition is, however, an isolated exception within an otherwise consistent pattern: the ZnO-1.1-c conditions were consistently superior across every other line of evidence — WCA stability (98.5% average retention against 84.7% for ZnO-0.22, Section 4.2.1(III)), an order-of-magnitude higher surface Zn content (Table 15), and clear FTIR evidence of MA coordination, largely absent from the ZnO-0.22 spectra. Selection was therefore based on this combined, multi-technique evidence rather than on WCA magnitude alone.
Within the ZnO-1.1-c group, M1-A1-1.1c-50Et and M1-A2-1.1c-50Et were selected as the two best-performing conditions:

- M1-A1-1.1c-50Et presented the highest initial WCA across all Methodology 1 conditions (144.3°), the highest surface zinc content (29.44 wt.%), and clear FTIR evidence of MA coordination — consistent with the dense, well-covered coating confirmed by SEM.
- M1-A2-1.1c-50Et, statistically indistinguishable from M1-A1-1.1c-50Et per the Tukey test despite its slightly lower initial WCA (136.3°) and Zn content (19.33 wt.%), exhibited the best WCA stability of all conditions tested (99.7% retention). This condition was retained to evaluate the effect of the acetic acid cleaning treatment at the higher ZnO concentration in the subsequent durability testing.

4.3. Methodology 2

This process begins with sequential immersion of the leather in tannic acid (TA) and zinc salt solutions. TA is a polyphenolic compound rich in galloyl groups, which are known to bind extensively to the collagen matrix through hydrogen bonding and hydrophobic interactions — a mechanism analogous to that exploited in vegetable retanning [14,19,22]— while simultaneously acting as an effective metal-chelating agent. TA has been widely reported to form coordination complexes with metal ions through pH-dependent, multivalent bonding of its phenolic hydroxyl groups, most notably with Fe^{3+}, where this coordination chemistry has been exploited to build thin films and coatings on a wide range of substrates [59,60]. A broadly similar coordination behaviour with Zn^{2+} may be expected, given the comparable affinity of phenolic hydroxyl groups for divalent and trivalent transition metal ions. This dual affinity is expected to enable TA to serve as a molecular bridge between the leather substrate and the subsequently precipitated zinc species, potentially promoting more controlled, substrate-adhered nucleation of ZnO compared with the electrostatically driven deposition of preformed nanoparticles described in Methodology 1.

Precipitation itself is subsequently induced in a final bath, through the gradual addition of a base, which progressively raises the pH of the solution. This pH increase drives the system towards supersaturation with respect to zinc hydroxide and related zincate species, promoting their conversion into solid zinc oxide (or an intermediate zinc hydroxide phase) directly at the leather surface [18] consistent with the nucleation and growth principles discussed in Section 4.1.1. This localised, substrate-templated formation of ZnO contrasts with the *ex-situ* synthesis and subsequent deposition approach used in Methodology 1, and may result in differences in nanoparticle morphology, distribution, and surface adhesion, which are examined in the following subsections in relation to the process variables tested.

4.3.1. Effect of zinc salt, base, solvent and final bath conditions on WCA

Figure 22 presents the water contact angle (WCA) results obtained for all conditions tested under this methodology, compared to the untreated leather (control).

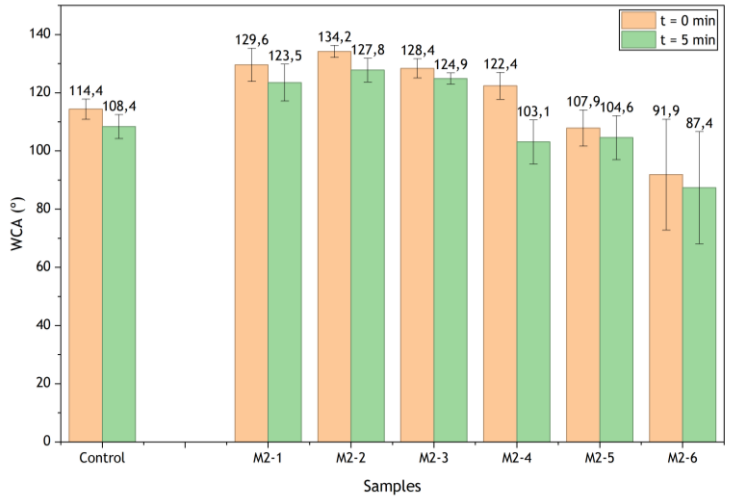


Figure 22 - Water contact angle (WCA) at t=0 min and t=5 min for the untreated control and all Methodology 2 conditions (M2-1 to M2-6). Error bars represent standard deviation across replicate measurements

Because the design tested here does not correspond to an orthogonal factorial structure — each pair of conditions instead isolates one process variable at a time (zinc salt/base type, solvent, final bath heating, supplementary zinc salt) — the seven samples (control plus six treated conditions) were compared using a Welch's one-way ANOVA, which does not assume equal variance across groups, followed by Games-Howell post-hoc pairwise comparisons (n = 5 replicate measurements per condition). Table 17 ranks the seven conditions by mean WCA and identifies which are statistically distinguishable from one another.

Table 17 - Ranking of Methodology 2 conditions by mean WCA at t = 5 min, with Games-Howell statistical grouping (α = 0.05). Conditions sharing a letter are not significantly different from each other.

Rank	Condition	Mean WCA ± SD (°)	Games-Howell group
1	M2-2	127.8 ± 4.05	a
2	M2-3	124.9 ± 1.95	a
3	M2-1	123.5 ± 6.34	a
4	Control	108.4 ± 4.12	b
5	M2-5	104.6 ± 7.55	b
6	M2-4	103.1 ± 7.55	b
7	M2-6	87.4 ± 19.27	ab

M2-1, M2-2 and M2-3, the three conditions prepared with final-bath heating, form a high-performing group significantly superior to the control, M2-4 and M2-5, identifying final-bath heating as the principal factor distinguishing high- from low-performing conditions within this methodology. These results are examined in detail below.

Among the six conditions tested, M2-5 and M2-6 — prepared with the lower zinc nitrate concentration (1.0%) — were the only two to fall at or below the untreated control (Table 17), though this difference was not itself statistically significant, likely reflecting their wide variability, especially for M2-6. This is most likely explained by the tannic acid (TA) pre-treatment used in this methodology, which is itself strongly hydrophilic due to its abundant phenolic hydroxyl groups. At lower zinc concentration, the resulting ZnO precipitation is likely insufficient to provide either the surface roughness required for a

Cassie-Baxter state or enough Zn^{2+} sites to anchor a dense MA layer capable of shielding the underlying, polar TA and collagen surface — allowing their hydrophilic character to dominate overall wettability. A less likely additional contribution may come from the sequential solvent immersion steps, which could in principle partially strip loosely bound fatliquoring agents responsible for the leather's intrinsic hydrophobicity, although this was not directly verified in this work.

Comparing M2-3 and M2-4, which differ only in final-bath heating (at 2.0% zinc nitrate), heating produced a significantly higher WCA — the only pairwise comparison in this section to reach significance. This is consistent with the role of temperature in converting zinc hydroxide intermediates into crystalline ZnO: precipitation at room temperature likely yields a more amorphous, poorly crystalline phase, whereas thermal activation promotes more complete dehydration and condensation into ZnO, potentially strengthening interfacial bonding with the TA-anchored surface and improving mechanical robustness.

Comparing M2-2 and M2-3, which differ in the addition of a supplementary zinc salt to the final bath, this addition made no meaningful statistical difference to WCA. This indicated that adding supplementary zinc to an already-heated bath offers no advantage over heating alone.

Taken together, final-bath heating emerges as the principal factor distinguishing high- from low-performing conditions within Methodology 2. Notably, M2-4 shares the same zinc nitrate concentration (2.0%) as M2-3 without heating yet performs significantly worse — indicating that zinc availability alone does not explain coating performance here, heating instead governs the effective conversion and anchoring of the available zinc as ZnO onto the leather surface. Zinc salt/base type, solvent choice, and supplementary zinc salt addition showed no statistically significant effect at the sample sizes tested (n = 5).

4.3.2. Surface morphology and chemistry (SEM/EDS, FTIR)

(I) SEM/EDS

Backscattered electron SEM micrographs of the untreated control and of the five Methodology 2 conditions analysed (M2-2 to M2-6) are presented in Figure 23.

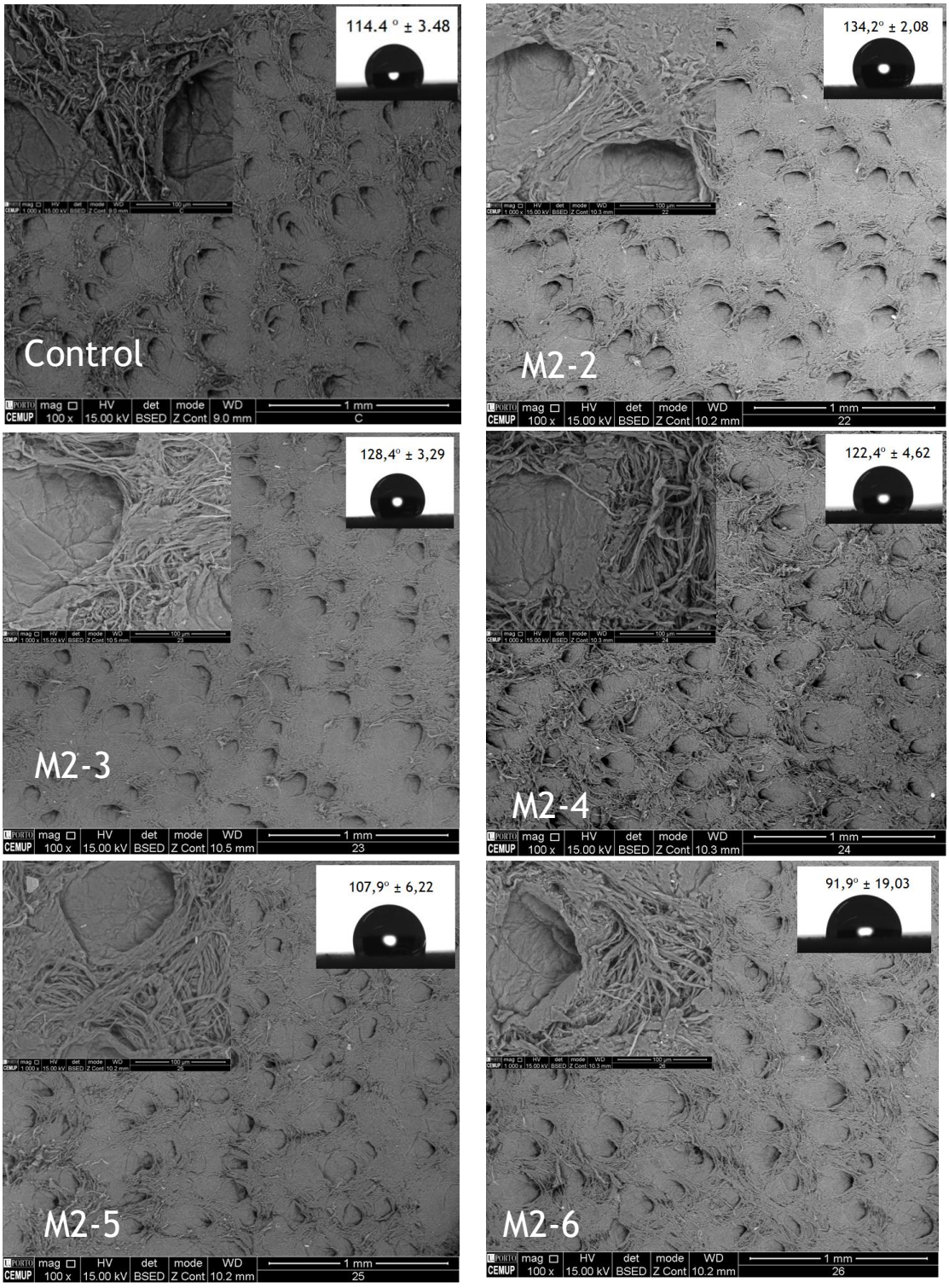


Figure 23 - Backscattered electron SEM micrographs at 100× (panoramic) and 1000× (detail) magnification of the untreated control and Methodology 2 conditions M2-2 to M2-6. Insets show the corresponding water contact angle for each condition

Surface morphology across the Methodology 2 conditions showed more subtle variations than the distinct concentration regimes observed in Methodology 1. None of the *in-situ* formulations displayed the dense, continuous particulate layer or the near-complete masking of individual collagen fibres characteristic of the ZnO-1.1-c conditions. This morphology is consistent with the intermediate water contact angles recorded across

Methodology 2, which remained lower than the peak values achieved in Methodology 1.

The SEM micrographs divide the samples into two morphological groups based on final-bath heating. The heated conditions (M2-1, M2-2 and M2-3) presented the flattest and most compact surfaces, with reduced visibility of individual fibres relative to the control. M2-5 and M2-6, despite also being heated, displayed an open, fibrous structure closely resembling both the untreated control and the ZnO-0.22 conditions of Methodology 1 — most likely reflecting their lower zinc concentration (1.0%) rather than the absence of heating. Notably, none of the Methodology 2 conditions displayed the localised, brighter regions attributable to zinc observed for the higher-concentration conditions of Methodology 1, suggesting a comparatively lower or less concentrated surface deposition of ZnO across this methodology as a whole.

This pattern is most clearly illustrated by M2-3 and M2-4, which share the same zinc nitrate concentration (2.0%) but differ in final-bath heating: only M2-3 displays the compact morphology of the heated group, while M2-4 retains an open, fibrous structure despite its equal zinc concentration. This directly supports, at the morphological level, the statistical finding that heating, rather than zinc concentration alone, governs both the conversion of zinc hydroxide intermediates into crystalline ZnO and the extent to which the resulting material forms a continuous surface coating rather than isolated, poorly adhered deposits.

This difference may be further explained by the distinct deposition mechanisms underlying the two methodologies. In Methodology 1, pre-formed ZnO nanoparticles, already present at a defined concentration in suspension, are directly applied to the leather surface through repeated immersion cycles, promoting their deposition and retention at the substrate. In Methodology 2, by contrast, zinc oxide precipitation occurs throughout the entire volume of the final bath, rather than being confined to the leather surface. As a result, only a fraction of the precipitated zinc species is expected to nucleate and remain attached to the substrate, with the remainder likely persist in suspension within the bulk solution. Despite the higher zinc precursor concentrations used in Methodology 2 (1.0–2.0%) compared to the 1.1% used for ZnO-1.1-c in Methodology 1, overall WCA and morphological outcomes remained inferior to those achieved by the best Methodology 1 conditions, suggesting a comparatively lower effective surface deposition despite the greater zinc precursor available. The extent to which this mechanism explains the comparatively lower ZnO deposition observed in Methodology 2 is examined further through semi-quantitative EDS analysis.

Table 18 presents the semi-quantitative EDS zinc content for the Methodology 2 conditions. M2-2 and M2-3 present the highest surface zinc content (8.81% and 7.28%, respectively), comparable to or higher than the ZnO-0.22 conditions of Methodology 1 (1.04–3.79 wt.%, Section 4.2.2). This partially addresses the hypothesis raised in Section 4.3.2: rather than being lost to homogeneous precipitation in the bath, a meaningful fraction of zinc does reach and remain on the leather surface, yet without translating into WCA values matching the best Methodology 1 conditions.

Table 18 - Semi-quantitative EDS analysis of zinc content on the leather surface for Methodology 2 conditions (M2-1 to M2-6)

Sample	Zn (wt.%)
M2-1	-
M2-2	8.81
M2-3	7.28
M2-4	4.69
M2-5	3.53
M2-6	3.45

This is particularly evident for M2-5 and M2-6, which contain more than double the surface zinc content of M1-A2-0.22-50Et (1.60%, WCA 140º, Section 4.2.2) yet achieved substantially lower WCA (107.9º and 91.9º, respectively). A plausible contributing factor is the tannic acid (TA) pre-treatment specific to Methodology 2: if TA remains present or partially exposed to the surface alongside the deposited zinc, its hydrophilic character could counteract the intended hydrophobic effect, independently of zinc content.

Once again, surface zinc content alone does not predict hydrophobic performance in this methodology — as observed for Methodology 1 (Section 4.2.2), how zinc is deposited and distributed matters at least as much as the total amount present. This distinction is further examined through FTIR analysis, to assess whether MA binding to the zinc species differs between methodologies.

(II) FTIR

ATR-FTIR spectra of the untreated control, M2-2 to M2-6, and pure myristic acid (MA) are presented in Figure 24. As with Methodology 1, none of the leather spectra display the band at ~1700 cm^{-1} characteristic of the free carboxylic acid group of MA, suggesting that, where present, MA is chemically bound rather than physically deposited in its free acid form across all Methodology 2 conditions.

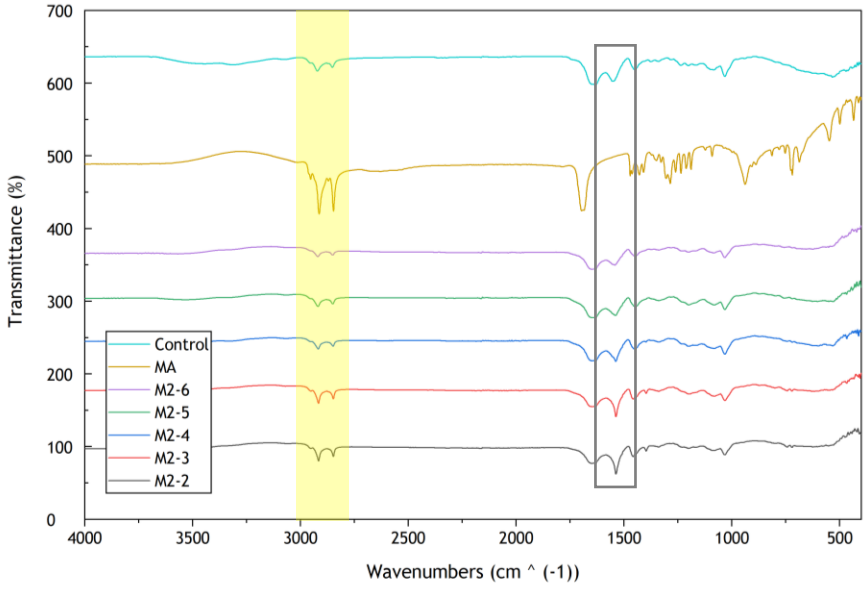


Figure 24 - FTIR-ATR spectra of the untreated (Control) leather, M2-2 to M2-6 conditions from Methodology 2, and pure myristic acid (MA)

Some differentiation is nonetheless visible in the band at ~1540 cm^{-1}, associated with $Zn–COO^-$ coordination. This band is more pronounced in M2-2 and M2-3, the two conditions with the highest surface zinc content and among the statistically best-performing conditions. While M2-5 and M2-6 show a comparatively weaker signal in this region, and M2-4 presents an intermediate intensity. This gradient is broadly consistent with the EDS-based ranking of surface zinc content (M2-2 > M2-3 > M2-4 > M2-5 ≈ M2-6, Table 18), suggesting that more surface zinc is associated with somewhat more effective MA coordination in this methodology as well.

This distinction is, however, considerably less pronounced than the contrast observed between the ZnO-0.22 and ZnO-1.1-c conditions in Methodology 1, where the ~1540 cm^{-1} band was essentially absent at the lower concentration and clearly resolved at the higher one. The comparatively subtler variation across Methodology 2 conditions is consistent with the smaller range of surface zinc content among these samples relative to the roughly 10-fold difference between the two Methodology 1 concentrations, and may also reflect the less controlled, in situ deposition mechanism discussed in Section 4.3.2, which is expected to yield zinc species that are less uniformly coordinated with MA even when present in comparable amounts.

4.3.3. Selection of best-performing conditions

Among the six conditions tested within Methodology 2, M2-1, M2-2 and M2-3 presented the most promising results, forming a statistically indistinguishable high-performing group (Section 4.3.1) — performances broadly comparable to some of the intermediate conditions of Methodology 1.

Despite these encouraging results, Methodology 2 was not pursued further, in favour of Methodologies 1 and 3 — a practical prioritisation within the scope of this work, rather than a rejection of its viability. This decision mainly reflected its greater processing complexity (multiple immersion/rinsing steps, controlled heating, gradual pH adjustment) and the handling and safety concerns associated with ammonia as the base used in most conditions, both relevant limitations for scalable, industrial application. Further optimisation, including alternative bases and simplified bath sequences, is suggested as a direction for future work.

4.4. Methodology 3

Methodology 3 combines ZnO nanoparticles with carnauba wax, applied as a bilayer system that can be repeated to build up multiple layers of coating [38,44]. As in Methodology 1, leather samples were first pre-treated with tannic acid (TA) [59,60], and ZnO nanoparticles were subsequently applied to introduce nanoscale surface roughness. However, rather than using myristic acid (MA) as the low-surface-energy component, this methodology employs carnauba wax — a natural wax rich in long-chain fatty acid esters [41]— applied as a second layer over the deposited nanoparticles.

The expected hydrophobic mechanism follows the same general principles discussed for Methodology 1 (Section 4.2): ZnO nanoparticles are expected to introduce surface roughness, while the wax itself is expected to contribute a low-surface-energy outer layer

through its long aliphatic ester chains, together promoting a Cassie-Baxter-type wetting behaviour [17,38,41].

A key distinguishing feature of this methodology is the bilayer approach itself, which allows the number of ZnO/wax cycles to be varied (1, 3, or 5 bilayers, Section 3.4.3), providing an additional means of controlling coating thickness and, potentially, its resulting hydrophobic performance and durability — a variable not explored within Methodologies 1 or 2 [14,38,44,50] . The opposing surface charges of the negatively charged carnauba wax and the positively charged ZnO nanoparticles are expected to favour strong electrostatic adhesion between the two layers, further supporting the structural integrity of each bilayer [38,44]. The following subsections examine the effect of this variable, alongside a comparison between the exploratory preliminary trials and the standardised bilayer protocol subsequently adopted.

4.4.1. Preliminary trials (M3-(1B+3W) / M3-(2B+3B)) vs. standardised protocol

Figure 25 presents the WCA results obtained for the untreated control, the exploratory preliminary trial conditions, and the standardised bilayer protocol conditions tested within Methodology 3.

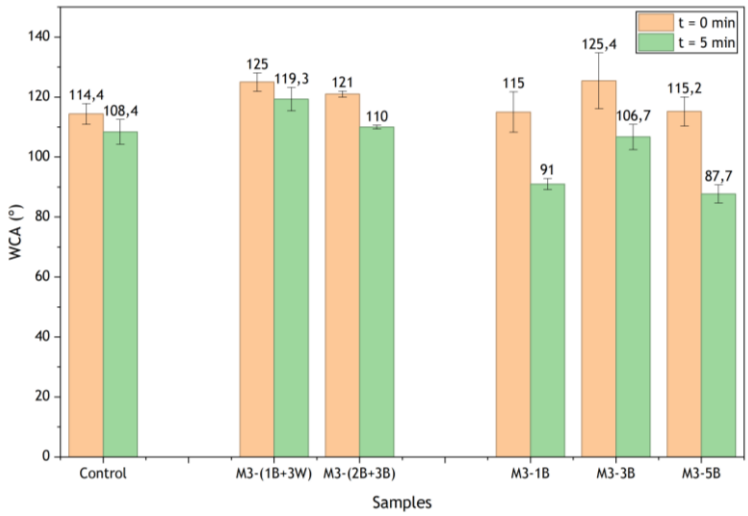


Figure 25 - Water contact angle (WCA) at t=0 min and t=5 min for the untreated control, the preliminary trial conditions (M3-(1B+3W) and M3-(2B+3B)), and the standardised bilayer protocol conditions (M3-1B, M3-3B, M3-5B). Error bars represent the standard deviation a

Because the standard deviations differ considerably between conditions (ranging from 0.63º for M3-(2B+3B) to 4.20º for M3-3B), the six samples were compared using a Welch's one-way ANOVA, followed by Games-Howell post-hoc pairwise comparisons (n = 5 replicate measurements per condition). Results are summarised in Table 19.

Table 19 - Games-Howell grouping of WCA at t = 5 min for the untreated control and all Methodology 3 conditions (α = 0.05). Conditions sharing a letter are not significantly different from each other

Sample	Contact angle (°), mean ± SD	Group
M3-(1B+3W)	119.3 ± 3.92	a
M3-(2B+3B)	110.0 ± 0.63	b
Control	108.4 ± 4.12	b
M3-3B	106.7 ± 4.20	b
M3-1B	91.0 ± 1.85	c
M3-5B	87.7 ± 3.00	c

The Welch's ANOVA indicates a highly significant overall effect, separating the six conditions into three statistical groups (Table 19). M3-(1B+3W) alone forms the top group, significantly outperforming both the control and the standardised protocol conditions ($p < 0.05$ throughout). M3-(2B+3B), the control, and M3-3B form an intermediate group, statistically indistinguishable from one another — meaning neither M3-(2B+3B) nor M3-3B improves on the untreated control. M3-1B and M3-5B form the lowest group, both significantly below all other conditions. M3-(1B+3W) is thus the only condition within Methodology 3 to achieve a statistically significant improvement over the control.

At t = 0 min, M3-(1B+3W) achieved a WCA of 125.0°, with excellent stability after 5 minutes (95.4% retention). M3-(2B+3B) reached a comparable initial WCA (121.0°) but showed somewhat lower stability (90.9% retention), consistent with its statistical equivalence to the control. The standardised protocol conditions (M3-1B, M3-3B, M3-5B), despite reasonably high initial WCA values, showed substantially poorer stability (79.1%, 85.1%, and 76.1% retention) — consistent with M3-1B and M3-5B falling significantly below the control, and M3-3B, despite its higher retention, remaining statistically equivalent to it rather than distinguishable as an improvement.

A key procedural difference between the preliminary trials and the standardised protocol lies in the presence/absence of an intermediate drying step prior to the application of reinforcement layers. In the preliminary trials, a base bilayer was first applied and oven-dried, after which the reinforcement material — either additional wax layers (M3-(1B+3W)) or additional bilayers (M3-(2B+3B)) — was applied consecutively on top, without further intermediate drying between these individual reinforcement steps. In the standardised protocol, by contrast, no intermediate drying was applied at any stage, with the full number of bilayers deposited consecutively from the outset (Section 3.4.3). Both approaches therefore involve an element of "wet-on-wet" deposition — within the reinforcement steps of the preliminary trials, and throughout the entire process in the standardised protocol — but differ in whether this occurs on top of an already-consolidated base layer or directly onto the untreated leather surface. Such wet-on-wet processes are known, in layer-by-layer coating systems, to promote partial blending, redissolution, or disruption of the underlying layer during subsequent immersion steps, rather than the formation of clearly defined, discrete layers [38,44]; this effect would be expected to be more pronounced when it occurs from the very first deposition step, as in the standardised protocol, than when it is confined to reinforcement layers applied over an already-dried base.

The single intermediate oven-drying step included in the preliminary trials (65 ºC, Section 3.4.3) allowed the base bilayer to consolidate before the reinforcement material was applied. Although this temperature remains below the reported melting point of carnauba wax (approximately 80–86 ºC), it may nonetheless have promoted partial solvent evaporation and some initial structural consolidation of the wax layer; it is noted, however, that complete film consolidation and superhydrophobic behaviour in carnauba wax coatings have been reported to require thermal annealing above the wax melting point [41], suggesting that the consolidation achieved at 65 ºC in this work was likely partial rather than complete. Similar wax-based low-surface-energy mechanisms have been reported for other natural waxes, such as beeswax [50].

The two preliminary trial conditions differ in reinforcement type: M3-(1B+3W) received three additional wax-only layers over a single base bilayer, while M3-(2B+3B) received three additional full bilayers (ZnO and wax) over a two-bilayer base. Despite the extra ZnO deposited with each bilayer, M3-(2B+3B) performed no better than the control, whereas wax-only reinforcement (M3-(1B+3W)) was the only condition to significantly improve on it. Since ZnO is itself hydrophilic and contributes to hydrophobicity only indirectly, through surface roughness, repeatedly reintroducing it without a matching increase in wax may fail to improve — or could even dilute — the coating's hydrophobic character. Once a base layer of ZnO-induced roughness is established, reinforcing the wax layer specifically therefore appears more effective than repeated full bilayer deposition. Wet-on-wet deposition, rather than the number of reinforcement steps, is likely the more important factor behind the standardised protocol's reduced efficacy, and a relevant parameter for future optimisation. M3-(1B+3W)'s success using a wax-based emulsion of only water and carnauba wax is also appealing from a sustainability standpoint. However, this trend was only identified after the preliminary trials had already been conducted, leaving no time to design a systematic set of conditions to explore it further. Subsequent efforts therefore focused on the conditions with superior overall performance, namely those selected within Methodology 1 (Section 4.2.3); further investigation of this reinforcement strategy, particularly the effect of intermediate drying, is suggested for future work.

4.4.2. Effect of number of bilayers on WCA

As shown in Table 19 (Section 4.4.1), the number of bilayers did not produce a linear improvement in WCA: M3-3B is statistically indistinguishable from the control, but significantly higher than M3-1B and M3-5B, which are themselves statistically identical.
This non-linear trend suggests that adding bilayers beyond an intermediate point does not improve the coating and may be counterproductive. Given the wet-on-wet deposition regime (Section 4.4.1), a higher number of bilayers means more consecutive wet-on-wet depositions, potentially increasing blending, redissolution, or disruption of previously deposited material — M3-5B would accumulate more of this disruption than M3-1B or M3-3B, despite receiving the most ZnO and wax overall. Alternatively, or additionally, excessive bilayers may smooth over the nanoscale roughness required for hydrophobicity rather than reinforcing it.

M3-3B's intermediate performance may reflect a balance between these effects: enough bilayers for meaningful roughness and low-surface-energy coverage, without yet reaching the disruption apparent at five. This is consistent with the earlier finding that the absence of intermediate drying, rather than the number of reinforcement steps, limits the standardised protocol's durability.

Within the range tested, three bilayers is therefore the most favourable condition of the standardised protocol — though it still falls short of a genuine improvement over the control, unlike M3-(1B+3W).

4.4.3. Surface morphology and chemistry (SEM, FTIR)

(I) SEM

SEM characterisation was performed on a subset of Methodology 3 conditions — M3-(1B+3W), M3-1B, and M3-3B — selected as representative examples of the best-performing preliminary trial condition (Section 4.4.1) and of the standardised bilayer protocol (Section 4.4.2). This characterisation aimed to assess the presence and distribution of zinc and wax at the leather surface, complementing the WCA results discussed above. Figure 26 presents SEM micrographs of M3-(1B+3W).

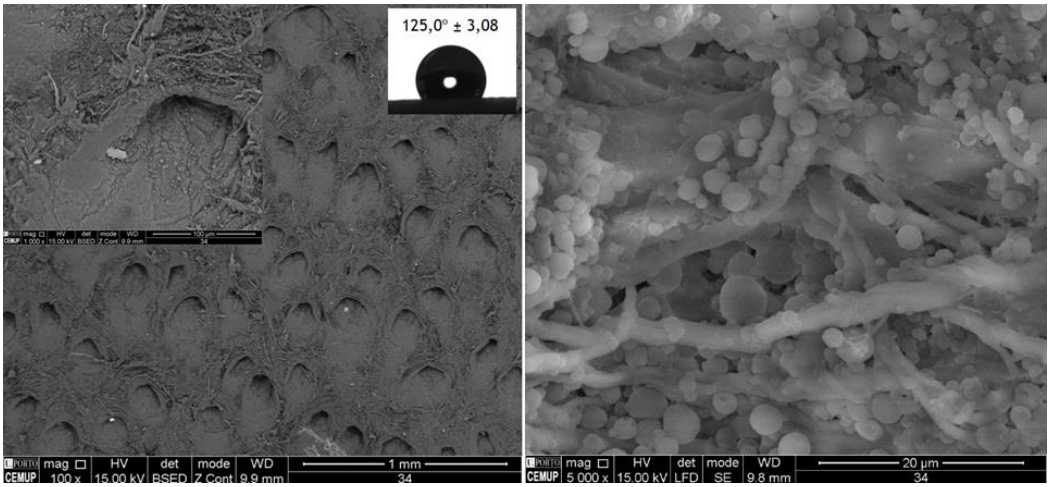


Figure 26 - SEM micrographs of sample M3-(1B+3W): (left) backscattered electron image at 100× (panoramic) and 1000× (detail) magnification, with inset showing the corresponding water contact angle (125.0° ± 3.08); (right) secondary electron image at 50

At 100× and 1000× magnification, backscattered electron imaging shows no obvious brightness contrast attributable to zinc — consistent with the surface being well covered by the outer wax layer, which is expected to obscure the underlying zinc from detection in this mode. At higher magnification (5000×, secondary electron mode), spherical particulate structures are clearly visible across and between the leather fibres. EDS cannot directly confirm the organic composition of these structures, but similar spherical morphologies have been reported in the literature for carnauba wax dispersions [38,41], supporting their tentative attribution to deposited wax — an interpretation further consolidated through FTIR analysis.

Comparing M3-1B and M3-3B (Figure 27), the 100× panoramic view (BSED) does not allow a confident assessment of the presence or absence of zinc-associated bright regions in either condition — any localised brightness, if present, is too faint to be reliably

distinguished from the surrounding surface at this magnification. As with M3-(1B+3W) above, this is consistent with the outer wax layer common to all Methodology 3 conditions, which is expected to attenuate the Z-contrast signal from any underlying zinc and generally limit the interpretability of BSED imaging at lower magnification across this methodology.

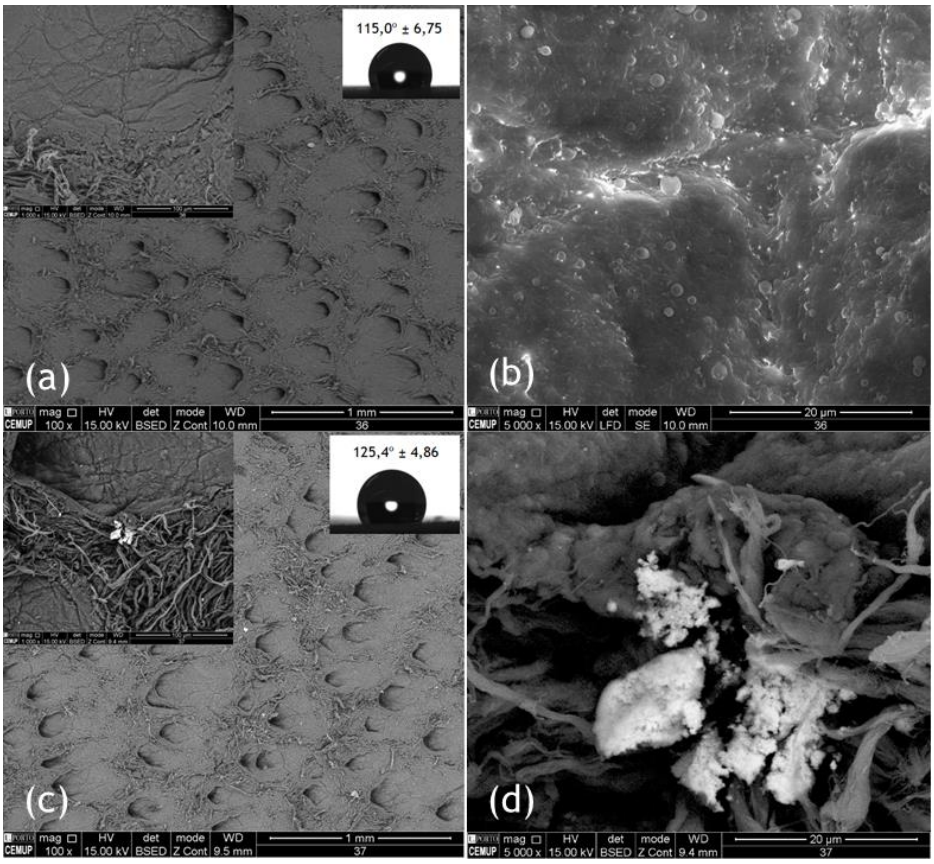


Figure 27 - SEM micrographs of samples M3-1B (a, b) and M3-3B (c, d): (a, c) backscattered electron images at 100× magnification, with insets showing the corresponding water contact angle; (b) secondary electron image at 5000× magnification of sample M3-1B, showing surface detail; (d) backscattered electron image at 5000× magnification of sample M3-3B, corresponding to a higher-magnification view of the region shown in (c).

At higher magnification, secondary electron images showed pronounced charging effects on this non-conductive substrate, limiting their use for compositional analysis. For M3-1B, secondary electron mode (5000×, Figure 27b) still resolved isolated spherical structures consistent with those seen in M3-(1B+3W) (Figure 26), tentatively attributed to carnauba wax, though the charging noted above warrants some caution in this interpretation. For M3-3B, backscattered electron mode (5000×, Figure 27d) was used instead; although no clear bright region was distinguishable at 100×, a small area of distinctly higher brightness was identified at higher magnification, tentatively attributable to a localised zinc-rich feature. A few spherical structures like those in M3-1B could also be faintly distinguished nearby, partially overlapping this brighter feature.

Given how faint and localised this feature is, it cannot be taken as evidence that M3-3B's surface is broadly zinc-dominated — only that some zinc-rich material is present and

detectable at sufficiently high magnification, unlike the more uniformly wax-like appearance of M3-1B and M3-(1B+3W). Since BSED brightness reflects atomic number, this raises the possibility of localised, heterogeneous zinc agglomeration, potentially in a core-shell-like arrangement — a zinc-rich core partially encapsulated by wax — rather than a fully phase-separated or homogeneous coating. This remains speculative and was not further confirmed in this work.

This morphological observation aligns loosely with the statistical grouping in Section 4.4.1 (Table 19): M3-(1B+3W), the only condition with clearly resolved, wax-dominated surface features and no detectable zinc signal at any magnification, is also the only one to significantly outperform the control, while M3-3B — for which a discrete zinc-rich feature was identified, albeit only at high magnification — remains statistically equivalent to it. Given the limited and localised nature of this evidence, this association should be treated as suggestive rather than conclusive.

Taken together, these observations suggest that the low surface energy of a well-distributed wax layer played a more decisive role in M3-(1B+3W)'s performance than the roughness contributed by ZnO — a departure from the combined roughness-and-chemistry mechanism proposed for Methodology 1, where both components were considered comparably important. This remains speculative and would require further investigation, such as separately assessing the individual contributions of ZnO and wax, to be more firmly established.

(II) FTIR

Figure 28 presents ATR-FTIR spectra of the untreated (control) leather, M3-(1B+3W), M3-1B, M3-3B, and pure carnauba wax. The pure wax spectrum displays a distinct carbonyl stretching band at approximately 1734 cm^{-1}, characteristic of the fatty acid ester component of carnauba wax [38]. This band is closely matched in the spectrum of M3-(1B+3W), appearing markedly more pronounced than the weak feature already present in the control spectrum in this region — the latter likely arising from minor contributions of the collagen substrate.

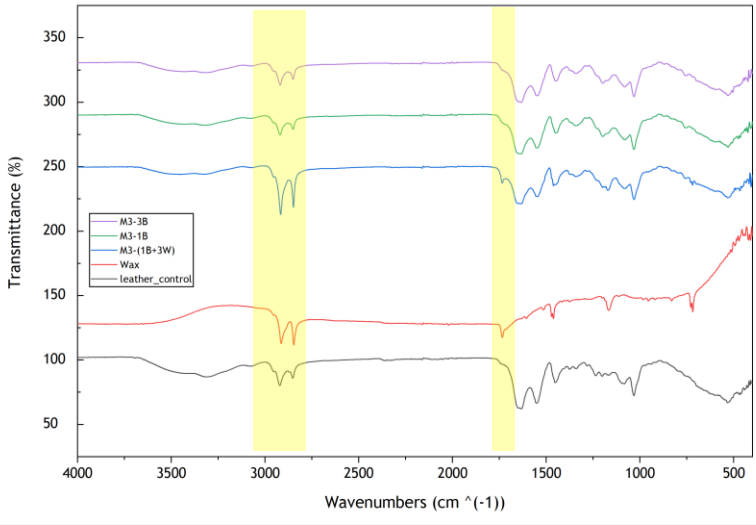


Figure 28- ATR-FTIR spectra of the untreated (control) leather Methodology 3 conditions M3-(1B+3W), M3-1B, and M3-3B

In contrast, M3-1B and M3-3B show only a slight increase in intensity at this position relative to the control, considerably less pronounced than that observed for M3-(1B+3W). This pattern is consistent with the SEM findings discussed above, which identified M3-(1B+3W) as displaying the most distinct wax-like particulate morphology among the three conditions analysed. By comparison with the pure carnauba wax spectrum, we can confirm that wax is present at the surface of M3-(1B+3W) to a substantially greater extent, and in a more readily identifiable form, than in M3-1B and M3-3B.

A further, broad band centred around 3500 cm^{-1}, associated with O–H stretching, is markedly more pronounced in the control spectrum than in any of the functionalised conditions. Since this region reflects hydroxyl groups available for hydrogen bonding with water, its attenuation upon functionalisation is consistent with a reduction in surface hydrophilicity, reinforcing the hydrophobic character imparted by the applied coatings.

4.5. Comparison across methodologies

4.5.1. WCA comparison

Table 20 summarises the water contact angle (WCA) at t = 0 and t = 5 min, retention, and surface zinc content (where available) for the best-performing conditions identified within each methodology.

Table 20 - Summary of water contact angle (WCA) at t=0 and t=5 min, retention, and surface zinc content (where available) for the best-performing conditions identified within each methodology

Condition	WCA t=0 min (°)	WCA t=5 min (°)	Retention (%)	Zn (wt.%)
M1-A1-1.1c-50Et	144.3 ± 5.6	141.8 ± 5.7	98.3	29.44
M1-A2-1.1c-50Et	136.3 ± 8.0	135.9 ± 7.3	99.7	19.33
M2-1	129.6 ± 5.8	123.5 ± 6.3	95.3	-
M2-2	134.2 ± 2.1	127.8 ± 4.1	95.2	8.81
M2-3	128.4 ± 3.3	124.9 ± 2.0	97.3	7.28
M3-(1B+3W)	125.0 ± 3.1	119.3 ± 3.9	95.4	-
M3-3B	125.4 ± 9.3	106.7 ± 4.2	85.1	-

Methodology 1 clearly outperformed Methodologies 2 and 3 across all metrics considered, achieving both the highest WCA at t = 5 min and the most consistently high retention, relative to the untreated control (108.4°, 94.8% retention). M1-A1-1.1c-50Et represents the single best-performing condition identified across this work, combining the highest WCA with high stability, while M1-A2-1.1c-50Et achieved the best overall stability of any condition tested. Both conditions were confirmed statistically as the top-performing group within Methodology 1 (Section 4.2.3).

Notably, the strategies that achieved a statistically confirmed improvement over the control — the pre-synthesised ZnO nanoparticles of Methodology 1, the heated *in-situ* route of Methodology 2 (M2-1/M2-2/M2-3), and the wax-only reinforcement of M3-(1B+3W) — share a common feature despite their different deposition mechanisms: each involves a step that consolidates the deposited material, whether through repeated immersion (Methodology 1), thermal conversion to crystalline ZnO (Methodology 2), or intermediate drying before reinforcement (Methodology 3). By contrast, the conditions that failed to improve on the control — unheated or low-concentration M2 conditions, and the

continuous wet-on-wet standardised M3 protocol — all lacked this consolidation step. The *ex-situ*/*in-situ* distinction alone therefore does not determine performance; an adequate consolidation mechanism appears necessary, regardless of route, for the dual-component system — ZnO roughness plus a well-bound low-surface-energy phase — to yield durable hydrophobicity.

This trend is further reinforced when surface zinc content is considered alongside WCA within Methodologies 1 and 2. M1-A2-1.1c-50Et achieved the best overall stability of any condition tested despite requiring less than half the surface zinc content of the top WCA condition, M1-A1-1.1c-50Et. Similarly, M2-2 presented a substantially higher zinc content than M2-3, yet the two conditions were not statistically distinguishable in WCA. Zinc content could not be reliably compared for Methodology 3, as the outer wax layer was found to obscure the underlying zinc signal at the surface; nonetheless, M3-(1B+3W) achieved the best stability of any Methodology 2 or standardised Methodology 3 condition using only a single base bilayer reinforced with wax rather than additional ZnO. Taken together, these comparisons converge on a central conclusion of this work: the total quantity of zinc deposited is, on its own, a poor predictor of hydrophobic performance. What appears to matter most is how that zinc — and the accompanying low-surface-energy component — is deposited, consolidated, and distributed across the leather surface.

Given this consistently superior performance, the two best-performing Methodology 1 conditions — M1-A1-1.1c-50Et and M1-A2-1.1c-50Et — were selected for the abrasion resistance and stain resistance testing presented in Section 4.6. These two conditions were deliberately chosen to reflect a trade-off between the two performance dimensions considered throughout this work: M1-A1-1.1c-50Et represents the highest achievable WCA, while M1-A2-1.1c-50Et represents the most durable, stable hydrophobic performance over time. Evaluating both conditions in the subsequent durability tests allows this work to assess whether either dimension — peak hydrophobicity or long-term stability — translates more effectively into resistance against mechanical abrasion and staining.

4.6. Durability and functional performance of selected coatings

Building on the trade-off identified in Section 4.5.1, the two best-performing conditions of Methodology 1 — M1-A1-1.1c-50Et, representing peak initial hydrophobicity, and M1-A2-1.1c-50Et, representing the most stable hydrophobic behaviour over time — are further evaluated in this section through mechanical abrasion and stain resistance testing, providing an additional basis for distinguishing between these two conditions under more demanding, functionally relevant conditions.

4.6.1. Abrasion resistance

As described in Section 3.5.4, abrasion testing required the preparation of larger leather specimens than those used in the remaining characterisation techniques, in order to ensure a consistent applied pressure across the tested surface [7]. Non-abraded control specimens of the same larger dimensions were also prepared and evaluated by WCA, allowing this test to serve a secondary, indirect purpose beyond assessing abrasion resistance itself: verifying the reproducibility of the WCA results obtained at the smaller

sample scale used throughout the rest of this work, when the same coating conditions are applied to a larger surface area.

The primary outcome considered throughout this section is WCA, measured on both abraded and non-abraded specimens, rather than a direct quantification of material or mass loss, since hydrophobicity remains the central performance metric of interest in this work.

Figure 29 presents the WCA results for M1-A1-1.1c-50Et and M1-A2-1.1c-50Et before abrasion and after 20 and 50 abrasion cycles. To determine whether these changes are statistically meaningful, a one-way ANOVA was performed for each condition separately (t = 5 min, n = 5 per cycle count), followed by Tukey HSD pairwise comparisons; the two conditions were also compared directly at each cycle count.

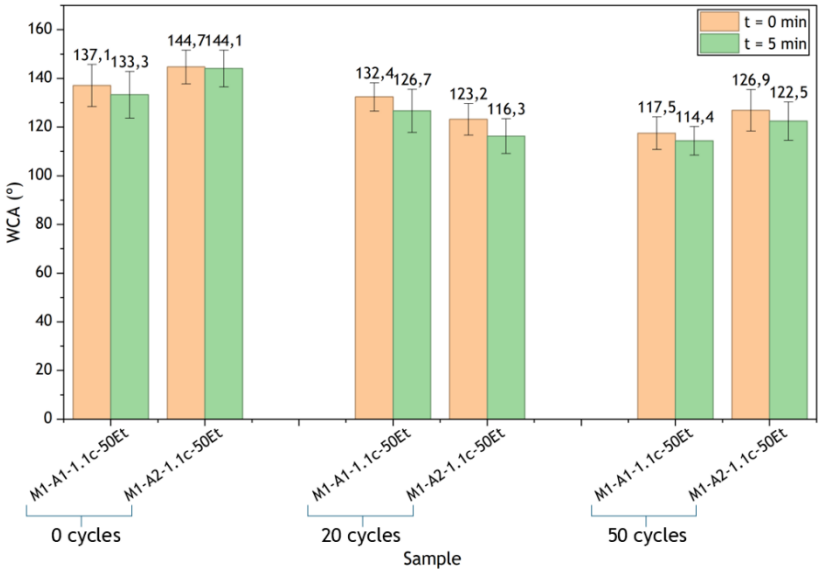


Figure 29- Water contact angle (WCA) at t=0 min and t=5 min for M1-A1-1.1c-50Et and M1-A2-1.1c-50Et before abrasion (0 cycles) and after 20 and 50 abrasion cycles

The water contact angle decreased significantly with abrasion cycles for both M1-A1-1.1c-50Et and M1-A2-1.1c-50Et (one-way ANOVA, $p < 0.05$), but with distinct patterns over time, as shown by the Tukey HSD pairwise comparisons in Table 21.

Table 21 - Tukey HSD pairwise comparisons between abrasion cycle counts, for each condition (α = 0.05)

Condition	Comparison	Difference (°)	Tukey p	Significant?
M1-A1-1.1c-50Et	0 vs 20 cycles	6.6	0.443	No
	0 vs 50 cycles	18.9	0.0094	Yes
	20 vs 50 cycles	12.3	0.087	No
M1-A2-1.1c-50Et	0 vs 20 cycles	27.8	0.0002	Yes
	0 vs 50 cycles	21.6	0.0018	Yes
	20 vs 50 cycles	6.2	0.419	No

For M1-A1-1.1c-50Et, only the overall drop from 0 to 50 cycles reached significance, the decrease up to 20 cycles alone was not statistically distinguishable from the non-abraded specimen. For M1-A2-1.1c-50Et, the significant decline occurred almost entirely within the first 20 cycles, with no further significant change between 20 and 50 cycles. This confirms that the numerically higher value at 50 cycles reflects measurement variability

rather than genuine recovery. No statistically significant difference was found between the two conditions at any cycle count, despite numerical gaps of 8–11°.

Despite this decrease, WCA stability after 5 minutes remained consistently high throughout (94.4–99.6% retention). In this case, abrasion reduces the initial extent of hydrophobicity without compromising short-term stability of the remaining coating.

To complement the statistical analysis above, the two conditions were also examined by SEM before and after abrasion. Figure 30 presents backscattered electron micrographs of M1-A1-1.1c-50Et at 0, 20 and 50 abrasion cycles, and Figure 31 presents the corresponding series for M1-A2-1.1c-50Et.

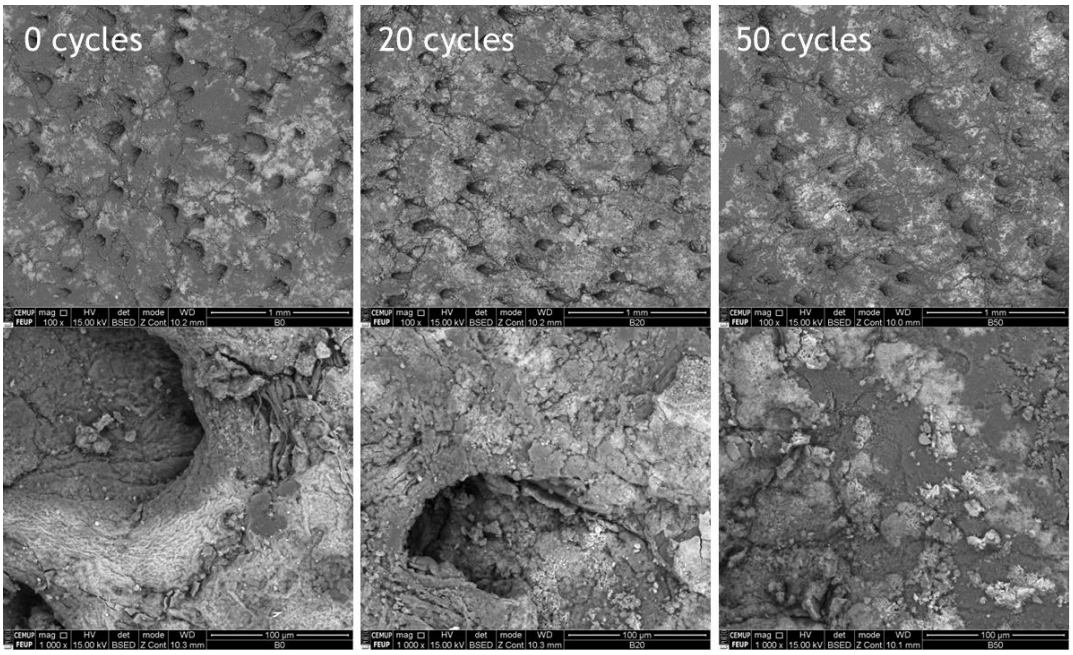


Figure 30- Backscattered electron SEM micrographs of sample M1-A1-1.1c-50Et after 0, 20 and 50 abrasion cycles, at 100× (top row) and 1000× (bottom row) magnification

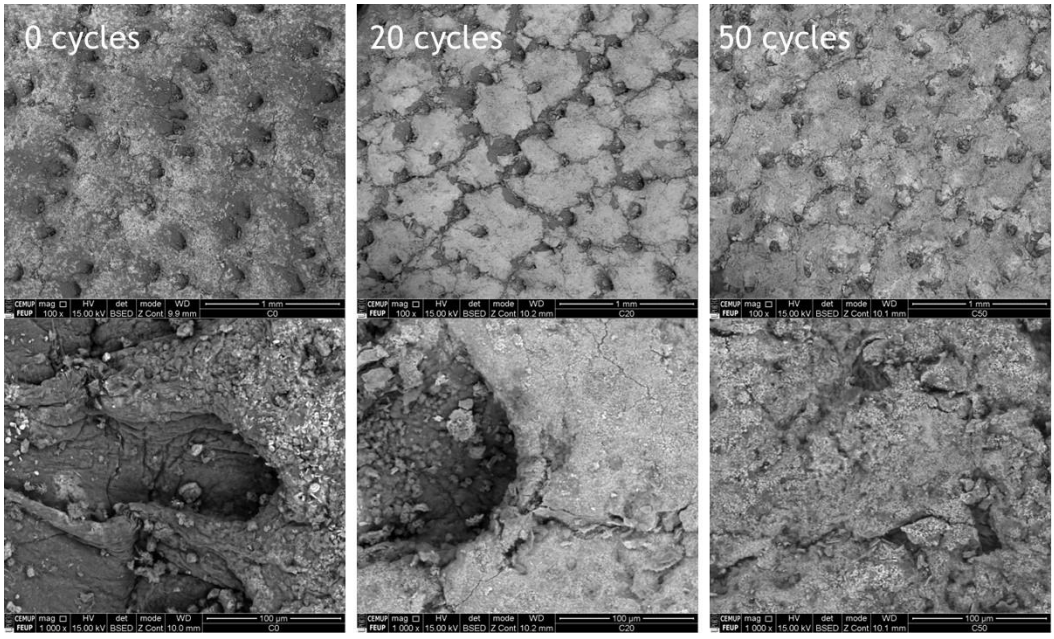


Figure 31- Backscattered electron SEM micrographs of sample M1-A2-1.1c-50Et after 0, 20 and 50 abrasion cycles, at 100× (top row) and 1000× (bottom row) magnification

Across all cycle counts and both conditions, the surface retains the pore-dominated topography characteristic of the higher ZnO concentration within Methodology 1, with no return of the loose, fibrous appearance of the untreated control even after 50 cycles. The two conditions differ, however, in the distribution of the brighter, Zn-rich regions: for M1-A1-1.1c-50Et these appear more dispersed across the surface, whereas for M1-A2-1.1c-50Et they form more localised aggregates, most notably at 20 cycles. Cracking is visible in both conditions after abrasion but is markedly more pronounced for M1-A2-1.1c-50Et. For M1-A1-1.1c-50Et at 50 cycles, the pores also appear somewhat flattened and aligned along a preferential direction, plausibly reflecting the direction of the applied abrasion.

These morphological differences are consistent with the distinct statistical patterns identified above (Table 21): the more extensive cracking and Zn aggregation already present at 20 cycles for M1-A2-1.1c-50Et align with its earlier, more abrupt WCA decline, whereas the comparatively more dispersed coating and less pronounced cracking for M1-A1-1.1c-50Et are consistent with its more gradual loss of hydrophobicity, only reaching significance by 50 cycles.

The SEM micrographs show that the ZnO-rich, pore-dominated topography persists throughout for both conditions, consistent with the coating's structural integrity being retained even after 50 abrasion cycles. The timing of WCA decline, statistically distinct for each condition (M1-A2 drops early, M1-A1 only by 50 cycles), matches what SEM shows: M1-A2 has more cracking and zinc aggregation already at 20 cycles, while M1-A1 stays more dispersed with less cracking. This reinforces the broader conclusion of the work — distribution and consolidation matter more than total amount.

At 0 cycles, the WCA values obtained for the larger specimens differ from those previously recorded at the smaller scale, with the relative ranking of the two conditions reversed. This is consistent with the substantial batch-to-batch heterogeneity of the leather substrate noted throughout this work. The reversal in relative ranking between scales (M1-A1 outperforming M1-A2 by 8.0° at the smaller scale, versus the opposite by 7.6° at the larger scale) is best explained by substrate heterogeneity rather than a genuine scale effect. This highlights an important limitation for practical scale-up: while the underlying functionalisation mechanism remains robust across scales — both conditions consistently exceeding the control regardless of specimen size — absolute WCA values should be interpreted as representative of a range of outcomes shaped by natural substrate variability, rather than as precise, universally reproducible figures.

4.6.2. Stain resistance

Stain resistance was evaluated on M1-A1-1.1c-50Et, M1-A2-1.1c-50Et, and the untreated control (Figure 32), following the protocol described in Section 3.5.5.

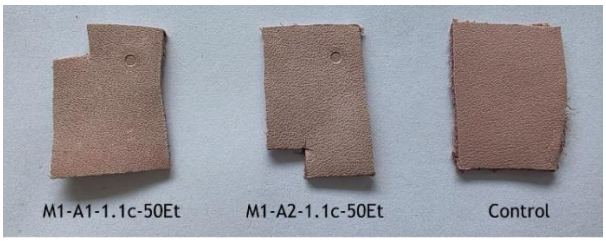


Figure 32- Leather specimens used for stain resistance testing: M1-A1-1.1c-50Et, M1-A2-1.1c-50Et, and the untreated control

Figure 33 presents the visual evolution of both staining agents on the three specimens, from droplet deposition to droplet removal after 10 minutes.

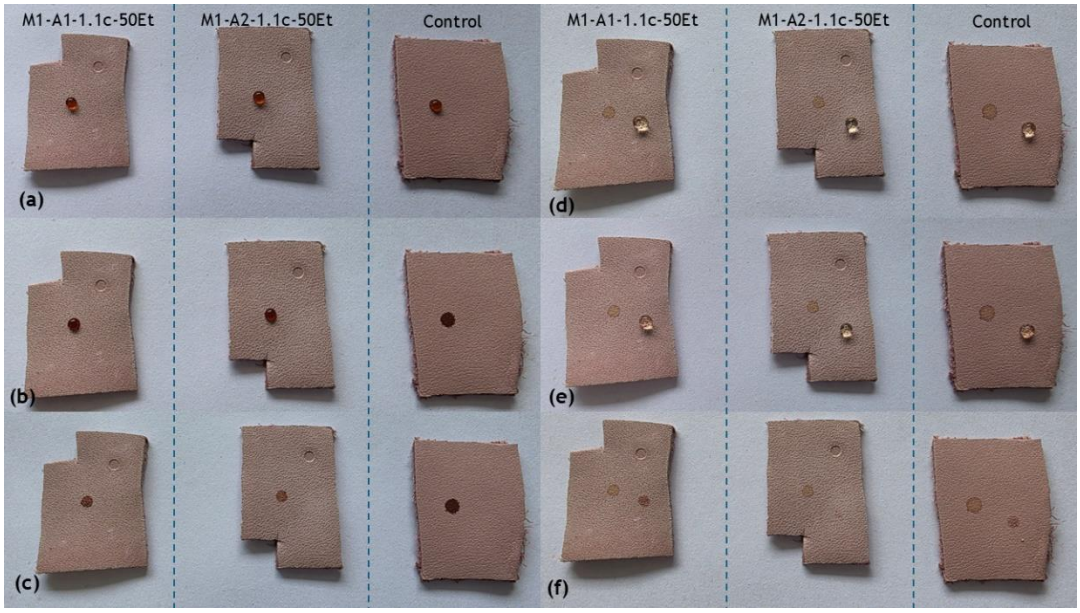


Figure 33- Stain resistance testing on M1-A1-1.1c-50Et, M1-A2-1.1c-50Et, and the untreated control, using coffee (a–c) and green tea (d–f) as staining agents. Rows show, from top to bottom: immediately after droplet deposition, after 10 minutes, and after droplet removal

In the case of green tea (Figure 33d–f), each specimen was previously used for the coffee staining test (Figure 33a-c); the fainter mark visible in these images corresponds to the residual coffee droplet from that earlier test. Residual liquid remained visible on the surface immediately after droplet removal for all samples, including the untreated control; however, no residual staining was detected once the specimens had fully dried. This behaviour is consistent with the baseline hydrophobicity of the pristine leather substrate, which appears sufficient to inhibit noticeable liquid penetration under the evaluated contact duration and low pigment load.

Conversely, coffee exposure (Figure 33a–c) left a visible mark across all specimens following droplet removal and subsequent air drying (Figure 34).

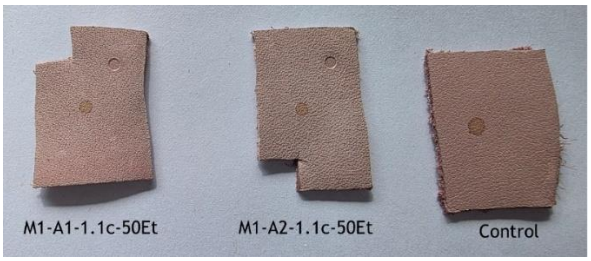


Figure 34- Final appearance of the coffee-stained specimens after droplet removal and complete drying

Crucially, a distinct contrast in stain intensity was evident between the functionalised surfaces and the control. While the untreated control developed a dark, well-defined mark, both M1-A1-1.1c-50Et and M1-A2-1.1c-50Et exhibited visibly fainter marks, with no appreciable difference in performance between the two coating conditions. These observations indicate that while the functional coating did not completely prevent staining from coffee — likely reflecting its higher chromophore concentration and more complex composition compared to green tea — it appears to have mitigated chromophore penetration and surface adsorption to some extent. This is consistent with the barrier functionality of the coating in restricting aqueous uptake, though the qualitative, visual nature of this assessment should be noted as a limitation.

5. Conclusion

This work developed and characterised a sustainable, PFAS-free surface coating for leather, based on the combination of ZnO nanoparticles with naturally occurring low-surface-energy agents — myristic acid and carnauba wax — aimed at imparting hydrophobicity and stain resistance.

ZnO nanoparticles were successfully synthesised and characterised by DLS, revealing that particle size increased with increasing precursor concentration, consistent with the LaMer nucleation-growth model and trends reported in the literature.

Application parameters were optimised across three distinct functionalisation methodologies, evaluating the effects of cleaning protocol, ZnO precursor concentration, dispersion medium, zinc salt type, base type, solvent, heating, and bilayer number on the resulting hydrophobic performance. Hydrophobicity was evaluated by water contact angle throughout all methodologies, statistically validated using ANOVA and post-hoc comparisons appropriate to each experimental design, and the coatings were extensively characterised chemically and morphologically by SEM, EDS, and FTIR.

Among the three investigated methodologies, Methodology 1 achieved the best overall, statistically confirmed performance, reaching a maximum WCA of 144.3º ± 5.6 and up to 99.7% stability retention after 5 minutes, driven primarily by ZnO concentration and cleaning protocol. Methodology 2 only achieved a statistically significant improvement over the control when final-bath heating was applied. Methodology 3 achieved its only significant improvement through a wax-only reinforcement strategy following an intermediate drying step, rather than through additional ZnO deposition.

The two best-performing Methodology 1 conditions demonstrated meaningful mechanical durability and provided complete resistance to green tea staining, alongside

a partial, though incomplete, reduction in coffee staining relative to the untreated control.

Several limitations of this work should nonetheless be acknowledged. The natural heterogeneity of the bovine leather substrate introduced considerable variability into WCA measurements, particularly evident in the reversal of relative performance ranking observed between smaller-scale and larger abrasion-test specimens. Stain resistance was assessed only qualitatively, based on visual inspection, rather than through quantitative colorimetric analysis.

Overall, this work demonstrates the feasibility of developing effective, sustainable, fluorine-free hydrophobic and stain-resistant leather coatings using ZnO nanoparticles combined with natural, bio-based low-surface-energy agents, representing a meaningful contribution towards more environmentally responsible finishing solutions for the leather industry. ZnO's known antimicrobial and UV-shielding properties, though not assessed here, represent a further potential benefit of this approach.

6. Future works

Based on the findings and limitations identified throughout this work, several directions are proposed for future research.

The isoelectric point of ZnO, used throughout this work to justify pH-based electrostatic deposition mechanisms, should be experimentally confirmed rather than assumed from general literature values. Additionally, DLS characterisation of the ZnO-1.1-c dispersion — the final, best-performing nanoparticle condition — should be completed to allow direct comparison with the substoichiometric conditions characterised in this work.

Although Methodology 2 achieved the lowest overall hydrophobic performance, it displayed several promising results (M2-1, M2-2, M2-3) that were not further pursued within the scope of this work, due to the greater procedural complexity and reagent safety considerations associated with this approach. Future work could explore alternative bases with a more favourable safety and handling profile, simplified bath sequences, and a more systematic experimental design to better isolate the effect of individual process variables.

In Methodology 3, the preliminary trial condition M3-(1B+3W) achieved the only statistically significant improvement over the control, using a low-zinc, wax-based reinforcement strategy, but this approach was not systematically explored due to time constraints. Future work should investigate the specific role of intermediate drying between reinforcement layers, and evaluate whether a wax-only reinforcement strategy, potentially requiring less zinc oxide overall, could offer a more sustainable and effective alternative to the standardised bilayer protocol. The effect of bilayer number on coating performance would also benefit from further investigation, testing additional intermediate values beyond those explored here.

ZnO nanoparticles were selected, in part, for their recognised potential to confer UV shielding and antimicrobial properties to leather; however, these properties were not experimentally evaluated within the scope of this work. Future studies should assess these functional properties directly, further exploring the multifunctional potential of the developed coatings.

Stain resistance in this work was evaluated only qualitatively, based on visual inspection. Future work should incorporate quantitative colorimetric analysis (e.g., ΔE measurements) to objectively assess both staining severity and any potential impact of the functionalisation treatments on the natural appearance of the leather.

The reversal in relative WCA performance observed between smaller-scale and larger abrasion-test specimens highlights the influence of substrate heterogeneity on reproducibility. Future work aimed at industrial scale-up of this coating should systematically assess performance across larger sample sizes and multiple hide sources, in order to establish more robust, widely applicable perform.

7. References

[1] F. Fierro, M. Iuliano, C. Cirillo, C. Florio, G. Maffei, A. Loi, T. Batakliev, R. Adami, M. Sarno, Multifunctional leather finishing vs. applications, through the addition of well-dispersed flower-like nanoparticles, Scientific Reports 2024 14:1 14 (2024) 2163-. https://doi.org/10.1038/s41598-024-51775-4.

[2] EU Green Week: Leather - A Natural Choice for the Circular Economy | EU Textiles Ecosystem Platform, (n.d.). https://transition-pathways.europa.eu/textiles/articles/eu-green-week-leather-natural-choice-circular-economy (accessed April 26, 2026).

[3] Leather: an example of circular economy - Gruppo Mastrotto, (n.d.). https://www.mastrotto.com/en/leather-experience/an-example-of-circular-economy (accessed April 26, 2026).

[4] R. Naffa, C. Maidment, M. Ahn, B. Ingham, S. Hinkley, G. Norris, Molecular and structural insights into skin collagen reveals several factors that influence its architecture, Int. J. Biol. Macromol. 128 (2019) 509–520. https://doi.org/10.1016/J.IJBIOMAC.2019.01.151.

[5] B.M. Haines, J.R. Barlow, The anatomy of leather, J. Mater. Sci. 10 (1975) 525–538. https://doi.org/10.1007/BF00543698/METRICS.

[6] S.J. Kelly, H.C. Wells, K.H. Sizeland, N. Kirby, R.L. Edmonds, T. Ryan, A. Hawley, S. Mudie, R.G. Haverkamp, Artificially modified collagen fibril orientation affects leather tear strength, J. Sci. Food Agric. 98 (2018) 3524–3531. https://doi.org/10.1002/JSFA.8863.

[7] S.A.F. Neves, S. Pinho, M.F. Almeida, M.A. Lopes, C. Fonseca, R. Frias, A Simple and Scalable Two-Step Process for Durable Hydrophobic and Stain-Resistant Leather Coatings, Coatings 2026, Vol. 16, Page 471 16 (2026) 471. https://doi.org/10.3390/COATINGS16040471.

[8] News - All you need to know about the Portuguese footwear industry - Portuguese Shoes, (n.d.). https://www.portugueseshoes.pt/en/news/all-you-need-to-know-about-the-portuguese-footwear-industry/ (accessed April 26, 2026).

[9] How Much Does It Cost to Make a Pair of Shoes in Portugal? - Portugal Production, (n.d.). https://www.portugalproduction.com/how-much-does-it-cost-to-make-a-pair-of-shoes-in-portugal/ (accessed April 26, 2026).

[10] Portugal launches campaign to export leather goods, (n.d.). https://www.satra.com/bulletin/article.php?id=3222 (accessed August 18, 2026).

[11] Tony. Covington, Tanning chemistry : the science of leather, (2009) 483. https://books.google.com/books/about/Tanning_Chemistry.html?hl=pt-PT&id=Og7OwDQp0CwC (accessed April 26, 2026).

[12] M. Parisi, A. Nanni, M. Colonna, Recycling of Chrome-Tanned Leather and Its Utilization as Polymeric Materials and in Polymer-Based Composites: A Review,

Polymers 2021, Vol. 13, Page 429 13 (2021) 429. https://doi.org/10.3390/POLYM13030429.

[13] M. Pollution Control Agency - Maya Gilchrist, L. McLain, PFAS in the textile and leather industries, (2023). www.pca.state.mn.us. (accessed April 26, 2026).

[14] P. Jerič, B. Likozar, U. Novak, Biobased Hydrophobic Solutions for Natural Textiles—Moving Beyond PFAS, Journal of Composites Science 2025, Vol. 9, Page 81 9 (2025) 81. https://doi.org/10.3390/JCS9020081.

[15] Per- and polyfluoroalkyl substances (PFAS) - ECHA, (n.d.). https://echa.europa.eu/hot-topics/perfluoroalkyl-chemicals-pfas (accessed April 26, 2026).

[16] An assessment on PFAS in textiles in Europe's circular economy | PFAS in textiles in Europe's circular economy | European Environment Agency (EEA), (n.d.). https://www.eea.europa.eu/en/analysis/publications/pfas-in-textiles-in-europes-circular-economy/an-assessment-on-pfas-in-textiles-in-europes-circular-economy (accessed April 26, 2026).

[17] S.R. Sani, F. Atrafshan, A.M. Ali, Study of the superhydrophobic properties of modified ZnO-coated cotton fabric by fatty acids, Inorg. Chem. Commun. 156 (2023) 111260. https://doi.org/10.1016/J.INOCHE.2023.111260.

[18] M.A. Arfaoui, P.I. Dolez, M. Dubé, David, Development and characterization of a hydrophobic treatment for jute fibres based on zinc oxide nanoparticles and a fatty acid, Appl. Surf. Sci. 397 (2017) 19–29. https://doi.org/10.1016/J.APSUSC.2016.11.085.

[19] I.N. Amirrah, Y. Lokanathan, I. Zulkiflee, M.F.M.R. Wee, A. Motta, M.B. Fauzi, A Comprehensive Review on Collagen Type I Development of Biomaterials for Tissue Engineering: From Biosynthesis to Bioscaffold, Biomedicines 10 (2022) 2307. https://doi.org/10.3390/BIOMEDICINES10092307.

[20] S. Ferraris, F. Gamna, T. Luxbacher, G. Maculotti, L. Giorio, J. Kholkhujaev, G. Genta, M. Galetto, A. Sarnataro, M. Nogarole, C. Florio, Comparative characterization of leather from different tanning processes as a contribution for a sustainable development of the leather industry, Scientific Reports 2025 15:1 15 (2025) 10608-. https://doi.org/10.1038/s41598-025-94531-y.

[21] S. Mehta, An Experimental Investigation on Optimizing Liquid Repellency of Fluorochemical Urethane Finish and Its Effect on the Physical Properties of Polyester/Cotton Blended Fabric, Fibers 2020, Vol. 8, Page 72 8 (2020) 72. https://doi.org/10.3390/FIB8120072.

[22] Y. Wang, W. Huang, H. Zhang, L. Tian, J. Zhou, B. Shi, Surface Charge and Isoelectric Point of Leather: A Novel Determination Method and its Application in Leather Making, Journal of the American Leather Chemists Association 112 (2017) 224–231. https://journals.uc.edu/index.php/JALCA/article/view/3766 (accessed April 28, 2026).

[23] C. Siebler, R.S. Erdmann, H. Wennemers, From azidoproline to functionalizable collagen, Chimia (Aarau). 67 (2013) 891–895. https://doi.org/10.2533/CHIMIA.2013.891.

[24] Y.; Zhang, Z.; Zhang, J.; Yang, Y.; Yue, H.A. Zhang, S. Kulinich, Y. Zhang, Z. Zhang, J. Yang, Y. Yue, H. Zhang, A Review of Recent Advances in Superhydrophobic Surfaces and Their Applications in Drag Reduction and Heat Transfer, Nanomaterials 2022, Vol. 12, Page 44 12 (2021) 44. https://doi.org/10.3390/NANO12010044.

[25] Q. Zuo, C. Wuyong, P. Hlavacek, Effect of Surfactants on Enzyme and Skin in Bating Process, (n.d.).

[26] A. Ibrahim Nasr, Influence of some mechanical finishing processes on manufactured leather properties, 33 (2017) 99–107. https://doi.org/10.20543/mkkp.v33i2.3139.

[27] O. Serenko, Z. Nizamova, M. Kalinin, Y. Ostrovsky, L. Polukhina, A. Muzafarov, Effect of the Morphology of Leather Surface on the Hydrophobic-Hydrophilic Properties, Advances in Materials Physics and Chemistry 4 (2014) 13–19. https://doi.org/10.4236/AMPC.2014.42003.

[28] Contact angle definition and simulation The well-known equation (1)... | Download Scientific Diagram, (n.d.). https://www.researchgate.net/figure/Contact-angle-definition-and-simulation-The-well-known-equation-1-Young-Laplace_fig1_399920841 (accessed August 18, 2026).

[29] Objective quantification of surface roughness parameters affecting superhydrophobicity - RSC Advances (RSC Publishing) DOI:10.1039/D0RA03137B, (n.d.). https://pubs.rsc.org/en/content/articlehtml/2020/ra/d0ra03137b (accessed April 29, 2026).

[30] L. Cui, Y. Yao, E.K.F. Yim, The effects of surface topography modification on hydrogel properties, APL Bioeng. 5 (2021). https://doi.org/10.1063/5.0046076.

[31] K. Seo, M. Kim, D.H. Kim, Re-derivation of Young's Equation, Wenzel Equation, and Cassie-Baxter Equation Based on Energy Minimization, Surface Energy (2015). https://doi.org/10.5772/61066.

[32] Y. Cho, C.H. Park, Objective quantification of surface roughness parameters affecting superhydrophobicity, RSC Adv. 10 (2020) 31251–31260. https://doi.org/10.1039/D0RA03137B.

[33] X.F. Xiang, P.J. Li, B.F. Liu, Tuning the Superhydrophobic Properties of Hierarchical Nano-microstructural Silica Biomorph Arrays Grown at Triphasic Interfaces, Sci. Rep. 10 (2020). https://doi.org/10.1038/s41598-020-61530-0.

[34] W. Huang, D. Bai, L. Li, H. Wei, Z. Shi, H. Cheng, Y. Li, The synthesis of ultrasmall ZnO@PEG nanoparticles and its fluorescence properties, Journal of Sol-Gel Science and Technology 2015 74:3 74 (2015) 718–725. https://doi.org/10.1007/S10971-015-3653-0.

[35] Z. Wang, J. Byun, S. Lee, J. Seo, B. Park, J.C. Kim, H.Y. Jeong, J. Bang, J. Lee, S.H. Oh, Vacancy driven surface disorder catalyzes anisotropic evaporation of ZnO (0001) polar surface, Nature Communications 2022 13:1 13 (2022) 5616-. https://doi.org/10.1038/s41467-022-33353-2.

[36] M. Vorochta, V. Mansfeldova, S. Chakraborty, L. Kavan, Work function and electrochemistry of ZnO (wurtzite) single crystals (F-1:L07), Ceram. Int. 51 (2025) 12346–12354. https://doi.org/10.1016/J.CERAMINT.2024.11.066.

[37] A. Sirelkhatim, S. Mahmud, A. Seeni, N. Haida, M. Kaus, L. Chuo, A.• Siti, K. Mohd Bakhori, H. Hasan, D. Mohamad, A. Sirelkhatim, Á.S. Mahmud, Á.L.C. Ann, Á.S.K.M. Bakhori, A. Seeni, N.H.M. Kaus, H. Hasan, D. Mohamad, Review on Zinc Oxide Nanoparticles: Antibacterial Activity and Toxicity Mechanism, Nano-Micro Letters 2015 7:3 7 (2015) 219–242. https://doi.org/10.1007/S40820-015-0040-X.

[38] A. Lozhechnikova, H. Bellanger, B. Michen, I. Burgert, M. Österberg, Surfactant-free carnauba wax dispersion and its use for layer-by-layer assembled protective surface coatings on wood, Appl. Surf. Sci. 396 (2017) 1273–1281. https://doi.org/10.1016/J.APSUSC.2016.11.132.

[39] Fatty Acid Structure | Examples | Types | Physical & Chemical Properties, (n.d.). https://ibiologia.com/fatty-acid-structure/ (accessed April 29, 2026).

[40] J.R. Kanicky, D.O. Shah, Effect of Degree, Type, and Position of Unsaturation on the pKa of Long-Chain Fatty Acids, J. Colloid Interface Sci. 256 (2002) 201–207. https://doi.org/10.1006/JCIS.2001.8009.

[41] I.S. Bayer, D. Fragouli, P.J. Martorana, L. Martiradonna, R. Cingolani, A. Athanassiou, Solvent resistant superhydrophobic films from self-emulsifying carnauba wax–alcohol emulsions, Soft Matter 7 (2011) 7939–7943. https://doi.org/10.1039/C1SM05710C.

[42] R.U. Islam, T. Khan, P.M. Junaid, S. Naseem, Recent Developments in Sustainable Bio-Based Wax Nanoemulsions as Edible Coatings for Food Commodities: A Comprehensive Review, Packaging Technology and Science 37 (2024) 1175–1194. https://doi.org/10.1002/PTS.2854.

[43] S. Li, F. Luo, S.A. Chattha, C. Zhang, B. Peng, C. Mu, Surfactant-free beamhouse technology of leather manufacturing: Removing constraints for the breakdown of natural fats catalyzed by lipase, J. Clean. Prod. 261 (2020) 121187. https://doi.org/10.1016/J.JCLEPRO.2020.121187.

[44] A. Bashari, A.H. Salehi K, N. Salamatipour, Bioinspired and green water repellent finishing of textiles using carnauba wax and layer-by-layer technique, The Journal of The Textile Institute 111 (2020) 1148–1158. https://doi.org/10.1080/00405000.2019.1686881.

[45] Dias Ruivo – Fábrica de couros, (n.d.). https://www.diasruivo.com/en/about-us (accessed August 19, 2026).

[46] T. Mudalige, H. Qu, D. Van Haute, S.M. Ansar, A. Paredes, T. Ingle, Characterization of Nanomaterials: Tools and Challenges, Nanomaterials for Food Applications (2019) 313–353. https://doi.org/10.1016/B978-0-12-814130-4.00011-7.

[47] K.M. Kim, M.H. Choi, J.K. Lee, J. Jeong, Y.R. Kim, M.K. Kim, S.M. Paek, J.M. Oh, Physicochemical properties of surface charge-modified ZnO nanoparticles with different particle sizes, Int. J. Nanomedicine 9 (2014) 41. https://doi.org/10.2147/IJN.S57923.

[48] V.K. Lamer, R.H. Dinegar, Theory, Production and Mechanism of Formation of Monodispersed Hydrosols, J. Am. Chem. Soc. 72 (1950) 4847–4854. https://doi.org/10.1021/JA01167A001.

[49] Y. nan Wang, L. Hu, Essential role of isoelectric point of skin/leather in leather processing, Journal of Leather Science and Engineering 2022 4:1 4 (2022) 25-. https://doi.org/10.1186/S42825-022-00099-Y.

[50] Z. Zhang, Y. Sheng, S. Liao, J. Zhang, Y. Liu, L. Cui, Durable hydrophobic cotton fabric fabricated by synergistically modifying with zein nanoparticles and beeswax, Colloids Surf. A Physicochem. Eng. Asp. 725 (2025) 137552. https://doi.org/10.1016/J.COLSURFA.2025.137552.

[51] W. Huang, Y. Song, Y. Yu, Y. nan Wang, B. Shi, Interaction between retanning agents and wet white tanned by a novel bimetal complex tanning agent, Journal of Leather Science and Engineering 2020 2:1 2 (2020) 8-. https://doi.org/10.1186/S42825-020-00023-2.

[52] Isopropanol in Leather Processing: Applications, Benefits & Suppliers for Textile, apparel & leather at Ookto, (n.d.). https://www.ookto.com/chemicals/isopropanol-isopropyl-alcohol/textile-apparel-and-leather/leather-processing-finishes (accessed August 13, 2026).

[53] A. Ballantyne, S. Davis, Modelling the charge across pH and isoelectricpoint of bovine collagen during leather manufacture, (2019). https://pure.northampton.ac.uk/en/publications/modelling-the-charge-across-ph-and-isoelectricpoint-of-bovine-col/ (accessed August 13, 2026).

[54] H. Qin, X. Shen, Y. Chai, X. Xu, Increasing the waterproof performance of fatliquored leather by silane modification: a simple and feasible green treatment method, RSC Adv. 15 (2025) 1557. https://doi.org/10.1039/D4RA07246D.

[55] A. Azimi, P. He, Effect of gravity in the Cassie-to-Wenzel transition on a micropatterned surface, MRS Communications 2019 10:1 10 (2020) 129–134. https://doi.org/10.1557/MRC.2019.160.

[56] P. Papadopoulos, L. Mammen, X. Deng, D. Vollmer, H.J. Butt, How superhydrophobicity breaks down, Proceedings of the National Academy of Sciences 110 (2013) 3254–3258. https://doi.org/10.1073/PNAS.1218673110.

[57] A. Matei, M. Stoian, G. Crăciun, V. Țucureanu, Chemical Synthesis and Characterization of Fatty Acid-Capped ZnO Nanoparticles, Journal of Composites Science 2024, Vol. 8, Page 429 8 (2024) 429. https://doi.org/10.3390/JCS8100429.

[58] C. Badre, P. Dubot, D. Lincot, T. Pauporte, M. Turmine, Effects of nanorod structure and conformation of fatty acid self-assembled layers on superhydrophobicity of zinc oxide surface, J. Colloid Interface Sci. 316 (2007) 233–237. https://doi.org/10.1016/J.JCIS.2007.07.046.

[59] H. Ejima, J.J. Richardson, K. Liang, J.P. Best, M.P. Van Koeverden, G.K. Such, J. Cui, F. Caruso, One-step assembly of coordination complexes for versatile film and particle engineering, Science (1979). 341 (2013) 154–157. https://doi.org/10.1126/SCIENCE.1237265.

[60] M.A. Rahim, H. Ejima, K.L. Cho, K. Kempe, M. Müllner, J.P. Best, F. Caruso, Coordination-Driven Multistep Assembly of Metal–Polyphenol Films and Capsules, Chemistry of Materials 26 (2014) 1645–1653. https://doi.org/10.1021/CM403903M.